Studies of Neutron-rich Nuclei from ^{252}Cf and ^{238}U+^{9}Be Fission Fragments

By

Enhong Wang

Dissertation

Submitted to the Faculty of the

Graduate School of Vanderbilt University

In partial fulfillment of the requirements

for the degree of

DOCTOR OF PHILOSOPHY

in

Physics

May, 2015

Nashville, Tennessee

Approved:

Professor Joseph Hamilton

Professor Akunuri Ramayya

Professor Volker Oberacker

Professor David Ernst

Professor Richard Haglund

To my family,

my colleagues,

and

a large community of friends and mentors

ACKNOWLEDGEMENTS

I am especially grateful to Dr. Hamilton and Dr. Ramayya for their advice and game tickets. I would also like to thank the other members of my committee, Dr. Oberacker, Dr. Ernst and Dr. Haglund for their advice, instruction and constructive questioning of my dissertation. It has been my pleasure to work in collaboration with 1) N.T.Brewer, J.K. Hwang, S.H.Liu, Y.X. Luo, J.O. Rasmussen, S.J. Zhu and H.J.Li in the analysis of ^{252}Cf data, 2) A.Navin's group at GANIL in the analysis of ^{238}U+^{9}Be data, 3) Peking University group leaded by F.R.Xu and Shanghai Jiao Tong University group leaded by Y.Sun for theoretical calculations. It has also been a interesting part of my experience to work with undergraduate students J.M.Eldridge and J.Ranger. I would thank Mark Riley for urging our group to built the 4-fold data set to get more accurate intensities.

The work at Vanderbilt University and Lawrence Berkeley National Laboratory are supported by the US Department of Energy under Grant No. DE-FG05-88ER40407 and Contract No. DE-AC03-76SF00098. The work at Tsinghua University was supported by the National Natural Science Foundation of China under Grant No. 11175095. The work at JINR was supported by the Russian Foundation for Basic Research Grant No. 08-02-00089 and by the INTAS Grant No. 03-51-4496. One of GANIL (S.B.) acknowledges partial financial support through the LIA France-India agreement.

I would also thank for the help from S.L.Soren and the support of friends and family to me during this time.

TABLE OF CONTENTS

Page

DEDICATION..... ii

ACKNOWLEDGEMENTS..... iii

LIST OF FIGURES..... vii

LIST OF TABLES..... xiv

Chapter

1. Introduction..... 1

2. Nuclear Theory..... 3

2.1 Nuclear Decay Processes..... 3

γ decay..... 3

Fission..... 5

2.2 Nuclear Models..... 6

Shell model..... 6

Collective model..... 7

2.3 Modern Nuclear Theory..... 10

Mean filed theory..... 10

3. Experimental Techniques..... 13

3.1 ^{252}Cf Spontaneous Fission..... 13

3.2 ^{238}U + ^{9}Be Induced Fission..... 20

4. Results..... 22

4.1 New Levels and transitions in ^{96,100}Y..... 22

^{96}Y..... 22

^{100}Y..... 25

4.2 New Transitions and Levels in ^{107}Nb..... 32

4.3 Oblate Deformation and Signature Splitting in ^{118,119}Ag..... 36

^{118}Ag..... 37

^{119}Ag..... 39

4.4 Octupole Correlation in ^{147}Ce, and β and γ Vibrational Bands in ^{148}Ce..... 50

^{147}Ce..... 52

^{148}Ce..... 59

4.5 New Transitions, Levels and Mass Assignments of $^{143\text{-}153}$Pr..... 66

^{143}Pr..... 68

^{144}Pr..... 69

^{145}Pr..... 70

^{146}Pr..... 72

^{147}Pr..... 72

^{148}Pr..... 77

^{149}Pr..... 79

^{150}Pr..... 83

^{151}Pr..... 85

^{152}Pr..... 92

^{153}Pr..... 96

4.6 New Levels and Mass Assignments of ^{156,157}Pm..... 104

^{156}Pm..... 104

^{157}Pm..... 107

4.7 Possible Proton Two Quasiparticle Band in ^{158}Sm..... 113

5. Conclusions..... 119

REFERENCES..... 122

LIST OF FIGURES

Figure		Page
2. 2. 1.	Schematic of angular momenta and their projections as used in collective and Nilsson models	9
3. 1. 1.	Yields of ^{252}Cf SF fragments	14
3. 1. 2.	^{252}Cf SF schematic	15
3. 1. 3.	A cross section schematic of Gammasphere	16
3. 1. 4.	A cascade of two gammas from I_1 to I_2 to I_3 states	19
3. 2. 1.	Yield of ^{238}U + ^{9}Be induced fission fragments	21
4. 1. 1.	Level scheme of ^{96}Y obtained in the current work	22
4. 1. 2.	Partial γ ray coincidence spectrum by a) double gating on 122.3 keV transition in 96Y and 206.6 keV transition in ^{153}Pr fission partner, b) double gating on 122.3 and 731.3 keV transitions in ^{96}Y and c) double gating on 122.3 and 530.0 keV transitions in ^{96}Y	23
4. 1. 3.	Level scheme of ^{100}Y	25
4. 1. 4.	Mass- and Z- gated spectrum on ^{100}Y in ^{238}U+^{9}Be data	25
4. 1. 5.	Partial γ ray coincidence spectra by a) triple gating on 131.1, 195.5 and 217.4 keV transitions in ^{100}Y, b) triple gating on 219.8 and 330.3 keV transitions in ^{149}Pr and 162.8 keV transition in ^{100}Y and c) triple gating on 219.8 keV transition in ^{149}Pr and 193.4 keV transitions in ^{100}Y	27

4. 1. 6. Partial γ ray coincidence spectra by a) double gating on 179.2 keV transition in ^{100}Y and 219.8 keV transition in ^{149}Pr and b) double gating on 179.2 and 179.2 keV transitions in ^{100}Y..... 28

4. 1. 7. Moments of inertia of band (1) in ^{100}Y..... 30

4. 2. 1. The level scheme of ^{107}Nb..... 32

4. 2. 2. Mass- and Z- gated spectrum on ^{107}Nb from ^{238}U + ^{9}Be experiment..... 32

4. 2. 3. Partial γ coincidence spectrum by triple gating on the 156.5, 228.5 and 202.6 keV transitions in ^{107}Nb..... 33

4. 2. 4. Signature splitting in ground state bands of ^{101,103,105,107}Nb and ^{111}Rh..... 34

4. 3. 1. Level scheme of ^{118}Ag..... 37

4. 3. 2. Partial γ coincidence spectra by a) double gating on 162.3 and 168.1 keV for low energy region, b) double gating on 162.3 and 168,1 keV for high energy region, c) double gating on 277.8 and 549.7 keV..... 38

4. 3. 3. Level scheme of ^{119}Ag..... 40

4. 3. 4. Partial γ coincidence spectra by a) double gating on 130.0 and 689.4 keV, b) double gating on 130.0 and 507.2 keV transitions in ^{119}Ag..... 41

4. 3. 5. Partial γ coincidence spectra by gating on transitions from $^{115\text{-}119}$Ag..... 42

4. 3. 6. Comparison of energy levels of yrast negative parity bands in even A Ag isotopes of $^{104\text{-}118}$Ag..... 43

4. 3. 7. Comparison of E(I) - E(I-1) vs I of yrast negative parity bands in even A Ag isotopes of $^{104\text{-}118}$Ag..... 44

4. 3. 8. Comparison of calculated E2 transition energy with experimental data in ^{118}Ag..... 45

4. 3. 9. Comparison energy spacing in ^{115,117,119}Ag..... 46

4. 3. 10. Kinematic moment of inertia of the α=1/2 set of positive parity bands in ^{115,117,119}Ag..... 47

4. 3. 11. PSM calculation for the positive parity band in ^{119}Ag with oblate and prolate parameters..... 48

4. 4. 1. Level scheme of ^{147}Ce..... 52

4. 4. 2. Partial γ ray spectra by a) double gating on 283.5 and 251.4 keV, and b) double gating on 251.4 and 596.1 keV transitions in ^{147}Ce..... 54

4. 4. 3. Partial γ ray spectrum by triple gating on 283.5, 251.4 and 633.2 keV transitions in ^{147}Ce..... 55

4. 4. 4. Comparison of the levels of s=-i octupole bands in ^{145}Ba, ^{147}Ce and ^{149}Nd. 56

4. 4. 5. Comparison of δE(I) vs. I in ^{145}Ba, ^{147}Ce, ^{149}Nd..... 58

4. 4. 6. Comparison of rotational frequency ratio vs. I in ^{145}Ba, ^{147}Ce, ^{149}Nd..... 59

4. 4. 7. Partial level scheme of ^{148}Ce..... 60

4. 4. 8. Comparison of the ground state band, the 1β vibrational band and the 1γ vibrational band in ^{148}Ce , ^{150}Nd and ^{152}Sm..... 63

4. 4. 9. Angular momentum alignment vs. rotational frequency of the ground state band, the 1β vibrational band and the 1γ vibrational band in ^{148}Ce..... 64

4. 5. 1. Doppler corrected γ-ray energy as a function of the mass number (A) of the Pr (Z=59) fragment identified in VAMOS++..... 67

4. 5. 2. Partial ^{143}Pr mass- and Z- gated γ-ray spectrum obtained from ^{238}U + ^{9}Be induced fission data..... 68

4. 5. 3. Partial ^{144}Pr mass- and Z- gated γ-ray spectrum obtained from ^{238}U + ^{9}Be induced fission data..... 69

4. 5. 4. The new level scheme of ^{145}Pr in the present work. Transitions and levels previously reported in β decay work are labeled in black. New ones in the current work are labeled in red..... 70

4. 5. 5. Partial ^{145}Pr mass- and Z- gated γ-ray spectra obtained from ^{238}U + ^{9}Be induced fission data. Part (a) is single γ-ray spectrum. Part (b) is a projection spectrum on 211.6 keV and part (c) is a projection on 546.2. keV..... 71

4. 5. 6. Partial ^{146}Pr mass- and Z- gated γ-ray spectra obtained from ^{238}U + ^{9}Be induced fission data. Part (a) is single γ-ray spectrum. Part (b) is a projection spectrum on 188.9 keV..... 73

4. 5. 7. The new level scheme of ^{147}Pr in the present work..... 74

4. 5. 8. Partial ^{147}Pr mass- and Z- gated γ-ray spectra obtained from ^{238}U + ^{9}Be induced fission data..... 75

4. 5. 9. Partial γ-ray coincidence spectrum by gating on 138.7 and 256.6 keV transitions in ^{147}Pr from ^{252}Cf SF data..... 76

4. 5. 10. The new level scheme of ^{148}Pr..... 77

4. 5. 11. Partial ^{148}Pr mass- and Z- gated γ-ray spectra obtained from ^{238}U + ^{9}Be induced fission data..... 78

4. 5. 12. Partial γ-ray coincidence spectrum by gating on 132.1 and 290.5 keV transitions in ^{148}Pr from ^{252}Cf SF data..... 78

4. 5. 13. The new level scheme of ^{149}Pr in the present work..... 80

4. 5. 14. Partial ^{149}Pr mass- and Z- gated γ-ray spectra obtained from ^{238}U + ^{9}Be induced fission data..... 81

4. 5. 15. Partial γ-ray coincidence spectrum by gating on a) 132.1 and 290.5 keV transitions and b) 344.7 and 437.4 keV transitions in ^{149}Pr from ^{252}Cf SF data..... 81

4. 5. 16. The new level scheme of ^{150}Pr..... 83

4. 5. 17. Partial ^{150}Pr mass- and Z- gated γ-ray spectra obtained from ^{238}U + ^{9}Be induced fission data..... 84

4. 5. 18. Partial γ ray coincidence spectra by a) gating on 190.2 and 254.6 keV transitions, and b) by gating on 244.7 and 340.0 keV transitions in ^{150}Pr from ^{252}Cf SF data..... 84

4. 5. 19. The new level scheme of ^{151}Pr..... 86

4. 5. 20. Partial ^{151}Pr mass- and Z- gated γ-ray spectra obtained from ^{238}U + ^{9}Be induced fission data. Part (a) is a single γ-ray spectrum. Part (b) is a projection spectrum on 222 keV..... 87

4. 5. 21. Partial γ-ray coincidence spectra (a) by gating on 216.3 and 292.0 keV transitions, and (b) by gating on 298.8, 377.2 and 445.0 keV transitions in ^{151}Pr from ^{252}Cf SF data..... 89

4. 5. 22. Partial γ-ray coincidence spectra (a) by gating on 221.9.3 and 296.4 keV transitions, and (b) by gating on 221.3 and 291.9 keV transitions in ^{151}Pr from ^{252}Cf SF data..... 89

4. 5. 23. Partial γ-ray coincidence spectrum by gating on 296.4, 365.2 and 420.8 keV transitions in ^{151}Pr..... 90

4. 5. 24. The new level scheme of ^{152}Pr..... 93

4. 5. 25. Partial ^{152}Pr mass- and Z- gated γ-ray spectrum from ^{238}U + ^{9}Be data..... 94

4. 5. 26. Partial γ-ray coincidence spectra (a) by gating on 264.5 and 327.3 keV transitions, (b) by gating on 232.6, 295.3 and 353.4 keV transitions, and (c) by gating on 219.6, 274.1 and 306.9 keV transitions in ^{152}Pr from ^{252}Cf SF data..... 95

4. 5. 27. The level scheme of ^{153}Pr..... 96

4. 5. 28. Partial ^{153}Pr mass- and Z- gated γ-ray spectrum from ^{238}U + ^{9}Be data..... 97

4. 5. 29. Partial γ-ray coincidence spectra by gating on 221.9, 297.7 and 368.9 keV transitions in ^{153}Pr from ^{252}Cf SF data..... 97

4. 5. 30. Relative yield curves of yttrium by gating on transitions in ^{151}Pr ,^{152}Pr and ^{153}Pr from ^{252}Cf SF data..... 99

4. 6. 1. The level scheme of ^{156}Pm..... 105

4. 6. 2. Mass- and Z- gated γ- ray spectrum on ^{156}Pm from ^{9}Be+ ^{238}U induced fission..... 105

4. 6. 3. Partial γ coincidence spectra by a) double gating on 318.8 and 384.3 keV and b) 236.1 and 307.1 keV transitions in ^{156}Pm..... 107

4. 6. 4. The level scheme of ^{157}Pm..... 108

4. 6. 5. Mass- and Z- gated γ- ray spectrum on ^{157}Pm from ^{9}Be+ ^{238}U induced fission..... 108

4. 6. 6. Partial γ ray coincidence spectra by a) gating on 38.7 keV Pm x ray and the 103.6 keV in ^{157}Pm and b) gating on 38.7 keV and 264.1 keV transition in ^{157}Pm..... 110

4. 6. 7. Comparison of 5/2[532] band levels in ^{153,155,157}Pm..... 111

4. 6. 8. Moment of inertia of the 5/2- band in ^{153,155,157}Pm..... 111

4. 7. 1. The level scheme of ^{158}Sm..... 114

4. 7. 2. Partial γ-ray coincidence spectrum a) by gating on 167.5 keV transitions in ^{158}Sm and 707.1 keV transition in ^{90}Kr fission partner, and (b) by gating on 167.5 and 1082.0 keV transitions in ^{158}Sm from ^{252}Cf SF data..... 115

4. 7. 3. Comparison of level energies of ^{158}Sm with PSM calculation..... 117

LIST OF TABLES

Table	Page
1. Parameters of the energy calibration of ^{252}Cf SF data	17
2. Parameters of the efficiency calibration of ^{252}Cf SF data	18
3. The γ-ray relative intensities of ^{96}Y	24
4. The γ ray relative intensities of ^{147}Ce	53
5. The γ ray relative intensities of ^{148}Ce	61
6. The γ ray branching ratios of ^{148}Ce	62
7. Comparison of the E2 and ΔE2 energies in ^{149,151,153}Pr	101

CHAPTER 1

INTRODUCTION

Nuclear physics has many practical applications, including energy resource, national security, medical diagnosis and treatment, radioactive dating, and new materials. Studies of nuclear physics involve the structure and behavior of the inner core of the atom in the nucleus. One final goal of nuclear physics is to understand the strong nuclear force between protons and neutrons in the nucleus. Studies of neutron rich isotopes probe nuclear matter in an exotic region with unusual features and are a current frontier of much interest in nuclear physics. The fission process is a practical approach to populate neutron rich isotopes. The current techniques allow one to make precise measurements of nuclear matter in this regions with high temperature, high angular momentum, and high level density.

The present thesis comes in four basic chapters. The introduction parts of chapter 1, chapter 2 present the basic principles of nuclear theory used in the current work, namely, nuclear decay processes and nuclear models. The former one discusses the radioactivity of nuclei, and the latter one describe how the nucleons inside the nucleus move and behave in terms of the nuclear force. These two areas contain many various subsections while only the relevant parts are included. Chapter 3 introduces the current experimental techniques and procedures. This chapter deals with a ^{252}Cf spontaneous fission experiment with Gammasphere detectors and a ^{238}U + ^{9}Be induced fission experiment with Exogam detectors. Chapter 4 presents the main part of this thesis, which contains all

the experimental results and further discussions. New insights into the level schemes of 21 nuclei have been newly identified and the behavior of their structures are probed. Finally, conclusions are presented in chapter 5.

CHAPTER 2

NUCLEAR THEORY

2.1 Nuclear Decay Process

Gamma decay

According to quantum mechanics, nuclei can exist only in certain quantized energy states. A transition between two energy levels in a nucleus may lead to photon emission. This kind of photon energies are in the range from several keV to several MeV. By measuring the γ-ray energies and intensities, information of the energy states in a nucleus can be obtained.

The reduced transition probability is an important quantity and concept during the photon emission process. It is defined in the following equation related to the electric and magnetic multipole operators

$$B({}^{E}_{M}\lambda, I_i \to I_f) = \sum_{\mu M_f} | < I_f M_f \,|\, M({}^{E}_{M}\lambda, \mu) \,|\, I_i M_i > |^2$$

This expression can be simplified as

$$B({}^{E}_{M}\lambda, I_i \to I_f) = \frac{1}{2I_i + 1} | < I_f \,\|\, M({}^{E}_{M}\lambda) \,\|\, I_i > |^2$$

The reduced transition probability is proportional to the transition probability

$$B({}^{E}_{M}L, I_i \to I_f) = \frac{L[(2L+1)!!]^2 \hbar}{8\pi(L+1)} \left(\frac{\hbar c}{E_\gamma} \right)^{2L+1} \bullet P_\gamma({}^{M}_{E}L, I_i \to I_f)$$

or

$$B(EL, I_i \to I_f) = \frac{L[(2L+1)!!]^2 \hbar}{8\pi(L+1)e^2 b^L}\left(\frac{\hbar c}{E_\gamma}\right)^{2L+1} \bullet P_\gamma(EL, I_i \to I_f)$$

$$B(ML, I_i \to I_f) = \frac{L[(2L+1)!!]^2 \hbar}{8\pi(L+1)\mu_N{}^2 b^{L-1}}\left(\frac{\hbar c}{E_\gamma}\right)^{2L+1} \bullet P_\gamma(ML, I_i \to I_f)$$

The electromagnetic interaction weakly perturb the strong nuclear interaction and the corresponding operators have a well-known structure. Thus, comparison between experimentally determined γ-ray reduced transition probabilities and the theoretical predictions gives an effective approach to investigate the wave functions of nuclei.

Weisskopf single-particle estimates for the reduced transition probabilities are usually used for comparison. Such estimates are calculated by assuming a single proton making a transition from one shell model state to another.

In some cases, the nucleus goes from an exited state to a lower energy state by giving its excess energy to one of the atomic electrons outside the nucleus. This radioactive process is called internal conversion (IC) process. The ejected atomic electron is called and internal conversion electron. In this process, photon emission does not occur.

The competition between γ decay and internal conversion is quantified by the internal conversion coefficient. This coefficient is defined as the ratio of the internal conversion probability and the photon emission probability.

$$\alpha = \frac{N_e}{N_\gamma}$$

For low energy, high Z and high multipole transitions, the internal conversion process is significant.

In addition to photon emission and internal conversion, another approach for a nucleus to dexcite to a lower energy level is internal pair creation. In this process, the

excited nucleus gives up its energy through the creation of an electron-positron pair. The internal pair creation will become dominant at high energy.

Fission

The fission process is a good approach to study structural and dynamical aspects of quantum many body systems. In this process in certain heavy nuclei, hundreds of different neutron-rich isotopes far from stability are formed. Thus, it is also an important way to produce these nuclei far from stability and to study the structure of the fission products.

Spontaneous fission (SF) is a process with a long half life and competing with α decay. Spontaneously fissile nuclides have many useful applications. For example, ^{252}Cf is a very efficient compact energy source for many application. Also, ^{252}Cf is a useful very compact source of neutrons that eliminates the need for accelerators or reactors for many applications.

2.2 Nuclear Models

Shell model

Experimental data on nuclei revealed that there exists a series of magic numbers of protons and neutrons that give special stability to those nuclei which have such a Z and/or N number. It was found that when the proton number or the neutron number is equal to one of 2,8,20,28,50,82,126 the nucleus is particularly stable and has a spherical shape. The presence of such nuclear stability suggests some type of shell structure and shell closure.

The Mayer-Jensen shell model [1] presumes that the nucleons in a nucleus move independently in an average potential field. So the nucleons can be treated to move in a single particle spherical potential. The Hamiltonian is expressed as the following

$$H = \frac{p^2}{2m} + V(r) + V_{so}(r)\vec{s} \bullet \vec{l}$$

where a typical potential is

$$V = -\frac{V_0}{1+\exp[(r-R)/a]}$$

This model introduce a strong nuclear spin-orbit coupling force compared to the atomic electron Hamiltonian. The spin-orbit coupling gives rise to the energy splitting of a pair of levels with the same orbital angular momentum l into two levels $j = l \pm s$ (except for $l = 0$).

The single particle shell model assumes that the nucleons in a nucleus fill up orbitals for N and Z to a closed shell core, and the nuclear properties beyond the core are determined by the interactions of the valence nucleons outside the core. By introducing a

strong pairing interaction between nucleons, protons and neutrons tend to form pairs with both their spins and orbital angular momenta opposed. Such pairing interaction is part of the residue from the average interaction which cause a short range correlation between nucleons. Thus, 1) all even-even nuclei have zero total spin and even parity; 2) the ground state spin and parity in odd-even nuclei are determined by the unpaired particle, 3) the spins of odd-odd nuclei are determined by the coupling between the final unpaired odd neutron and odd proton. This model is suitable for spherical nuclei and well explains the shell closure magic numbers.

The Nilsson model [1] is a evolution of the basic single particle shell model in order to make it applicable to nearly all deformed nuclei. The Hamiltonian in the Nilsson model is

$$H = \frac{p^2}{2m} + \frac{1}{2}m(\omega_x{}^2 x^2 + \omega_y{}^2 y^2 + \omega_z{}^2 z^2) + C\vec{s} \bullet \vec{l} + D\vec{l}^{\,2}$$

where $\omega_x = \omega_y = \omega_0{}^2(1+\frac{2}{3}\varepsilon_2), \omega_z = \omega_0{}^2(1-\frac{4}{3}\varepsilon_2)$, and z is the nucleus symmetry axis. Spherical symmetry is broken. New quantum numbers are introduced. $\Omega^{\pi}[Nn_z\Lambda]$. Ω is the projection of the single particle angular momentum j onto the symmetry z axis. π is the parity. N is the principal number of the major oscillator quanta. n_z is the number of nodes of the wavefuntion along the z axis, and Λ is the projection of the single particle orbital angular momentum l onto the symmetry z axis.

Collective model

Despite the average potential presumed in the shell model, there exists residue interactions between nucleons. As mentioned above, part of the residue interaction gives

rise to the pairing force. Moreover, the long range correlation of the nucleons can deform the nucleus and cause a collective motion. This kind of collective motion can be classified by rotation and vibration.

For a simplified model of rotation, the Hamiltonian for a symmetrical ellipsoid rotor with a permanent deformation is

$$H_{rot} = \frac{R^2}{2\Im}$$

For even even nuclei, the shape is invariant to x-y plane reflection. Thus, only even I numbers are allowed. The energy levels are

$$E_{rot} = \frac{\hbar^2}{2\Im} I(I+1), I = 0,2,4\cdots$$

Nuclear surface vibrations can lead to the changes of deformation. On the other hand, surface vibrations can become unstable and provide a permanent nuclear deformation or nuclear fission. The shape of a deformed nucleus can be described by an expansion in terms of spherical harmonics where the

$$R(\theta',\phi') = R_0[1+\sum_{\lambda=0}^{\infty}\sum_{\mu=-\lambda}^{\lambda}\alpha_{\lambda\mu}Y_{\lambda\mu}(\theta',\phi')]$$

where the λ=0 vibration represents a change of volume. This phenomenon is called giant monopole resonance and usually occurs at relatively larger A (>40), and λ=1 is dipole vibration that corresponds to a translation where the proton and neutron fluids oscillate against each other. These two types of vibrational mode occur at high energy (at the order of 10MeV).

For quadrupole deformation, the radius of the surface with λ=2 expansion can be rewritten in terms of the angles θ and ϕ in the body-fixed system

$$R(\theta,\phi) = R_0\left[1+\beta_2\cos\gamma\, Y_{20}(\theta,\phi)+\frac{1}{\sqrt{2}}\beta_2\sin\gamma\{Y_{22}(\theta,\phi)+Y_{2-2}(\theta,\phi)\}\right]$$

where β is measured by the distance out from the origin and γ is the angle between the γ = 0 prolate and γ = 60° oblate axis.

In a pure spherical harmonic vibrator, the energy levels are generated by phonons.

Deformed nuclei can also vibrate. In quadrupole deformed nuclei, two types of vibrational states observed are: β vibration and γ vibration. These two most common types represent the vibration of β and γ parameters and are generated by β and γ phonons, respectively. Similarly, octupole vibrational states are observed and generated by octupole phonons.

In more complicated cases, nuclear behavior is a coupling of single particle motion and collective motion. The K quantum number is good quantum number and usually used for axial symmetric nuclei. This quantum number is defined as the projection of the total angular momentum onto the symmetry axis.

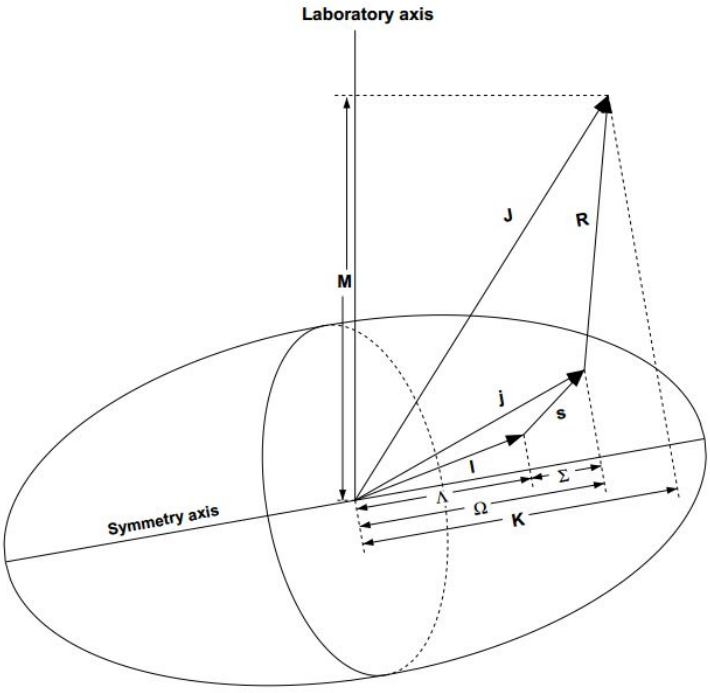

Figure 2. 2. 1. A schematic view of angular momenta and their projections as used in collective and Nilsson models [2].

2.3 Modern Nuclear Theory

Mean field theory

The *ab initio* approach is limited to very light nuclei. All the other nuclear structure theories need some kind of approximations. Mean field theory is one of them and can be applied to calculate the nuclear ground state properties of all nuclei. Mean field theory assumes the nucleons in a nucleus move independently in an average potential.

$$V(1,...,A) = \sum_{i,j}^{A} V(i,j) \approx \sum_{i}^{A} V(i)$$

The potential *V(i, j)* can be fitted to the experimental data. The nuclear wave-function is an anti-symmetrized product (Slater determinant) of the nucleon wave-functions.

$$\Phi(1,...,i,...,A) = \frac{1}{\sqrt{N!}} \begin{vmatrix} \varphi_1(1) & ... \varphi_1(A) \\ \vdots & \vdots \\ \varphi_A(1) & ... \varphi_A(A) \end{vmatrix}, \; i = \vec{r}_i, s_i, t_i$$

Here assume each φ is orthonomalized. From the variational principle, the best base gives the minimum energy of the system, or the ground state. Take E to φ_i variation.

$$\delta E[\Phi] = 0, \qquad E[\Phi] = \frac{<\Phi \mid H \mid \Phi>}{<\Phi \mid \Phi>}$$

If spin is neglected, one can get,

$$-\frac{\hbar^2}{2m}\nabla^2\varphi_i(\vec{r}) + \sum_{i'}\int d\vec{r}' \mid \varphi_{i'}(\vec{r}') \mid^2 \cdot V(\vec{r},\vec{r}') \cdot \varphi_i(\vec{r})$$
$$-\sum_{i'}\int d\vec{r}' \varphi_{i'}^{*}(\vec{r}')\varphi_i(\vec{r}') \cdot V(\vec{r},\vec{r}') \cdot \varphi_{i'}(\vec{r}) = E_i\varphi_i(\vec{r})$$

The nucleon wave-functions obey the Schrödinger equation of the mean field potential. To solve this equation, one needs an iteration method. In the first order, start with an approximate single-particle wave-function φ e.g. from shell model calculations.

Then substitute into the integral part of the left side and solve for the second order of the wave-functions. This is the so called Hartree-Fock (HF) method. Moreover, the multipole operator can be added to the variational principle to calculate the collective energy surface.

$$\delta[<\Phi_0^{HF} \mid H \mid \Phi_0^{HF}> -\sum_i \lambda_i <\Phi_0^{HF} \mid Q_i \mid \Phi_0^{HF}>] = 0$$

Similarly, the total angular momentum operator can be added to the variational principle to calculate the rotational bands.

$$\delta[<\Phi_0^{HF} \mid H \mid \Phi_0^{HF}> -\omega(I) <\Phi_0^{HF} \mid J_x \mid \Phi_0^{HF}>] = 0$$

Vibrational excitations can be built on the HF ground state using the Random Phase Approximation (RPA).

However, this method does not account for the pairing correlation and is not consistent with the observation that the ground states of even-even nuclei always have $J^{\pi}=0^{+}$. Such pairing forces can be added through a HF+Bardeen-Cooper-Schrieffer (BCS) or Hartree-Fock-Bogoliubov (HFB) approach.

Comparing to the HF method by doing variation of the single-particle wave-function, one can also rewrite the Hamiltonian in terms of local densities and currents and do variation of the density. This is called Hohenberg-Kohn-Sham (HKS) method. HKS is a kind of density functional theory.

The Schrödinger equation used above does not take relativistic effects into account. In the relativistic frame, nucleon-nucleon interactions are expressed in exchanging mesons. The HF method can also apply. This is called covariant density variation functional.

Mean field theory is a microscopic global theory of nuclear structure. Predictions can

be made with only an input of effective interaction. However, in some cases, this theory is not precise enough and has spontaneous symmetry breaking.

CHAPTER 3

EXPERIMENTAL TECHNIQUES

3.1 ^{252}Cf spontaneous fission

In 1995, an experiment was performed Lawrence Berkeley National Laboratory (LBNL) by using 72 Ge detectors of Gammasphere with a 28 μCi ^{252}Cf source sandwiched between two 11.3 mg/cm^2 Ni foils. In addition, 13.7 mg/cm^2 Al foils were added on both sides. The data were sorted into 9.8×10^9 γ-γ-γ and higher fold events and analyzed by RADWARE software [3].

In 2000, another experiment with ^{252}Cf was carried out at the LBNL. A 62 μCi ^{252}Cf source was sandwiched between two Fe foils of thickness 10mg/cm^2 and encased in a 7.62 cm polyethylene ball. By using 101 Ge detectors of Gammasphere, the raw data were sorted into 5.7×10^{11} γ-γ-γ and higher fold γ events and as reported for the first time in this thesis into 1.9×10^{11} γ-γ-γ-γ and higher fold γ coincident events. The basic unit in the raw data is event. Each event contains the information of γ multiplicity and every coincidence gamma's detector id, energy (in ADC channel number) and coincidence time. These γ coincident data were analyzed by the RADWARE software package. In order to compile the raw data into a 4d cube, one needs 1) the *lufwhm* program to generate a look-up table to map ADC channels to cube channels, 2) *make4cub* program to generate an empty cube, 3) *4play* program to scan the raw data and compile events into the 4d cube, 4) *split4cub* program to slice big size files into small ones, 5) *pro4d* program to

create a 3d cube projection and 6) *pro3d* program to create 1d and 2d projections. For the current 4d data, four ADC channels were compressed into one 4d cube channel. The energy range of 4d cube was narrowed from 33 keV to 2500 keV. The *xm4dg* program can be used to set a triple gate on the 4d cube data. The final 4d cube takes up 15GB space. Gamma-ray energies of the strong transitions have errors of 0.1 keV while the errors on the weak transitions could be as much as to 0.5 keV.

The ^{252}Cf is a radioactive source with 2.645 y half life where 96.91% of its decay branching is the α decay mode. The other 3.09% decay is spontaneous fission. The major part of ^{252}Cf SF is binary fission. Ternary fission contributes about less than 1%. In ^{252}Cf binary SF process, the parent nucleus splits into two daughter nuclei with roughly a 1.4:1 mass ratio between the heavy and light fragments. The distribution of the fission fragments is shown in Fig. 3. 1. 1.Afterwards, the primary fission fragments evaporate some neutrons with a total neutron distribution maximized at 3 or 4. The secondary fragments are usually populated to excited states. These excited secondary fission

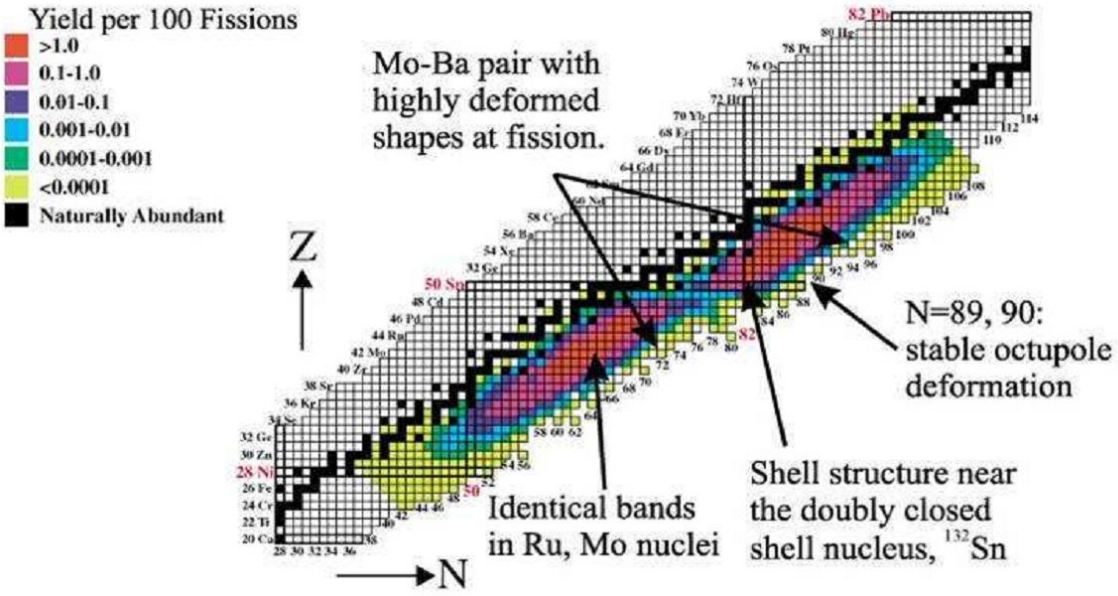

Figure 3. 1. 1 Yields of ^{252}Cf SF fragment [4].

fragments can decay to lower states by promptly emitting γ rays. The first and second stages of the binary fission occur very quickly in 10^{-18} to 10^{-15} seconds. In the present experiments, fission fragments and α particles were stopped by foils and neutrons as well as β rays were partially moderated and absorbed by the foils and plastic. The γ rays were detected in Gammasphere. Signals in Gammasphere detectors are collected in the data acquisition and saved in raw data in external memory (details in Ref. [5]).

Gammasphere is a powerful spectrometer and especially good at collecting γ ray data due to its high energy resolution, high granularity and high detection efficiency. It consists of 110 high purity germanium (HPGe) detectors in a spherical arrangement with about 47% angular coverage. The HPGe crystals are maintained at liquid nitrogen temperature in order to reduce the signal noise.

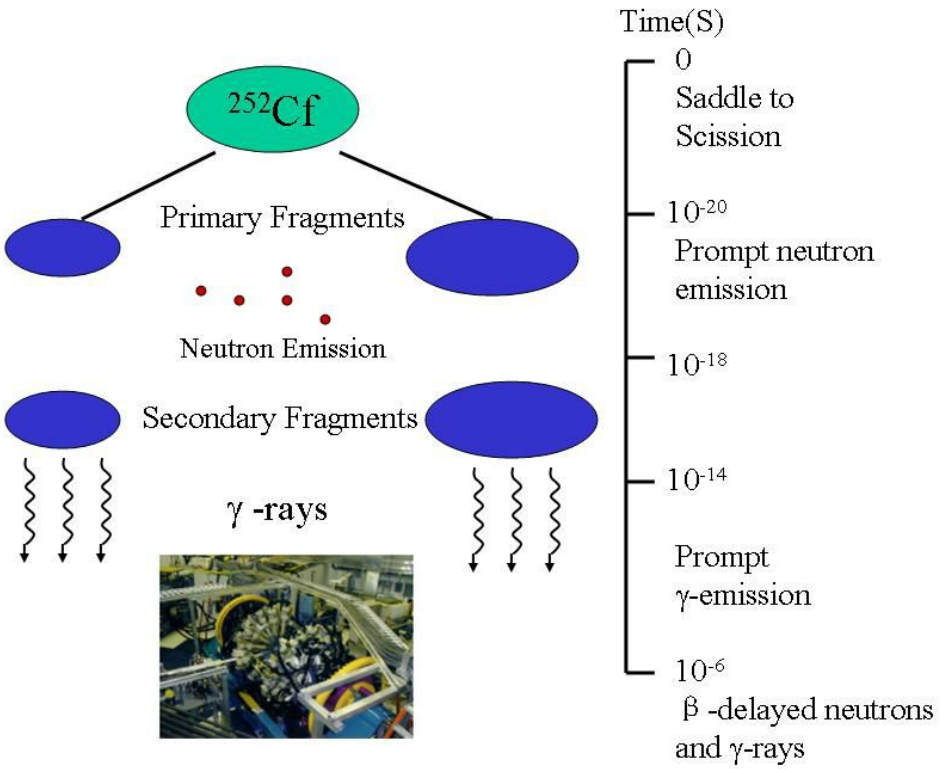

Figure 3. 1. 2. ^{252}Cf SF schematic [6].

In general, the interaction of photons with detector material atoms involves several processes: 1) Rayleigh scattering, a photon is deflected by the atom with no energy transfer, which is probable for very low energy photons and not in the γ ray region; 2) Compton scattering, a photon is elastic scattered by an atom electron and transfers a portion of its energy to the electron to cause an ejection of the electron from the atom orbital, which is predominant for medium energy of magnitude from 0.1 to 1 MeV; 3) photoelectric effect, a photon knocks out an electron from the atom and transfer all of its

Figure 3. 1. 3 A cross section schematic of Gammasphere [5].

energy to the electron so its own existence terminates, which is the dominant energy loss mechanism for photons of smaller than 50 keV energy but still important up to several MeV; 4) pair production, a photon with greater than 1.02 MeV energy converts into an electron and a position. Since Compton scattering is the dominant process in the region where most radiation is emitted, an additional bismuth germanium oxide (BGO) detector is placed between the HPGe in Gammasphere to detect and reject Compton events.

The efficiency of Gammasphere is about 10% with a peak to total ratio of 0.6% at 1.33 MeV. The energy calibration is fitted to a polynomial below using standard sources.

$$E = a + bN + cN^2 + dN^3$$

where E is energy and N is the Analog-to-Digital Converter (ADC) channel number. The fitted parameters are listed below.

a	-6.2734×10^{-1}
b	3.337×10^{-1}
c	-8.0093×10^{-8}
d	4.7999×10^{-12}

Table 1. Parameters of energy calibration.

It is noticed that there is a writing mistake for parameter c in Ref. [4, 7].

The relative efficiency for the 2000 experiment is fitted to the equation below using the relative γ ray intensities obtained from ^{252}Cf fission fragments.

$$eff = \exp[(A + Bx + Cx^2)^{-H} + (D + Fy + Gy^2)^{-H}]^{-1/H}$$

where x=Ln(E/100) with E as energy in keV, and y=Ln(E/1000) and A to H are parameters. The fitted parameters are listed below.

A	14.1597
B	9.18559
C	-2.7907
D	6.36297
F	-0.65056
G	0.0
H	2.09765

Table 2. Parameters of efficiency calibration.

Radware software is used to compile and analyze the raw data. With this software, raw data are built into 3 and 4 dimensional matrices, where the matrix elements are γ ray transition energies. By using a 3 dimensional matrix, Radware can give the γ ray spectrum in coincidence with any two other correlated γ transitions. This procedure is called a double gate on two γ ray transitions. Similarly, the 4 dimensional matrix can deduce the γ ray spectrum in coincidence with three γ transitions, which is a triple gate in short. However, γ ray the intensity measurements from the single gate in the triple coincidence data and from single and double gates in the four fold coincidence data are not accurate occasionally.

A triple gate spectrum loses statistics but improves the peak to background ratio compared to a double gate spectrum and so it is easy to eliminate the contamination peaks.

Software using the angular correlation method was developed to determine the spins and parities of nuclear states [8]. For a cascade shown in Fig. 3. 1. 4, the probability of detecting γ_1 and γ_2 with a θ angle between them can be expanded to a 4th order of Legendre polynomials

$$W(\theta) = 1 + A_2 P_2(\cos\theta) + A_4 P_4(\cos\theta)$$

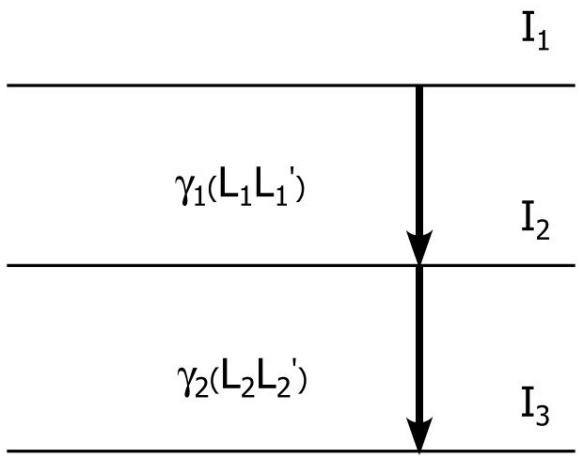

Figure 3. 1. 4 A cascade of two gammas from I_1 to I_2 to I_3 states [8].

Usually, one of the gammas was selected with known multiplicity. The multiplicity of the other gamma can be obtained by fitting the A2, A4 values with theoretical predictions for two successive quanta [9]. If the intermediate state I_2 has a lifetime, the angular correlation would be attenuated by the hyperfine magnetic field originated from the implantation of fission fragments in substitutional sties in the iron lattice. By measuring the attenuation, nuclear g factors can be obtained. Note that the *GSam* angular correlation program for theoretical calculations is wrong while the calculation involves the highest spin e.g. 19/2.

The 1995 ^{252}Cf experiment data were built according to several discrete coincidence time windows ranging from 4ns to 500ns of the γ rays [10, 11].

All the nuclei studied in the current work are analyzed by the 3 and 4 dimensional matrix from ^{252}Cf SF data. The high statistics of the data are very powerful in analyzing the γ coincidences.

3.2 ^{238}U + ^{9}Be induced fission

The measurements of transfer and fusion induced fission were performed at the GANIL laboratory in France using a ^{238}U beam at 6.2 MeV/u, with a typical intensity of 0.2 pnA, impinging on a 10-micron thick ^{9}Be target [12,13].The advantage of the inverse kinematics used in this work is that the fission fragments are forward focussed and have a large velocity, resulting in both an efficient detection and isotopic identification in the spectrometer. A single magnetic field setting of the large-acceptance spectrometer VAMOS++ [12], possessing a momentum acceptance of around ±20%, placed at 20° with respect to the beam axis, was used to identify uniquely the fission fragments. The detection system (1×0.15 m^2) at the focal plane of the spectrometer was composed of (i) a Multi-Wire Parallel Plate Avalanche Counter (MWPPAC), (ii) two Drift Chambers (x,y), (iii) a Segmented Ionization Chamber (ΔE), and (iv) 40 silicon detectors arranged in a wall structure (Er). The time of flight (TOF) was obtained by using the signals from the two MWPPACs, one located after the target and the other at the focal plane (flight path ~7.5 m). The parameters measured at the focal plane [(x,y), ΔE, Er, TOF] along with the known magnetic field were used to determine, on an event-by-event basis, the mass number (A), charge state (q), atomic number (Z), and velocity vector (v) after the reaction for the detected fragment. Isotopic identifications of elements were made up to Z=63 with a mass resolution of ΔA/A~0.4% [13]. The prompt γ rays were measured in coincidence with the isotopically-identified fragments, using the EXOGAM array [14] consisting of 11 Compton-suppressed segmented clover HpGe detectors (15 cm from the target). The velocity of the fragment along with the angle of the segment of the relevant

clover detector were used to obtain the γ-ray energy in the rest frame of the emitting fragment.

The $^{238}U + ^{9}Be$ induced fission data are used to identify the transitions in ^{100}Y, $^{144-153}Pr$, $^{156,157}Pm$ in the current work. These data have lower statistics than ^{252}Cf SF but have full mass and Z identification of the fragments.

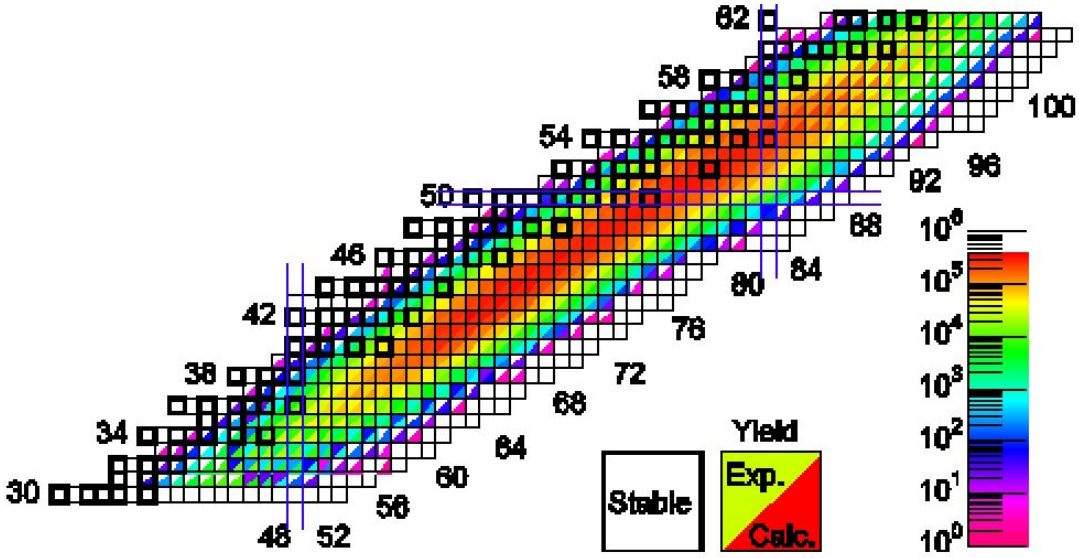

Figure 3. 2. 1. Yield of $^{238}U + ^{9}Be$ induced fission fragments [15].

CHAPTER 4

RESULTS

4.1 New Transitions and Levels in ^{96,100}Y

^{96}Y

The level scheme of ^{96}Y is shown in Fig. 4. 1. 1. Levels and transitions labeled in black were previously reported in ^{96}Sr β decay work [16] with spin and parity assignments. The ground state, 122.3, 652.3 and 931.7 keV state were tentatively assigned to $(\pi 2p_{1/2})(\upsilon 3s_{1/2})$, $(\pi 2p_{1/2})(\upsilon 3s_{1/2})$, $(\pi 2p_{1/2})(\upsilon 2d_{3/2})$ and $(\pi 1g_{9/2})(\upsilon 1g_{7/2})$

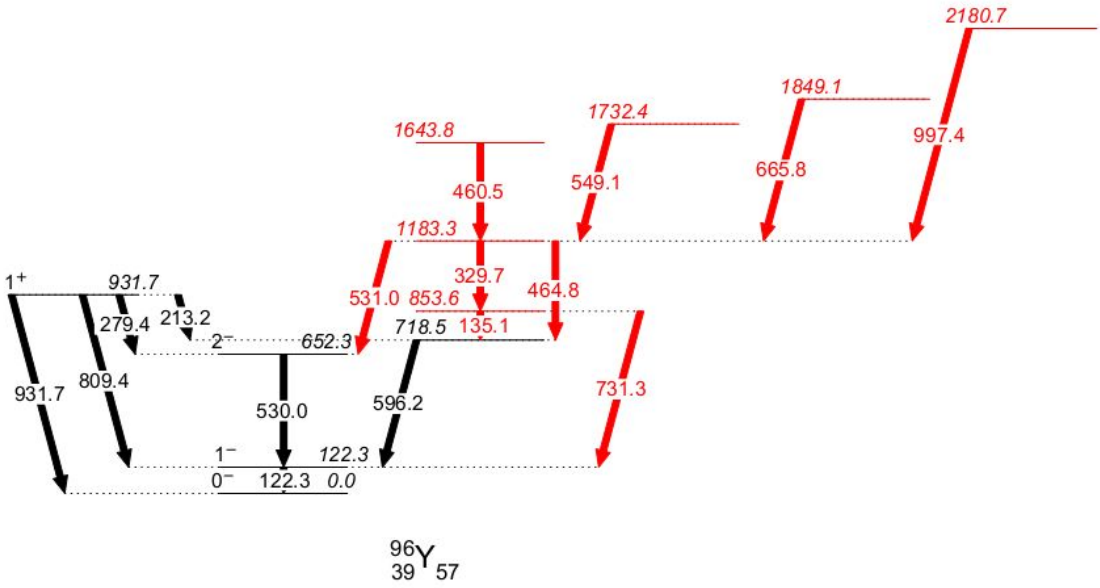

Figure 4. 1. 1. Level scheme of ^{96}Y obtained in the current work. New transitions and levels are labeled in red. Some levels and transitions from β decay to ^{96}Y are not placed.

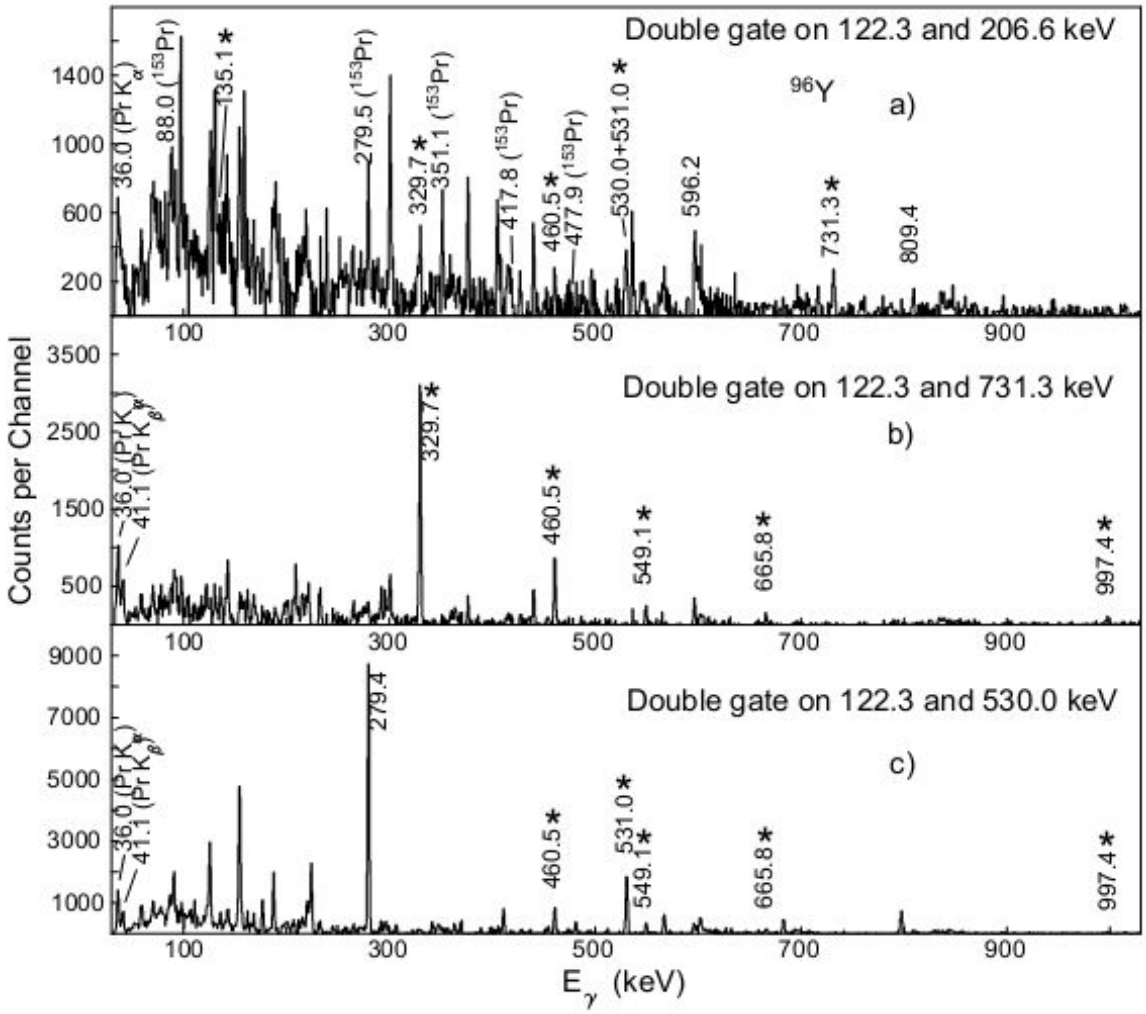

Figure 4. 1. 2. Partial γ ray coincidence spectrum by a) double gating on the known 122.3 keV transition in ^{96}Y and 206.6 keV transition in the ^{153}Pr fission partner, b) double gating on 122.3 and 731.3 keV transitions in ^{96}Y and c) double gating on 122.3 and 530.0 keV transitions in ^{96}Y. New transitions are labeled with asterisks.

configurations, respectively. The 718.5 keV level was assigned as 1^+ or 2^+ because the 213.2 keV γ ray was measured to be a M1(+E2) transition [16]. The 1287.9 and 1983.7 keV levels reported in Ref. [16] and the correlated transitions are not included in the level scheme. Although these transitions can be observed in the ^{252}Cf SF data, as discussed later, they are proposed to originate from the β decay of the ^{96}Sr ^{252}Cf fission fragment.

Fig. 4. 1. 2 a) shows a double gate on the 122.3 keV known transition in ^{96}Y and the 206.6 keV known transition in ^{153}Pr (3n fission partner). In this gate, the previously known 530.0, 596.2 and 809.4 keV transitions and the 135.1, 329.7, 460.5, 531.0 and 731.3 keV new transitions can be seen. The 596.2 keV transition is stronger than the 530.0 and 809.4 keV ones. Note that the relative intensity of the 809.4 keV transition was 94.0 compared to 1.2 of the 596.2 one reported in Ref. [16]. Therefore, the 931.7 keV level is strongly populated and the 718.5 keV one is weakly populated in ^{96}Sr β decay. In the contrast, the 718.5 keV level is strongly populated in the current ^{252}Cf SF work. Fig. 4. 1. 2 b) shows a γ ray coincidence spectrum by double gating on the 122.3 and 731.3 keV transitions. In this gate, the 329.7, 460.5, 549.1, 665.8, 997.4 keV new transitions can be

Table 3. The γ-ray intensities of ^{96}Y.

E_γ (keV)	Intensity	E_i (keV)	E_f (keV)
122.3		122.3	0
530.0	63 (4)	652.3	122.3
596.2	100 (5)	718.5	122.3
135.1	45 (3)	853.6	718.5
731.3	71 (5)	853.6	122.3
213.2		931.7	718.5
279.4		931.7	652.3
809.4	39 (3)	931.7	122.3
931.7		931.7	0
329.7	64 (5)	1183.3	853.6
464.8	18 (1)	1183.3	718.5
531	30 (2)	1183.3	652.3
460.5	45 (3)	1643.8	1183.3
549.1	14 (2)	1732.4	1183.3
665.8	9.1 (1)	1849.1	1183.3
997.4	8.2 (2)	2180.7	1183.3

seen. Fig. 4. 1. 2 c) shows a γ ray coincidence spectrum by double gating on the 122.3 and 530.0 keV transitions. The 460.5, 531.0, 549.1, 665.8 and 997.4 keV new transitions can be seen. The 279.4 keV transition previously reported in Ref. [16] is much stronger in this gate. The component of the 279.5 keV transition in ^{153}Pr in this peak should be small because the 206.6, 351.1 keV transitions in ^{153}Pr are weak in this gate.

The γ ray relative intensities are listed in Table 3 and normalized to the 596.2 keV γ transition. Note that in Ref. [16], the intensity ratio between the 279.4 and 809.4 keV transitions was reported as 10.8/94.0. By using this branching ratio, the estimated intensity of the 279.4 keV transition in the current work is 4.5, which is 15% of the 531.0 keV one. This result is in contradiction with the intensity ratio shown in the 122.3 - 530.0 keV double gate in Fig. 4. 1. 2 c). Thus, a major portion but not all of the 279.4 keV peak in Fig. 4. 1. 2 c) may come from the beta decay of the ^{96}Sr fragment to ^{96}Y.

^{100}Y

The level scheme of ^{100}Y is shown in Fig. 4. 1. 3. The ground state of ^{100}Y was assigned as 1^- or 2^- in β decay work [17]. A $1+ \pi 5/2[422] \otimes \upsilon 3/2[411]$ band was reported in Ref. [17, 18]. In the current work, this band (1) has been extended up to 10^+ with three new transitions and levels. The new bands (2), (3), (4) identified in the present work could decay to the ground state or a 145 keV 4^+ 0.94s isomeric state reported in Ref. [19-21]. Fig. 4. 1. 4 shows a Mass- and Z- gated spectrum on ^{100}Y from ^{238}U+^{9}Be induced fission work. In this spectrum ,the previously reported transitions in band (1) and new transitions in bands (2) and (3) can be clearly seen. The 125.0, 230.3, 310.8 keV transitions are not identified in the ^{252}Cf SF data so that they are not placed in the level

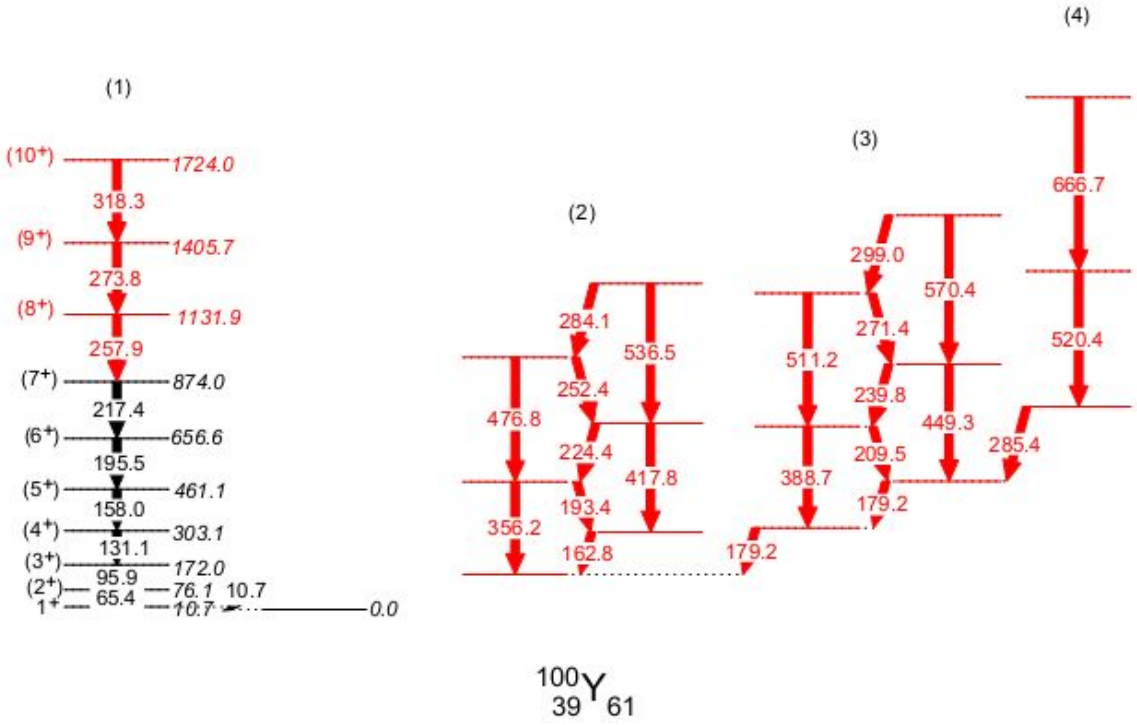

Figure 4. 1. 3. Level scheme of ^{100}Y obtained in the current work. New transitions and levels are labeled in red.

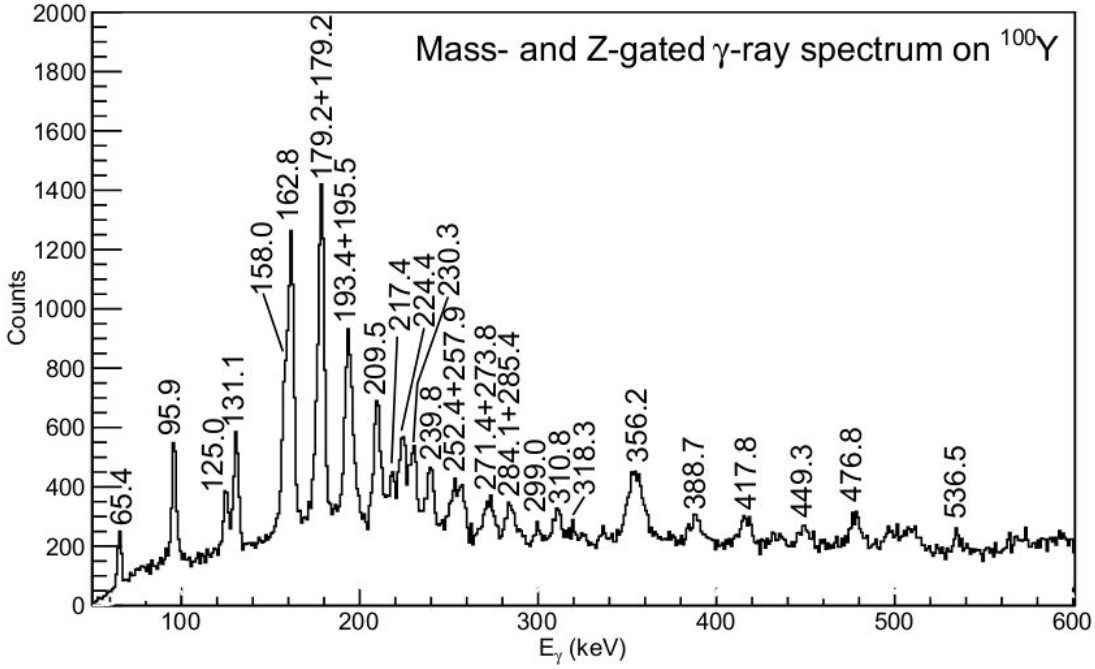

Figure 4. 1. 4. Mass- and Z- gated spectrum on ^{100}Y in ^{238}U+^{9}Be data.

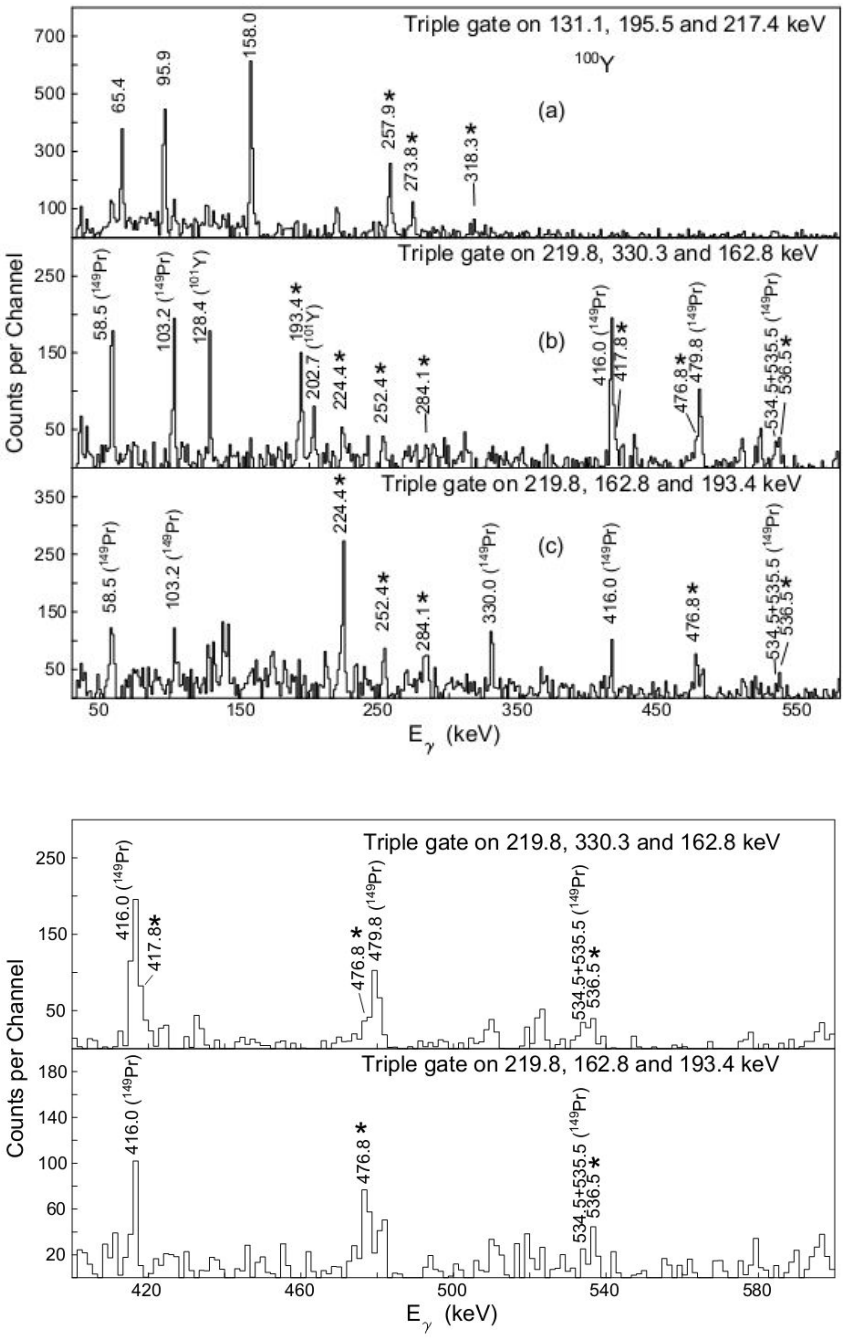

Figure 4. 1. 5. Partial γ ray coincidence spectra by a) triple gating on 131.1, 195.5 and 217.4 keV transitions in ^{100}Y, b) triple gating on 219.8 and 330.3 keV transitions in ^{149}Pr and 162.8 keV transition in ^{100}Y and c) triple gating on 219.8 keV transition in ^{149}Pr and 193.4 keV transitions in ^{100}Y. Note that ^{101}Y has a 163.3 keV transition to bring contamination transitions in part b). The enlarged part of b) and c) are shown in the lower figure. Transitions with * are new.

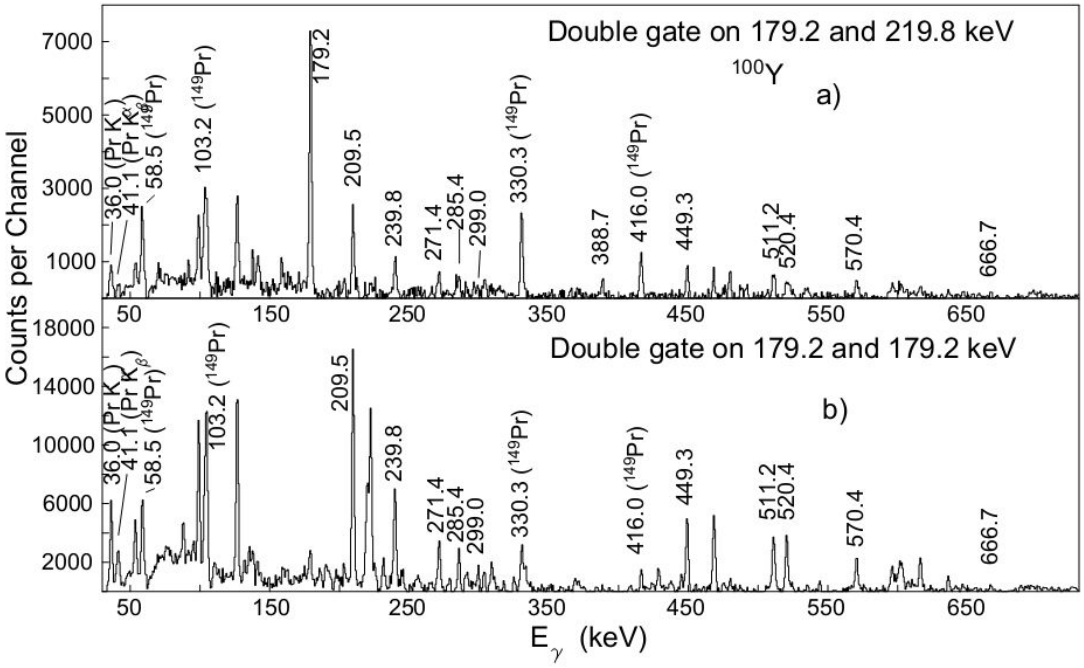

Figure 4. 1. 6. Partial γ ray coincidence spectra by a) double gating on 179.2 keV transition in ^{100}Y and 219.8 keV transition in ^{149}Pr and b) double gating on 179.2 and 179.2 keV transitions in ^{100}Y. All the labeled ^{100}Y transitions are new.

scheme. The 125.0 keV peak may come from the 125.3 keV transition in ^{99}Y. However, since the 128.4 keV transition in ^{101}Y, the 287.2 keV transition in ^{100}Sr, the 212.6 keV transition in ^{100}Zr are not clearly seen, this spectrum is clean to Z and higher mass gate. Note that the transitions in band (2) are identical to a band reported in ^{102}Nb. Since the intensities of the transitions leaking through ΔM=2 gates should be very small and no such leakage is seen in any other A/Z gated spectra in this thesis, the transitions in band (2) in the ^{100}Y mass- and Z- gated spectrum belong to ^{100}Y rather than ^{102}Nb.

Fig. 4. 1. 5 a) shows a γ ray coincidence spectrum by triple gating on three known transitions in band (1). The 257.9, 273.8 and 318.3 keV new transitions in band (1) can be seen. Fig. 4. 1. 5 b) shows a γ ray coincidence spectrum by gating on two transitions in the strongly populated 3n fission partner ^{149}Pr and the strong 162.8 keV transition

identified in the mass/Z gated spectrum in Fig. 4. 1. 4. Despite the contamination transitions in ^{101}Y (the 2n partner of ^{149}Pr), which originate from the 163.3 keV transition in ^{101}Y, the 193.4, 224.4, 252.4, 284.1 keV new transitions identified in the mass/Z gated ^{100}Y spectrum are clearly seen. The 224.4, 252.4, 284.1 and 476.8 keV transitions in band (2) are also seen in the coincidence spectrum gating on a strong transition in ^{149}Pr and the 162.8 and 193.3 keV transitions in Fig. 4. 1. 5 c). These coincidence spectra from ^{252}Cf SF further confirms that the somewhat broadened peak around 160 keV in Fig. 4. 1. 4 contains two components of 158 and 162 keV. Fig. 4. 1. 6 a) shows a γ ray coincidence spectrum by double gating on a strong transition in band (3) of ^{100}Y and a ^{149}Pr fission partner transition. All the correlated transitions in band (3) and band (4) can be seen. These transitions are also confirmed in the 179.2 and 179.2 keV double coincidence spectrum in Fig. 4. 1. 6 b). The ^{252}Cf SF data show some weak evidence that the 230 and 311 keV transitions seen in the mass/Z gated ^{100}Y spectrum might feed a 99.2 keV level reported previously in β decay. More work is needed to confirm these transitions.

Band (1) was assigned to a pairing free band with 1+ $\pi 5/2[522] \otimes \upsilon 3/2[411]$ configuration [17, 18]. The neutron pairing gap and proton pairing gap of this state are almost zero, which result in the moments of inertia very close to a rigid body one (Fig. 4. 1. 7).

Experimental measurements on Z=36-40 isotopes revealed a sudden onset of deformation at N≈60. For yttrium isotopes, deformation was small for N=48-58 and shape coexistence was reported for N=59 [21]. Then, the deformation suddenly changed to a higher one ($\beta_2 \sim 0.4$) for N=60, 62 with almost no triaxiality. Cheal *et al.* reported a tentative spin 3 for the ground state of ^{100}Y with 0.39(4) β_2 deformation from laser

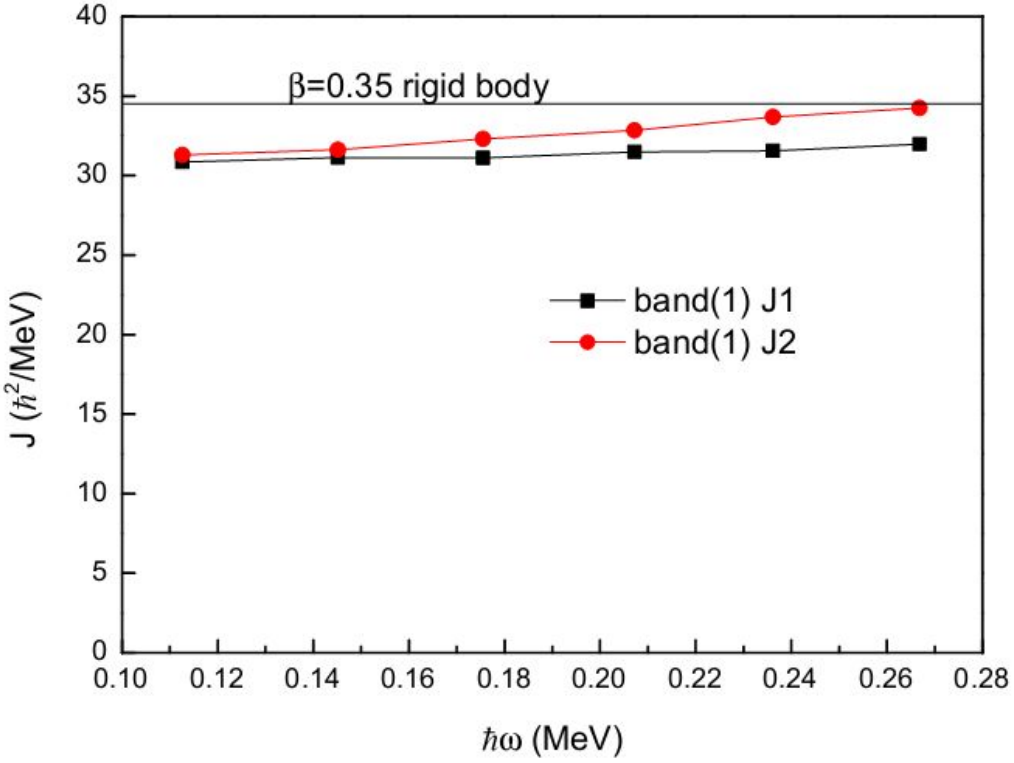

Figure 4. 1. 7. Moments of inertia of band (1) in ^{100}Y.

spectroscopy work [22]. Baczynska *et al.* reassigned this state as a 0.35(4) β_2 deformation, spin 4 isomeric state by using a similar experimental approach [21]. Probable 4^+ π5/2[422] $\otimes$ υ3/2[411] configuration was suggested from comparison of g factors between experiment and theory [21]. Similar and regular energy spacing with no signature splitting in bands (2) and (3) indicate a large rigid deformation, which is consistent with systematics. The new bands (2), (3), (4) may decay to the 1^-, 2^- ground state or this 145keV 4^+ isomer. If the band-head of band (2) is the 145 keV isomer and band (3) also decays to this state, the configuration of these bands would be 4^+ π5/2[422] $\otimes$ υ3/2[411] and 5^+ π5/2[422] $\otimes$ υ5/2[413] respectively. Band heads of (2) and (3) would form a π5/2[422] $\otimes$ υ[312 5/2,3/2] neutron pseudospin doublet. Bands (2) and (3) would also

become pairing free bands. However, more theoretical work on the energy levels and B(M1)/B(E2) branching ratios in bands (2) and (3) are needed to test and verify this proposal.

4.2 New Transitions and Levels in ^{107}Nb

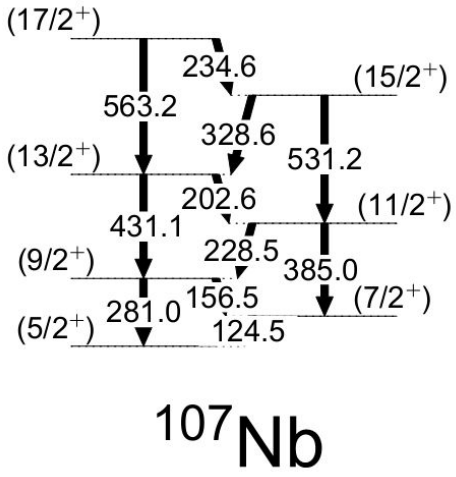

Figure 4. 2. 1. The level scheme of ^{107}Nb.

The level scheme of ^{107}Nb is shown in Fig. 4. 2. 1. The $5/2^+$ state could be the ground state of $\pi 5/2[422]$ from the systematic comparison of neighboring ^{101,103,105}Nb. No level

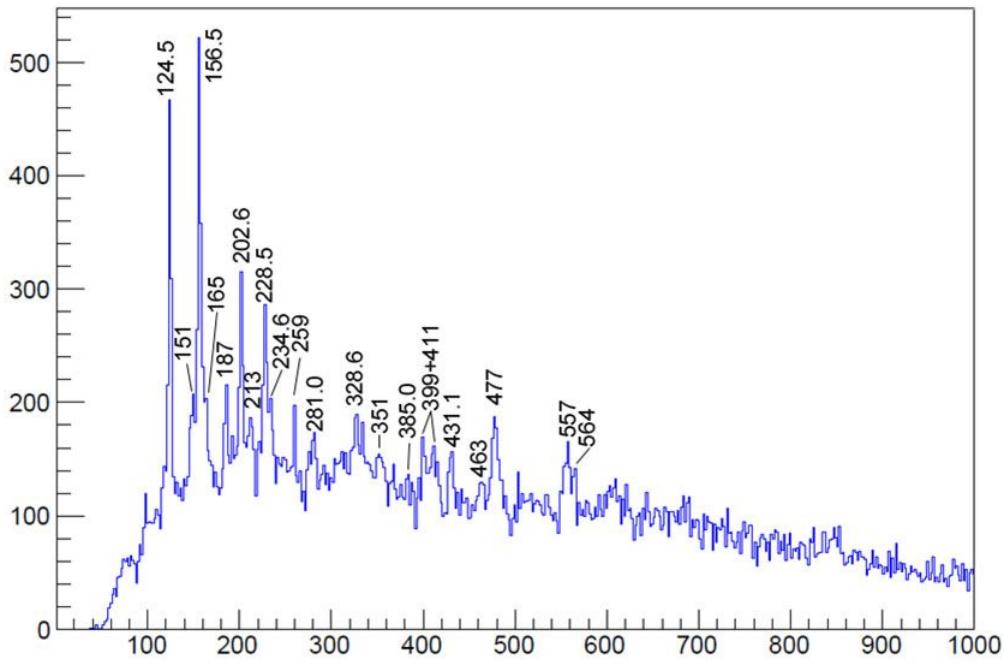

Figure 4. 2. 2. Mass- and Z- gated spectrum on ^{107}Nb from ^{238}U + ^{9}Be experiment [15].

scheme was established previously, so all the transitions are newly identified. These transitions are seen in the ^{107}Nb mass/Z gated spectrum with 2 keV per channel from ^{238}U + ^{9}Be induced fission data in Fig. 4. 2. 2. Since the strong 138, 145 keV transitions in ^{107}Mo are not clearly seen in Fig. 4. 2. 2, this spectrum is clean to a higher Z gate. The 124.5 and 156.5 keV transitions, 202.6 and 228.5 keV transitions are almost equal in intensity respectively in this figure, which may indicate an alternating B(M1)/B(E2) branching ratio in this band. The 151, 187 keV transitions labeled in the spectrum could be the members of a π5/2[303] band. The 119 (on left shoulder of 124.5), and 165 keV transitions could be the members of a π5/2[301] band. The ^{252}Cf SF data show some weak evidence for those speculations. The 477, 557 keV peaks are relatively strong and could be E2 transitions decaying from a 1γ vibrational band to the ground state band or from a 2γ band to the 1γ band. Note that both 1γ and 2γ vibrational bands were reported

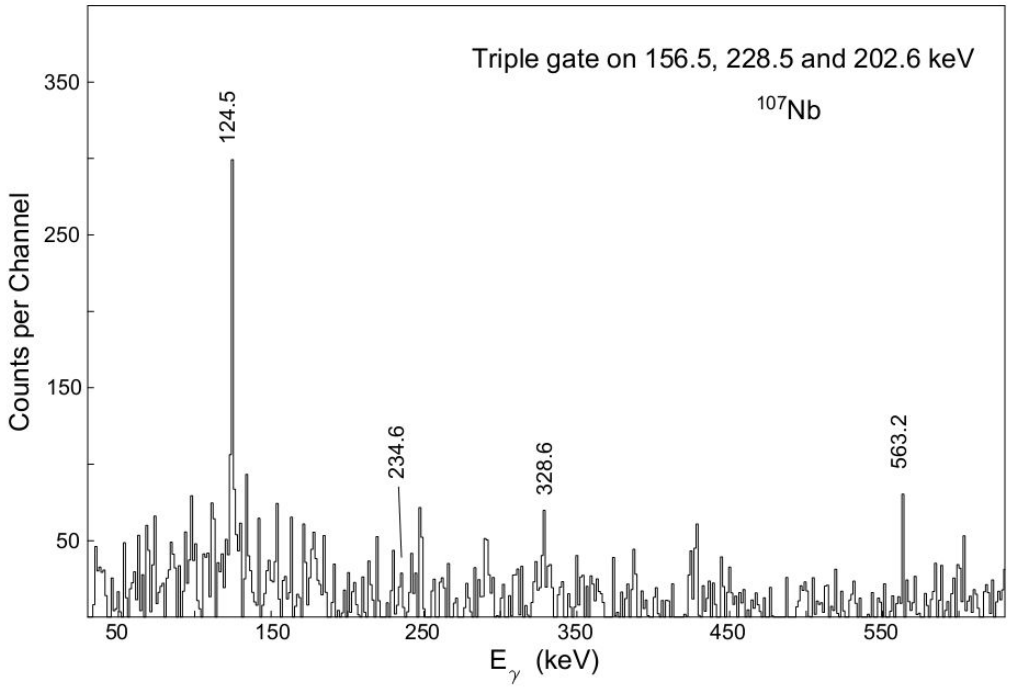

Figure 4. 2. 3. Partial γ coincidence spectrum by triple gating on the 156.5, 228.5 and 202.6 keV transitions in ^{107}Nb.

in $^{103, 105}$Nb [23, 24] and some other Mo, Tc, Ru nuclei previously [25-37]. Some other peaks not included in the level scheme are also labeled in this ^{107}Nb mass/Z gated spectrum.

Fig. 4. 2. 3 shows a γ ray coincidence spectrum gating on the 156.5, 228.5, 202.6 keV transitions. In this spectrum, the 124.5, 328.6 and 563.2 keV transitions can be clearly seen. The 234.6 keV transition is relatively weak. This transition is confirmed in the 124.5, 228.5 and 202.6 keV triple gate. More work on ^{252}Cf SF and ^{238}U + ^{9}Be data, especially for the ^{141}La fission partner, is needed to identify the coincidence of the weak transitions in Fig. 4. 2. 2.

In the A≈100 region, a shape transition from axially symmetric deformed Y nuclei to triaxial deformed Tc and Rh isotones occurs. Luo *et al.* reported this phenomenon in N=60, 62, 64 nuclei [38]. Theoretical calculations showed medium γ values (~15°) for

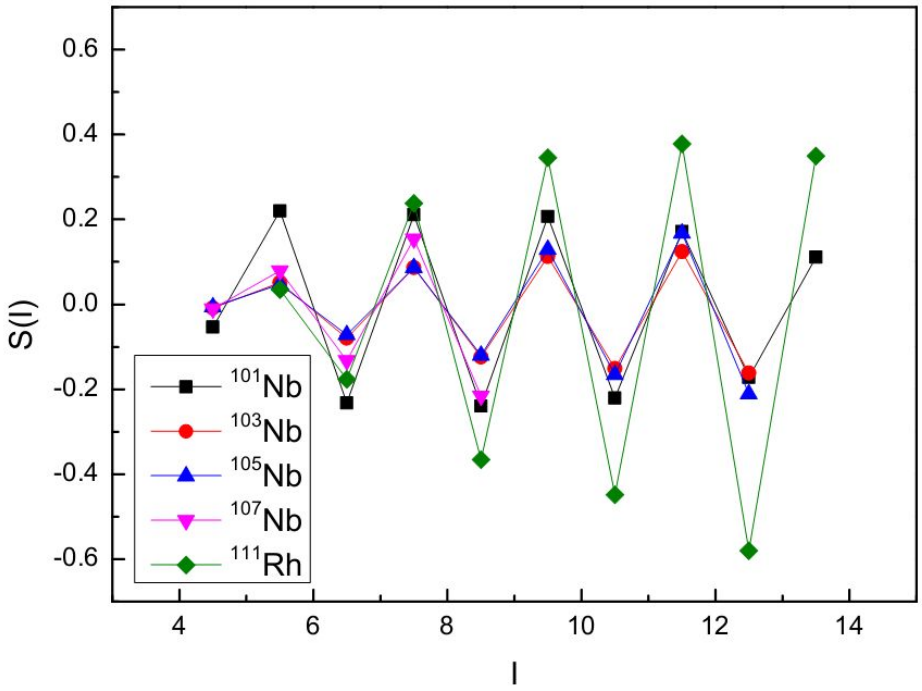

Figure 4. 2. 4. Signature splitting in ground state bands of ^{101,103,105,107}Nb and ^{111}Rh with data from Ref. [23, 24, 38, 39] and the current work.

these Nb nuclei [24,38]. The current work of ^{107}Nb, as discussed later, implies that N=66 nuclei also follow this trend.

Fig. 4. 2. 4 shows the signature splitting S(I) comparison of ^{107}Nb with the neighboring nuclei. S(I) was calculated by the same equation used in Ref. [38].

$$S(I) = \frac{E(I) - E(I-1)}{E(I) - E(I-2)} \frac{I(I+1) - (I-2)(I-1)}{I(I+1) - (I-1)I} - 1$$

S(I) values of ^{101,103,105,107}Nb are similar and apparently smaller than ^{111}Rh. This observation indicates that the triaxiality among Nb nuclei are similar but smaller than that in Rh nuclei. For Nb isotopes, S(I) decreases somewhat as N increases for ^{101,103,105}Nb. Nevertheless , S(I) for ^{107}Nb is larger than in $^{103, 105}$Nb and smaller than ^{101}Nb. This phenomenon might be related to the evolution of the gamma softness.

4.3 Oblate Deformation and signature splitting in ^{118,119}Ag

Signature quantum numbers (r and α) are used to describe the rotational invariance along the x axis. Historically, this number was first introduced in Cranked Shell Model calculation (CSM). In CSM, the Hamiltonian is expressed as

$$h(\omega) = h_0 - \hbar\omega j_x$$

When ω≠0, h does not commute with j_z. But h is invariant when rotating 180 degree along the x axis. The corresponding operator $R_x = e^{-i\pi J_x}$ is a good quantum number.

The R_x has eigenvalues r=±i for a fermion wave function and r=±1 for a boson wave function. The α is defined as

$$r = e^{-i\pi\alpha}$$

where r and α are called signature quantum numbers. A rotational band with ΔI=1 can be classified by α into two rotation sets [40]. For even A nuclei,

$$r = 1\ (\alpha = 0),\ I = 0, 2, 4, \cdots$$

$$r = -1\ (\alpha = 1),\ I = 1, 3, 5, \cdots$$

For odd A nuclei,

$$r = -i\ (\alpha = 1/2),\ I = 1/2, 5/2, 9/2, \cdots$$

$$r = i\ (\alpha = -1/2),\ I = 3/2, 7/2, 11/2, \cdots$$

Furthermore, these two sets are defined as a favored band and an unfavored band. For odd-A nuclei,

$$\alpha_f = \frac{1}{2}(-1)^{j-1/2},\ (I = j + even)$$

$$\alpha_u = \frac{1}{2}(-1)^{j+1/2},\ (I = j + odd)$$

j denotes the orbital angular momentum of the valence nucleon. For odd-odd nuclei,

$$\alpha_f = \frac{1}{2}(-1)^{j_p - 1/2} + \frac{1}{2}(-1)^{j_n - 1/2}$$

The energy spacing between these two bands are called the signature splitting energy. If the favored branch energy is lower than the unfavored branch, the phenomenon is called common signature splitting. However, if the favored branch energy is higher than the unfavored branch, the phenomenon is call signature inversion.

^{118}Ag

The level scheme obtained in the current work is shown in Fig. 4. 3. 1. All the

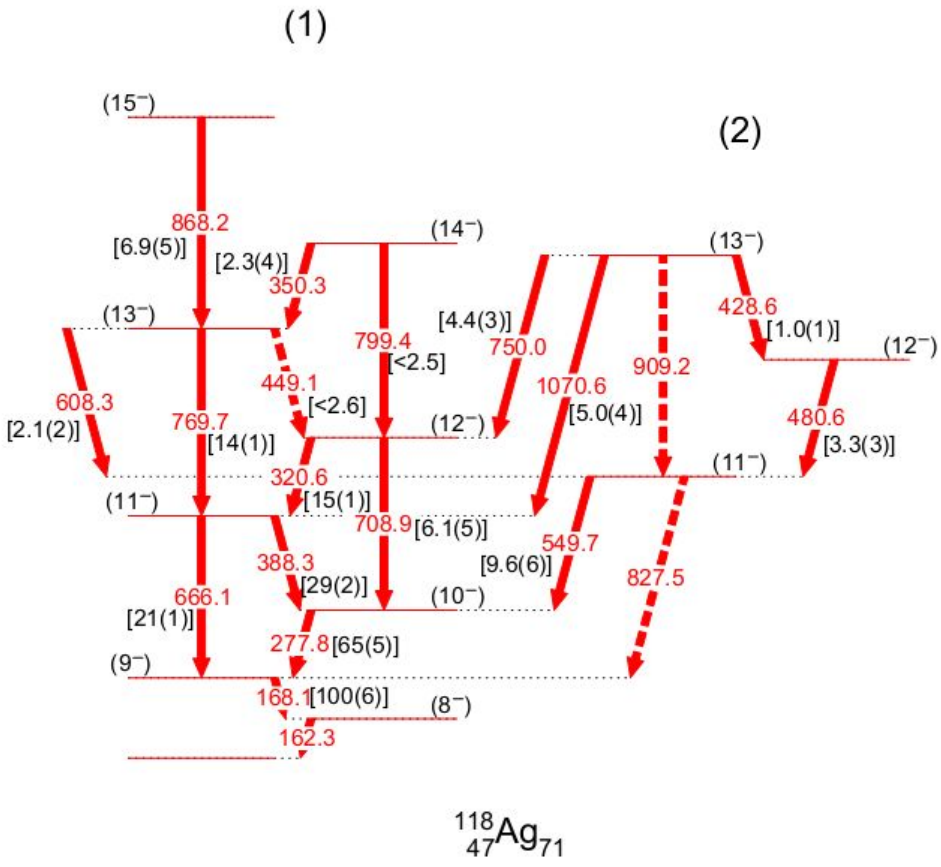

Figure 4. 3. 1. Level scheme of ^{118}Ag obtained in the current work. The γ-ray intensities are given in brackets.

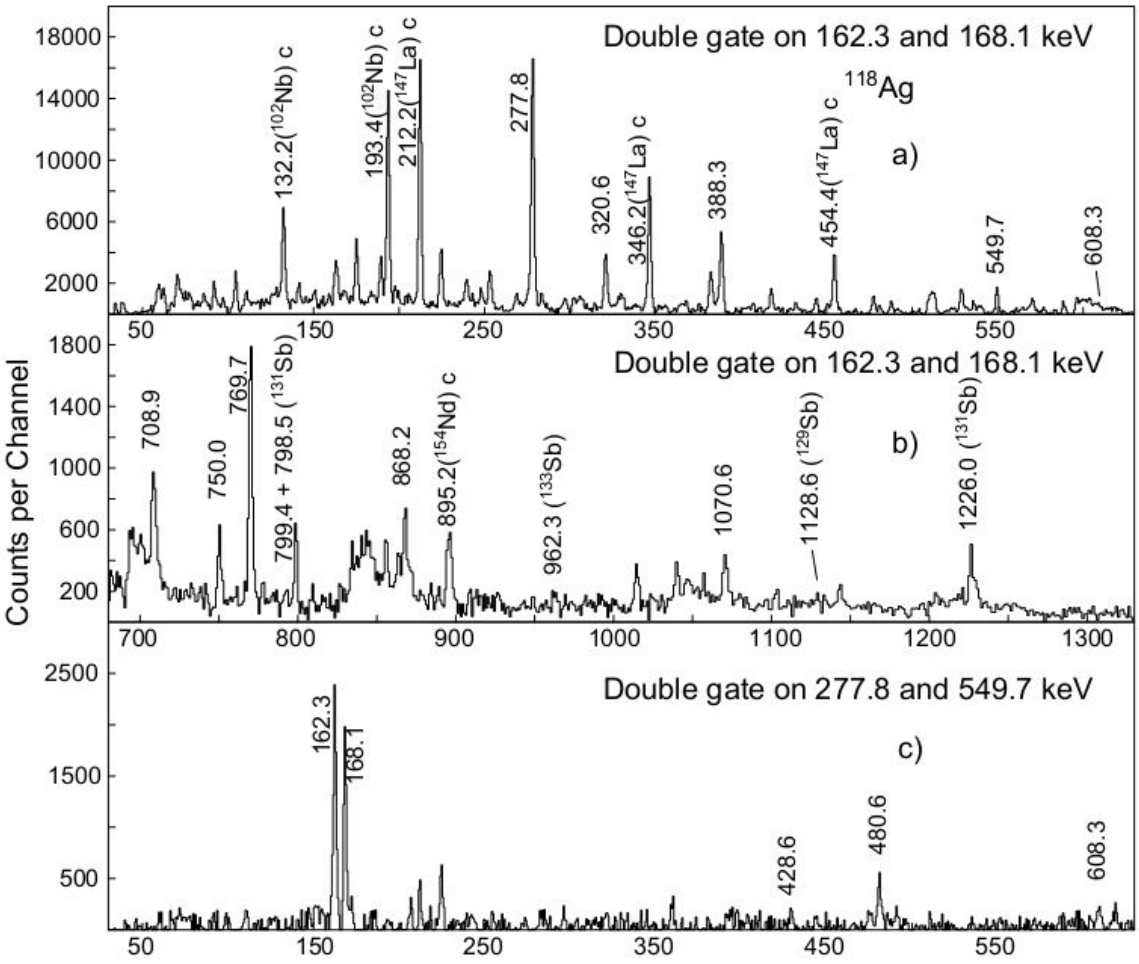

Figure 4. 3. 2. Partial γ coincidence spectra by a) double gating on 162.3 and 168.1 keV transition to show the low energy region, b) double gating on 162.3 and 168,1 keV to show the high energy region, and c) double gating on 277.8 and 549.7 keV to show low energy region.

transitions are newly identified. Spins and parities are tentatively assigned according to the similarity to ^{114,116}Ag nuclei. Some of the β decay work of ^{118}Pd and ^{118}Ag assigned $1^{(-)}$ for the ^{118}Ag ground state and $4^{(+)}$ for a 127.6 keV, 2.0 s isomer [41, 42], while others proposed $(2)^-$ for the ground state and $(5)^+$ for the 127.6 keV isomer [43]. Thus, it is more probable that the whole level scheme decays to the 127.6 keV isomer or to some other isomer. The level scheme seems to form two band structures (yrast and yrare). The E2

transition intensities of the odd spin are much stronger than the even spin ones, which may indicate an alternating B(M1)/B(E2) branching ratio.

Fig. 4. 3. 2 a) shows a γ coincidence spectrum in the low energy region gated on the 162.3 and 168.1 keV transitions. The 277.8, 320.8, 388.3, 549.7 and 608.3 keV correlated transitions in ^{118}Ag can be seen. The strong contamination transitions unlabeled in this spectrum mainly come from ^{102}Nb and ^{147}La because of the 162.8 keV transition reported in ^{102}Nb [18], and the coincidence 167.7 keV transition decaying from the 167.7 keV level to the ground state in its fission partner ^{147}La. Fig. 4. 3. 2 b) shows the high energy region of the same gate. The 708.9, 750.0, 769.7, 799.4, 868.2 and 1070.6 keV correlated transitions can be seen. The ^{129,131,133}Sb fission partner transitions are also seen. The strongest partner intensities are for ^{131}Sb to indicate that these cascades belong to ^{117}Ag or ^{118}Ag. Further analysis about mass assignment will be discussed later. Fig. 4. 3. 2 c) shows the low energy region of γ ray spectrum gating on the 277.8 and 549.7 keV transitions. The 162.3, 168.1, 428.6, 480.6 and 608.3 keV transitions can be seen.

^{119}Ag

The level scheme of ^{119}Ag is shown in Fig. 4. 3. 3. All the transitions are newly identified except for the 130.0 keV transition reported in ^{119}Pd β decay work [44]. In Ref. [44], Penttila *et al.* reported isomers with tentative $1/2^-$ and $7/2^+$ spin and parity assignments. A 507.2 keV transition was also identified in Ref. [44] to be weakly in coincidence with the 130.0 keV transition. This 507.2 keV transition is proposed to decay from a $11/2^+$ level to a $9/2^+$ one within the current work. The 689.4, 816.0 and 860.3 keV E2 transitions are strong in the positive parity bands in ^{119}Ag. The ^{117}Ag levels also show

this phenomenon even after the sudden onset of shrinking E2 transition energy at $21/2^+$. Therefore, the 306.0 and 338.9 keV γ rays in ^{119}Ag are tentatively assigned as E2 transitions according to the similarity to ^{117}Ag.

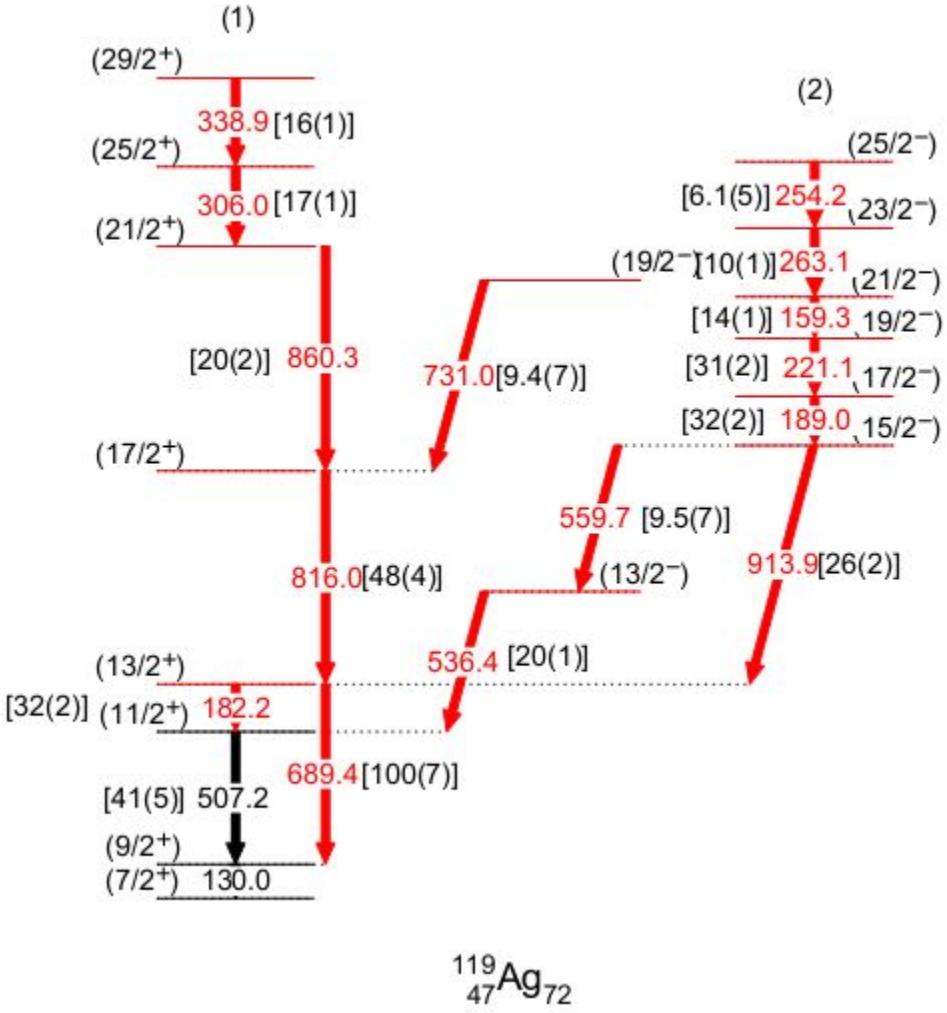

Figure 4. 3. 3. Level scheme of ^{119}Ag obtained in the current work. γ-ray intensities are also labeled with parenthesis without internal conversion correction.

Fig. 4. 3. 4 a) shows a γ ray coincidence spectrum by double gating on 130.0 and 689.4 keV. In this spectrum, the 816.0, 860.3, 306.0, and 338.9 keV transitions in band (1), the 731.0 keV transition, and all the transitions in band (2) can be seen. The intensities of the 189.0, 221.1, 159.3, 263.1, 254.2 keV transitions give their order in the high spin

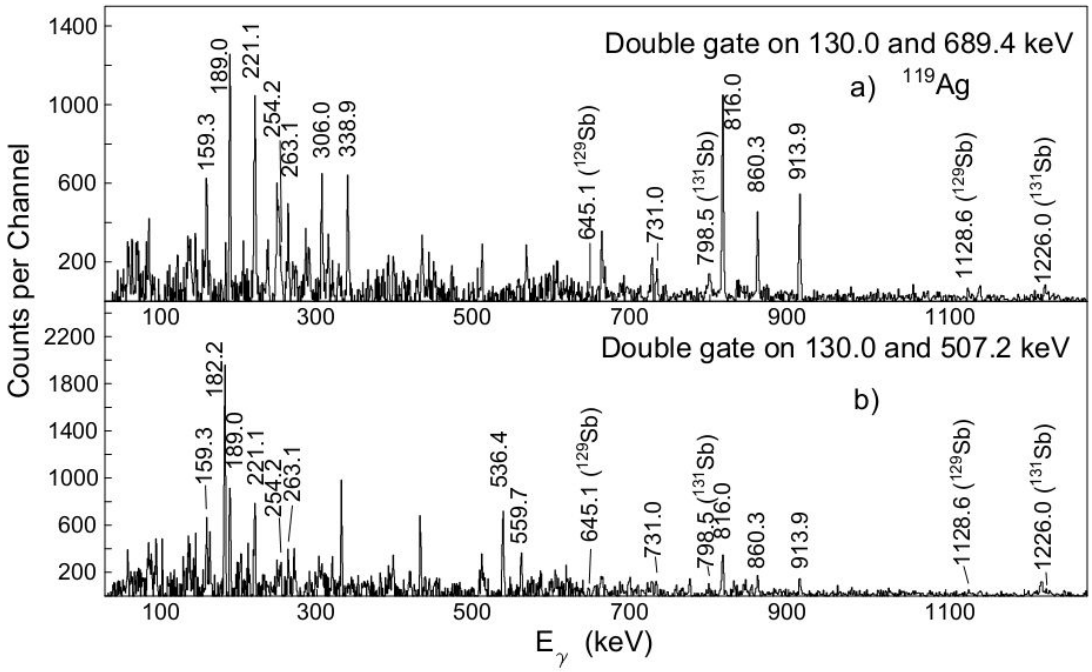

Figure 4. 3. 4. Partial γ coincidence spectra by a) double gating on 130.0 and 689.4 keV, b) double gating on 130.0 and 507.2 keV.

negative parity band. The theoretical internal conversion intensity prediction for a 159.3 keV transition in Ag isotopes is 0.12 for M1 and 0.28 for E2. Thus, these low energy transitions in the negative parity band would have an 10-30% more intensity correction. The presence of ^{129,131}Sb transitions and the absence of ^{133}Sb transitions in this spectrum confirm the current mass assignment of ^{119}Ag. Fig. 4. 3. 4 b) shows a γ ray coincidence spectrum gated on the 130.0 and 507.2 keV transitions. In this spectrum, the 182.2, 816.0, 860.3 keV transitions in the positive parity band, the 159.3, 189.0, 221.1, 254.2, 263.1 keV transitions in the negative parity band and the 536.4, 559.7, 913.9 keV interband transitions can be seen. The 330.8 and 431.4 keV peaks might be contamination transitions from ^{144}Ba. Further analysis about mass assignments will be discussed later.

Discussion

Fig. 4. 3. 5 shows the γ ray coincidence spectra gating on transitions in $^{115\text{-}119}$Ag from part a) to e). Only ^{129,131,133}Sb fission partner transitions are labeled in the spectra. Note that the 118.3-311.2 keV cascade was assigned to ^{115}Ag in ^{252}Cf SF [45] and then

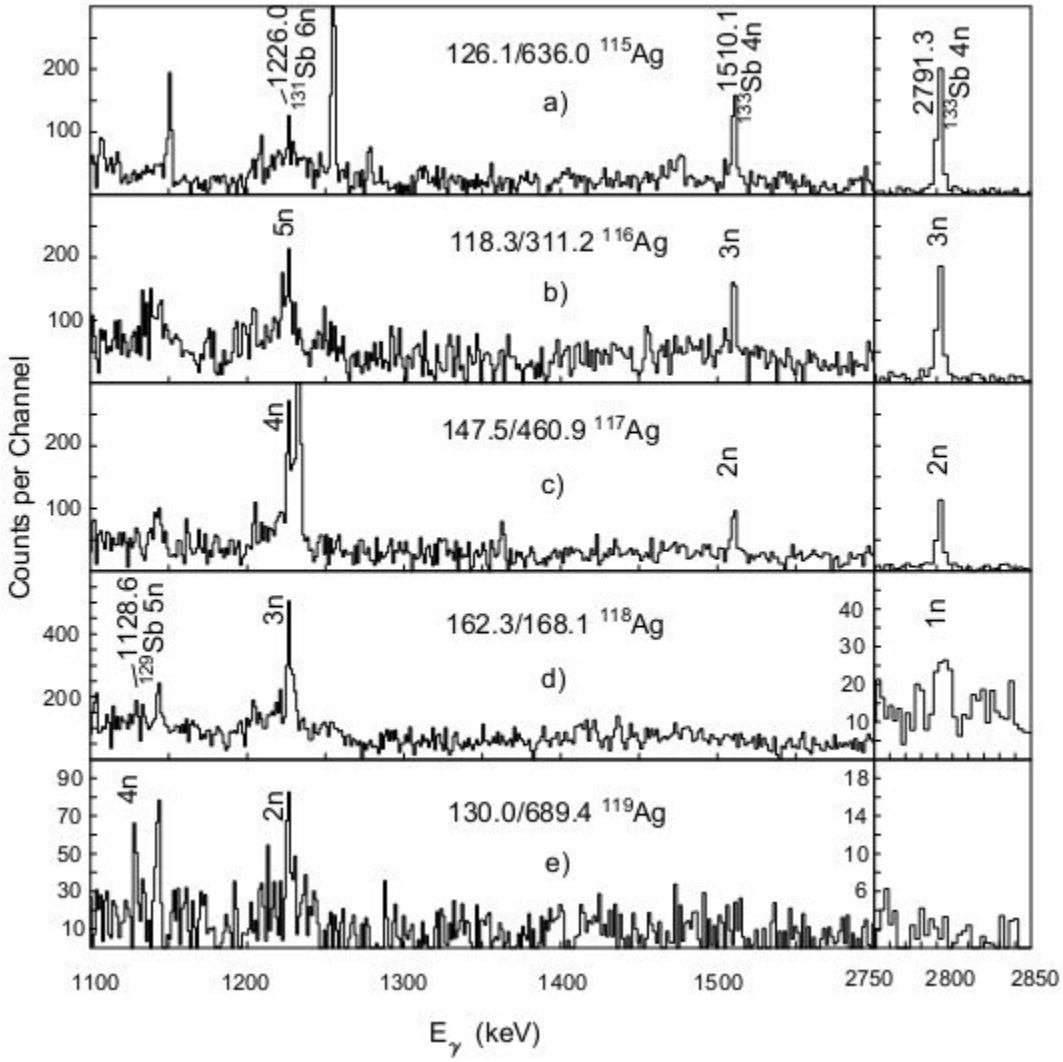

Figure 4. 3. 5. Partial γ coincidence spectra by gating on transitions from $^{115\text{-}119}$Ag. Transitions are taken from Ref. [45, 46] and the current work. The ^{129,131,133}Sb fission partner transitions are indicated with neutron evaporation numbers. Note that the count scale of the high energy regions of part d) and e) have been changed.

assigned to ^{116}Ag in ^{18}O + ^{208}Pb fusion fission work [46]. The relative intensities in the 1510.1 and 2791.3 keV transitions in ^{133}Sb transitions decrease as A increases from 115 to 118. The ^{133}Sb transitions are very weak in the ^{118}Ag transitions gate. In contrast, the intensity of the ^{131}Sb transition increases as A increases from 115 to 118. The intensity of the 1128.6 keV transitions in ^{129}Sb is much smaller than the 1226.0 keV on in ^{131}Sb in the ^{118}Ag gate in part d). In the ^{119}Ag transition gate in part e), these two transitions in ^{129,131}Ag are almost equal. Thus, these spectra give evidence for the mass assignments of ^{115,117}Ag in Ref. [45], ^{116}Ag in Ref. [46] and ^{118,119}Ag in the current work. Hwang *et al.* also reported a 223.8-178.3 keV cascade in ^{114}Ag [45]. In the present work, these two transitions are assigned to ^{133}Sb and proposed to feed the 4301.7 keV level.

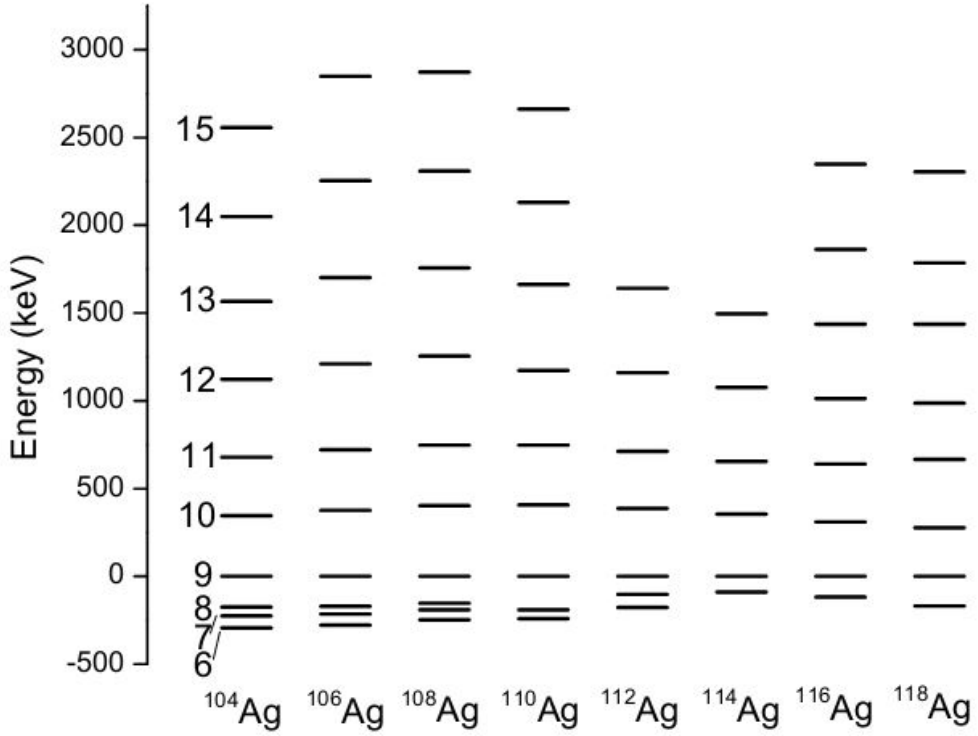

Figure 4. 3. 6. Comparison of energy levels (up to 15^-) of yrast negative parity bands in even A Ag isotopes of $^{104\text{-}118}$Ag. Level energies are normalized to the 9^- levels. [46, 47]

The levels of ^{118}Ag are similar to the yrast negative parity bands in neighboring odd-odd Ag isotopes as shown in Fig. 4. 3. 6. The energy spacing shows gradual increasing from ^{104}Ag to ^{108}Ag, decreasing from ^{108}Ag to ^{116}Ag and nearly the same in ^{116}Ag to ^{118}Ag. The smooth change supports the current spin and parity assignments. These bands in Ag isotopes were assigned to a $\pi g_{9/2} \otimes \upsilon h_{11/2}$ or $\pi g_{9/2}^{-1} \otimes \upsilon h_{11/2}$ configuration [46-52]. The shrinking $E(8^-) - E(6^-)$ energy spacing in ^{104,106,108}Ag may indicate two very low energy transitions lie between the 168.1 and 162.3 keV ones in ^{118}Ag so 6- state is not seen in 112 to 116. The interpretations of these bands have been controversial. Datta *et al.* gave a γ soft tiaxial shape for ^{104}Ag [48]. Joshi *et al.* suggested γ soft triaxial shape for the band in ^{106}Ag [49], while Lieder *et al.* proposed axially

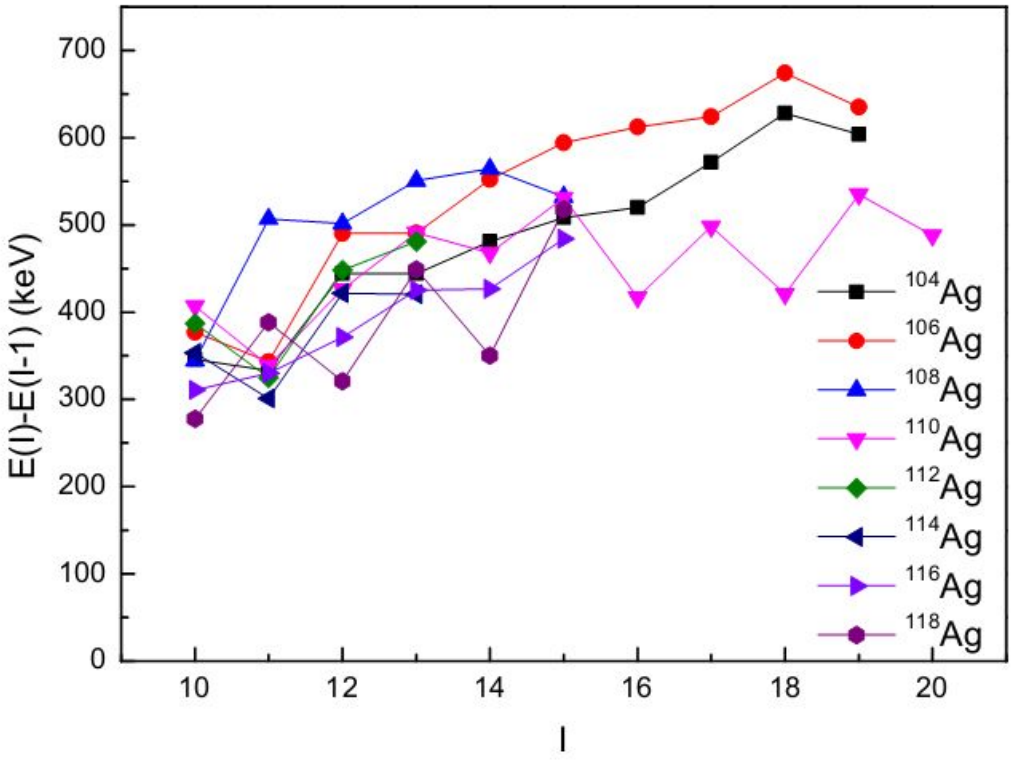

Figure 4. 3. 7. Comparison of E(I) - E(I-1) vs I of the yrast negative parity bands in even A Ag isotopes of $^{104-118}$Ag.

deformed shape (β=0.22, γ=0°) [50]. Similarly, ^{108}Ag was assigned to have an axially deformed shape (β=0.16, γ≈0°) by Liu *et al* [51]. Roy *et al.* suggested a triaxial shape (γ=20°) for ^{110}Ag [52]. The phenomena of shape evolution, signature inversion, magnetic rotation, and chiral doublet bands have been reported in the region of A<110 based on different deformations [48-51].

Fig. 4. 3. 7 shows the E(I) - E(I-1) curves in $^{104\text{-}118}$Ag nuclei. Pronounced staggering can be seen in ^{110}Ag and ^{118}Ag while the other curves are relatively smooth. Also, signature inversion occurs in ^{116}Ag. The large staggering in ^{118}Ag could be related to a change of γ values or the evolution from tilted axis rotation (TAR) to principal axis rotation (PAR). Note that PAR was presented in ^{110}Ag [52]. However, similar staggering of the B(M1)/B(E2) branching ratio has been observed in ^{118}Ag in the current work.

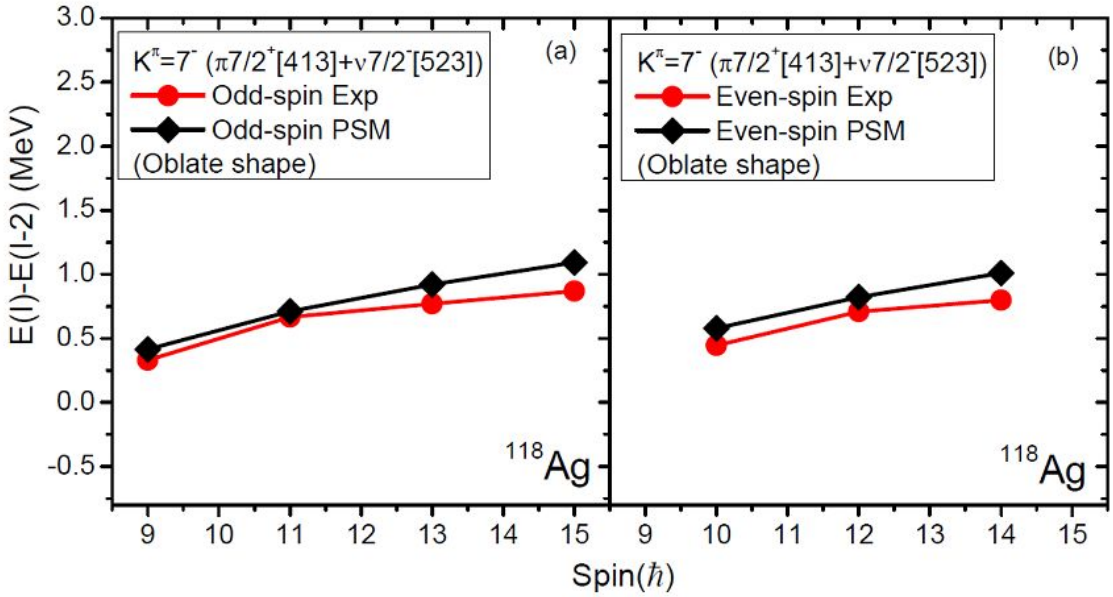

Figure 4. 3. 8. Comparison of calculated E2 transition energies with experimental data in ^{118}Ag.

A projected shell model (PSM) calculation has been carried out by Dr. Y. X. Liu for the transition energies in ^{118}Ag as shown in Fig. 4. 3. 8. PSM is especially suitable for the

nuclei with high A and large deformation. The calculation used ε_2=-0.240, ε_4=0.063 parameters. The ground state of ^{118}Ag was assumed to be 1- π1/2[301]+υ3/2[402] and the band-head of the current levels was assumed to be 7- π7/2[413]+υ7/2[523] isomer. The assumption was made according to the shape trends in the neighboring Pd isotopes. Note that shape evolution at low spins from triaxial prolate in ^{110}Pd (N=64) via triaxial oblate in ^{112}Pd (N=66) to nearly oblate in ^{114,116}Pd (N=68, 70), and then back to triaxial oblate in ^{118}Pd (N=72) was reported from TRS calculations [53]. The finite range liquid drop model also predicted oblate shapes in $^{112\text{-}119}$Ag [54]. The trend of the E2 transition energies was well reproduced by the PSM calculation. The calculation assumed the 162.3 keV transition decays from a 8^- state to a 7^- state. As discussed above, the transition energy from 8^- to 7^- is very low energy in ^{104,106,108}Ag. A turning point occurs at 11^- and 12^- for experimental data but the PSM calculation curves are smooth. Such small difference may be due to the missing of triaxiality in the calculation. However, since the

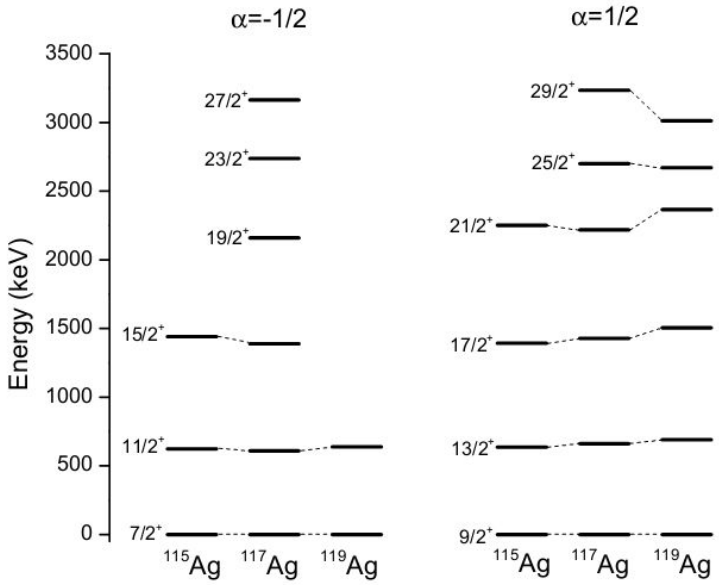

Figure 4. 3. 9. Comparison energy spacing in ^{115,117,119}Ag. Energies are normalized to the $7/2^+$, $9/2^+$ states respectively.

moments of inertia of these Ag isotopes have similar behavior, further TRS or triaxial relativistic mean field calculations are needed to give direct evidence for the speculation of an oblate shape in ^{118}Ag.

The energy levels in ^{119}Ag are similar to those in ^{115,117}Ag below the $21/2^+$ state (Fig. 4. 3. 9). The positive parity bands in ^{115,117}Ag were assigned as $\pi 7/2[413]$ [45]. The positive band in ^{119}Ag may have the same configuration. Alternatively, this band could have a $\pi g_{9/2}$ configuration if ^{119}Ag has a near spherical shape. Above the $21/2^+$ state, the energy spacings become smaller and back bending occurs for ^{117,119}Ag (see in Fig. 4. 3 .10). The back bending in ^{117,119}Ag may be due to the decoupling of a pair of protons and change of configuration because the E2 transitions are much stronger than M1. Back bending in ^{115}Ag was not observed according to the levels reported in Ref. [45]. The back bending frequency of ^{115}Ag should be larger than in ^{117,119}Ag from the trend. In ^{115,117}Ag γ

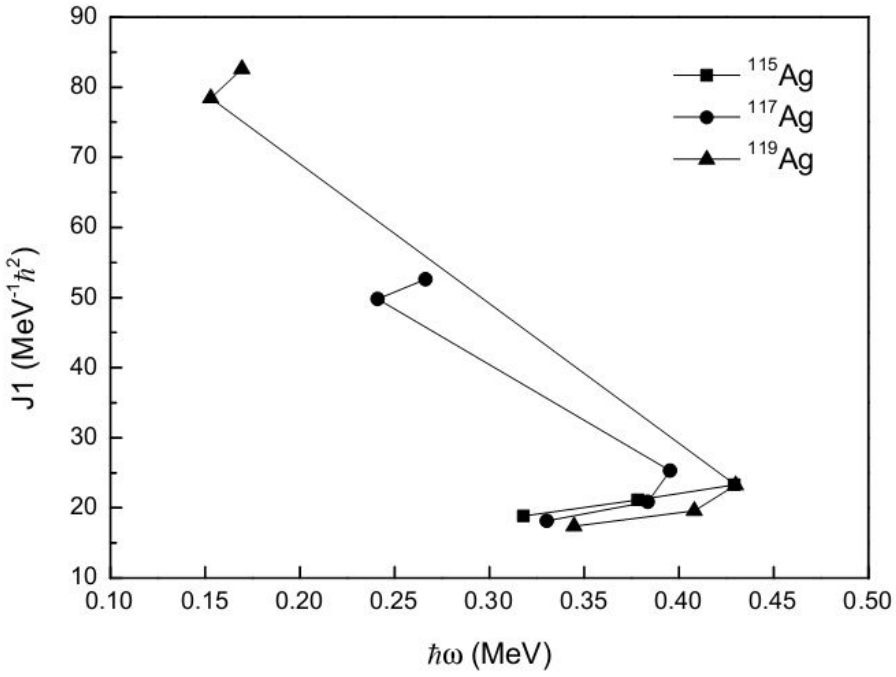

Figure 4. 3. 10. Kinematic moment of inertia of the $\alpha=1/2$ set of positive parity bands in ^{115,117,119}Ag.

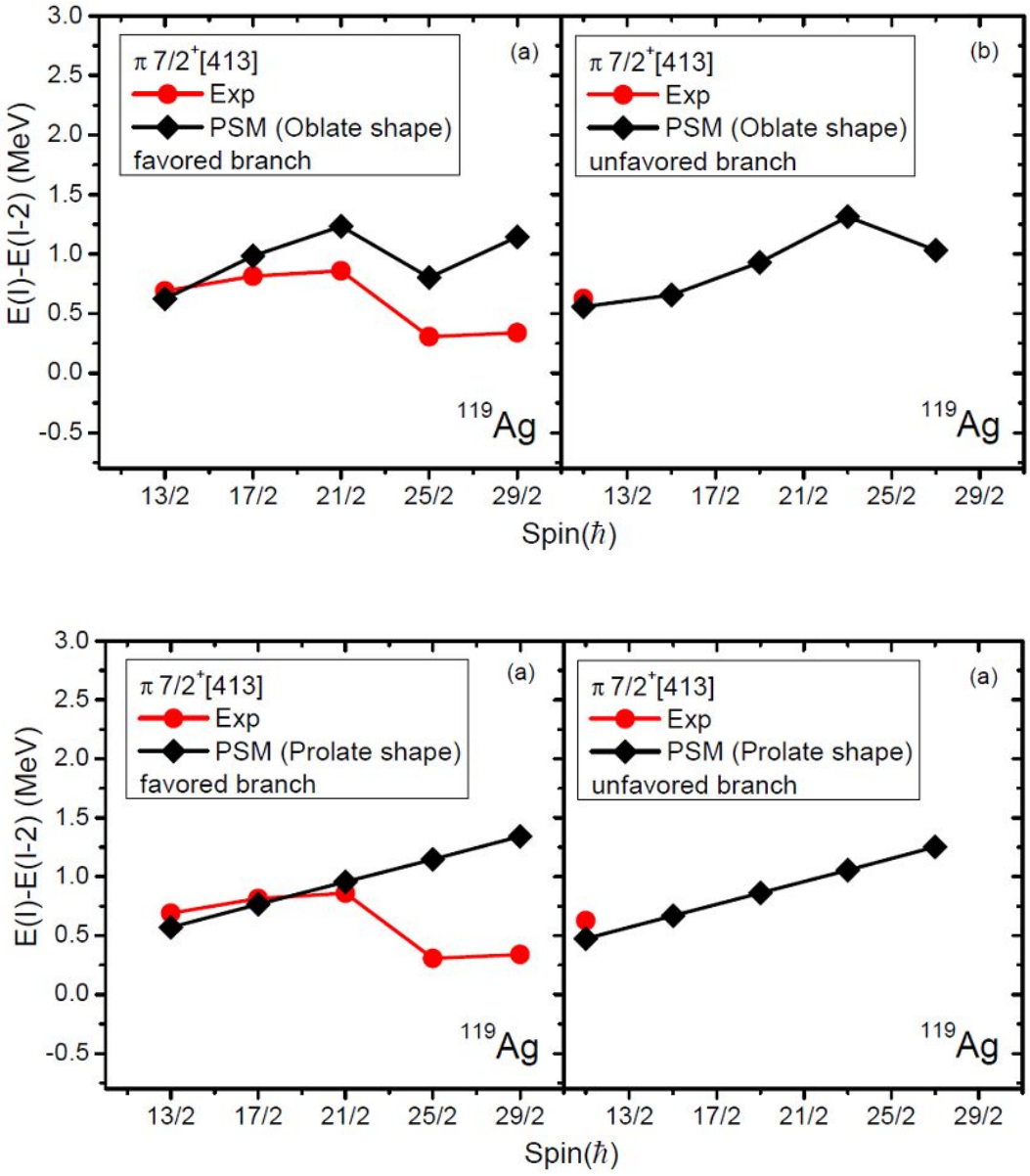

Figure 4. 3. 11. PSM calculation for the positive parity band in ^{119}Ag with oblate and prolate parameters.

soft was proposed in Ref. [45]. Signature splitting for these positive parity bands in ^{115,117,119}Ag are also similar. The signature splitting in ^{115,117}Ag were interpreted as large K mixing caused by triaxiality in the Ag isotopes in Ref. [55] and as the evolution of a

$\pi g_{9/2}^{-3}$ cluster in Refs. [56, 57].

PSM calculation has been carried out for the transition energies in ^{119}Ag as shown in Fig. 4. 3. 11. The calculations used ε_2=-0.260, ε_4=0.063 and ε_2=0.270, ε_4=0.063 parameters. The ground state of ^{119}Ag was assumed to be π1/2[301] and the new positive band was assumed to be π7/2[413]. According to the calculations, the back bending can be reproduced for oblate parameters but not for prolate parameters. This calculation shows evidence for an oblate shape in ^{119}Ag. More work on TRS calculations for the shape of ^{119}Ag is still needed.

The negative parity band in ^{119}Ag with 15/2$^-$ band-head is similar to the negative " bands C" reported in ^{115,117}Ag [45]. These bands could be magnetic rotation bands or 1 proton + 2 neutron three quasiparticle bands because of the strong M1 transitions and the unobserved E2 transitions. However, signature splitting in the negative parity bands in ^{119}Ag would weaken the evidence of magnetic rotation.

4.4 Octupole Correlation in ^{147}Ce, β and γ vibrational band in ^{148}Ce

In theory, static octupole deformation occurs when the Fermi level lies between two single particles with ΔN=1, ΔL=3, and Δj=3. The octupole coupling will give rise to parity symmetry breaking and result in a static octupole deformation. Theoretical predictions suggest such cases are located at Z or N= 34, 56, 88, 134. At Z=56 and N=88, those orbitals are $\pi d_{5/2}$, $h_{11/2}$ and $\nu f_{7/2}$, $i_{13/2}$ [58, 59].

The experimental behavior of octupole deformation is two sets of ΔI=1 levels with alternating spin and parity, and strong connecting E1 transitions. The simplex operator $S=\pi R_x^{-1}$ is introduced to describe the octupole deformation and explain the phenomenon. For even A nuclei, the eigenvalues are s=±1. The corresponding spins and parities are

$$S = 1,\ I^{\pi} = 0^{+},1^{-},2^{+},3^{-},\cdots$$

$$S = -1,\ I^{\pi} = 0^{-},1^{+},2^{-},3^{+},\cdots$$

For odd A nuclei, the eigenvalues are s=±i. The corresponding spins and parities are

$$S = i,\ I^{\pi} = \frac{1}{2}^{+},\frac{3}{2}^{-},\frac{5}{2}^{+},\frac{7}{2}^{-},\cdots$$

$$S = -i,\ I^{\pi} = \frac{1}{2}^{-},\frac{3}{2}^{+},\frac{5}{2}^{-},\frac{7}{2}^{+},\cdots$$

In odd-mass and odd-odd nuclei, another evidence of octupole deformation is pairs of states close in level energy with the same spin and opposite parity, which is called parity doublet.

The B(E1)/B(E2) reduce transition probability ratios are usually used to measure the strength of octupole deformation. This ratio is proposed to be proportional to the square of the β_3 deformation value.

$$\frac{B(E1)}{B(E2)} = .771 \frac{I_\gamma(E1)}{I_\gamma(E2)} \bullet \frac{E(E2)^5}{E(E1)^3} (10^{-6}\, fm^{-2})$$

A typical value is 10^{-6}fm^{-2}.

In more common cases, the octupole deformation is not very stable. The rotation of a octupole nucleus is coupled with vibration. The energy displacement δE between the opposite parity bands

$$\delta E = E(I^-) - \frac{1}{2}[E(I+1)^+ + E(I-1)^+]$$

and the corresponding rotational frequency ratios

$$\frac{\omega^-(I)}{\omega^+(I)} = \frac{2[E(I+1)^- - E(I-1)^-]}{[E(I+2)^+ - E(I-2)^+]}$$

can reflect the stability.

In the limit of stable octupole deformation these two values should approach zero and unity respectively. In the limit of aligned octupole vibration,

$$\frac{\omega^-(I)}{\omega^+(I)} = \frac{2I-5}{2I+1}$$

Static octupole deformation is observed around Z=56, N=88 and Z=88, N=134 regions in experiments. Small octupole deformation is also observed around Z=56 and N=56 region. In the Z=56, N=88 region, octupole correlations were reported in $^{140\text{-}146,148}$Ba, $^{144\text{-}146,148,150,152}$Ce, $^{141\text{-}143}$Cs, $^{143\text{-}145,147}$La, $^{147\text{-}150}$Nd [60-72].

The nuclear vibrational states decay to the ground state rotational band by essentially E2 radiation. For even even nuclei, energy levels can be expressed by

$$E_{n_\beta n_\gamma} = \left(n_\beta + \frac{1}{2}\right)\hbar\omega_\beta + \left(2n_\gamma + \frac{1}{2} + \frac{1}{2}|K|\right)\hbar\omega + \frac{\hbar^2}{2J}(I(I+1) - K^2)$$

This equation is suitable under the following hypotheses: the nuclear core vibrates harmonically in the γ and β directions, the vibration amplitude is small compared to the

static deformation, the moments of inertia are assumed to be equal. However, the β and γ vibrational states may mix with the ground state rotational band and result in deviations in the energies of the bands from the I(I+1) law. Furthermore, a deformed non-axial rotor, or a rotor soft to longitudinal and transverse quadrupole vibrations can also give rise to deviations.

^{147}Ce

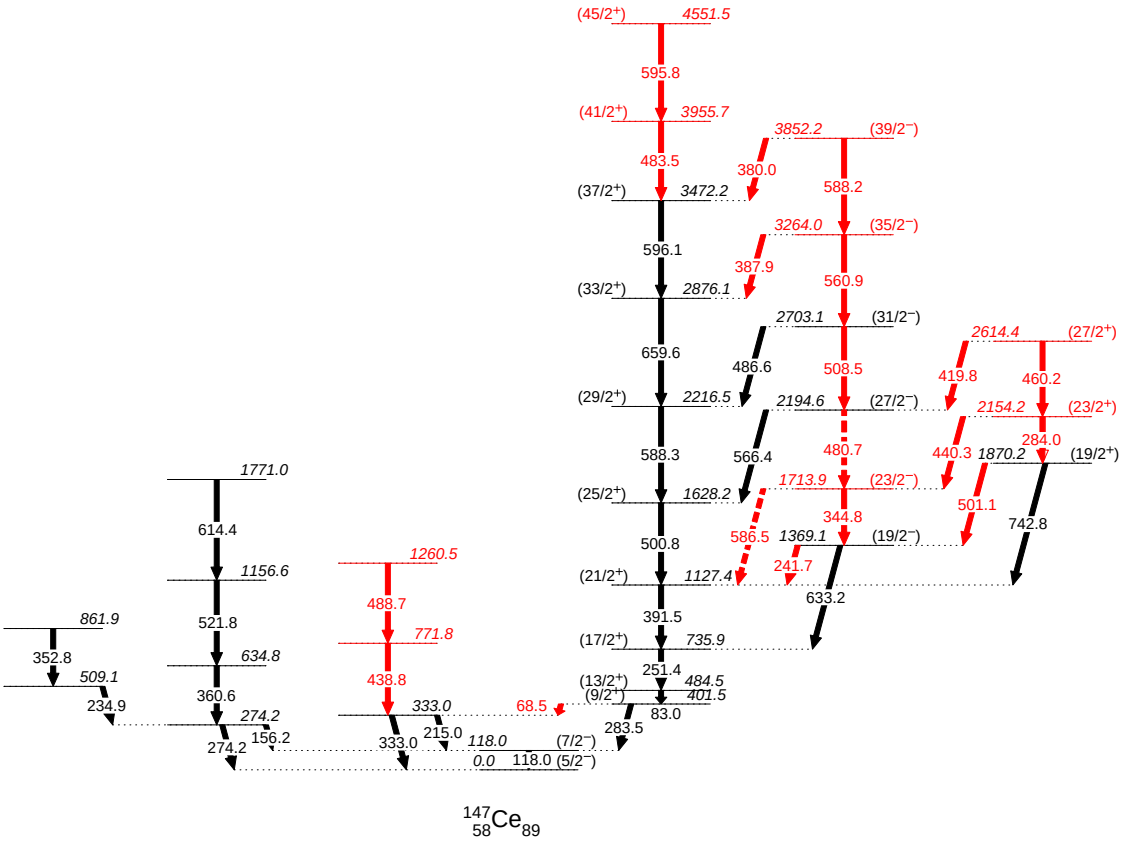

Figure 4. 4. 1. Level scheme of ^{147}Ce obtained in the current work. New transitions and levels are labeled in red. Part of the levels come from Ref. [73].

The level scheme of ^{147}Ce obtained in the current work is shown in Fig. 4. 4. 1 with

new transitions labeled in red. The levels can be classified into 6 band structures. The γ ray transition relative intensities are listed in Table 4. These intensities are normalized to the 283.5 keV one. Intensity errors are also listed in parenthesis.

Table 4. The γ ray relative intensities of ^{147}Ce. Part of values come from Ref. [73].

E_γ (keV)	Intensity	E_i (keV)	E_f (keV)	E_γ (keV)	Intensity	E_i (keV)	E_f (keV)
68.5	5.1(5)	401.5	333.0	460.2	0.7(1)	2614.4	2154.2
83.0	17.0(7)	484.5	401.5	(480.7)	(<0.5)	2194.6	1713.9
118.0	63.5(12)	118.0	0.0	483.5	1.2(1)	3855.7	3472.2
156.2	3.5	274.2	118.0	486.6	3.5(2)	2703.1	2216.5
215.0	10.5(6)	333.0	118.0	488.7	0.2	1260.5	771.8
234.9	2.7	509.1	274.2	500.8	32.3(8)	1628.2	1127.4
241.7	1.3(1)	1369.1	1127.4	501.1	1.8(1)	1870.2	1369.1
251.4	77.2(14)	735.9	484.5	508.5	1.1(1)	2703.1	2194.6
274.2	14.7	274.2	0.0	521.8	3.4	1156.6	634.8
283.5	100	401.5	118.0	560.9	1.0(1)	3264.0	2703.1
284.0	~1	2154.2	1870.2	566.4	4.8(3)	2194.6	1628.2
333.0	4.4(5)	333.0	0.0	586.5	<0.5	1713.9	1127.4
344.8	1.4(1)	1713.9	1369.1	(588.2)	(<0.5)	3852.2	3264.0
352.8	1.3	861.9	509.1	588.3	14.2(4)	2216.5	1628.2
360.6	8.0	634.8	274.2	595.8	<0.5	4551.5	3955.7
380.0	<0.5	3852.2	3472.2	596.1	2.5(2)	3472.2	2876.1
387.9	1.3(1)	3264.0	2876.1	614.4	0.8	1771.0	1156.6
391.5	53.0(10)	1127.4	735.9	633.2	4.5(3)	1369.1	735.9
419.8	1.1(1)	2614.4	2194.6	659.6	5.1(3)	2876.1	2216.5
438.8	1.7(1)	771.8	333.0	742.8	3.7(2)	1870.2	1127.4
440.3	0.8(1)	2154.2	1713.9				

The 3472.2 keV level was assigned to a side band in Ref. [74]. It is assigned to a member of band (1) in the current work. The 483.5 keV transition was reported to feed

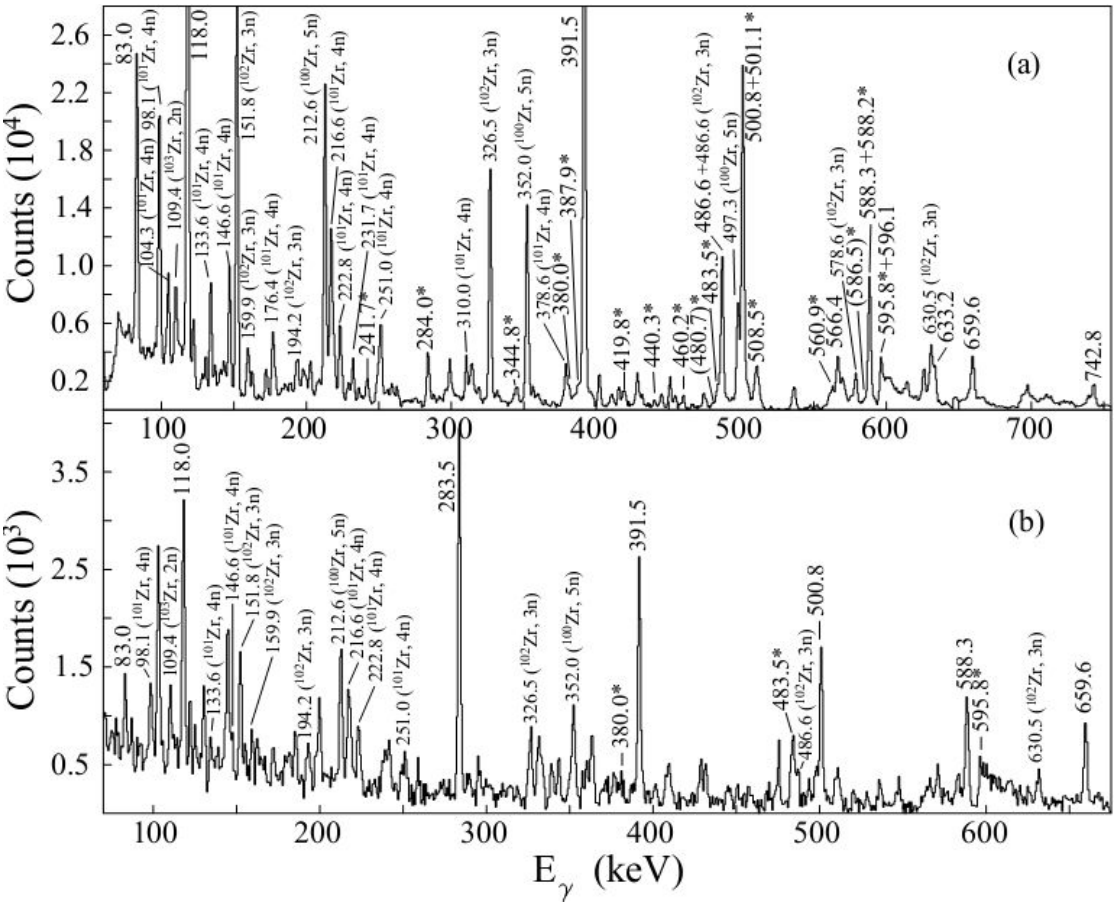

Figure 4. 4. 2. Partial γ ray spectra by a) double gating on 283.5 and 251.4 keV, and b) double gating on 251.4 and 596.1 keV transitions in ^{147}Ce. New transitions are labeled with an asterisk.

the 2876.1 keV level in Ref. [74]. In the current work, this transition is placed to feed the 3472.2 keV level. Another 4551.5 keV level and the corresponding 595.8 keV transition are assigned to band (1) in the current work. Three levels of 1369, 2195 and 2703 keV and their depopulation transitions were reported in Ref. [74] for the side band (2) as shown in black in Fig. 4. 4. 1. In the current work, band (2) is newly established with some interband and intraband linking transitions. Fig. 4. 4. 2 a) shows a coincidence spectrum by double gating on the 283.5 and the 251.4 keV transitions. The correlated

transitions in band (1), (2) and (3) as well as the Zr fission partner transitions can be seen. Fig. 4. 4. 2 b) shows a γ coincidence spectrum by double gating on 251.4 and 596.1 keV

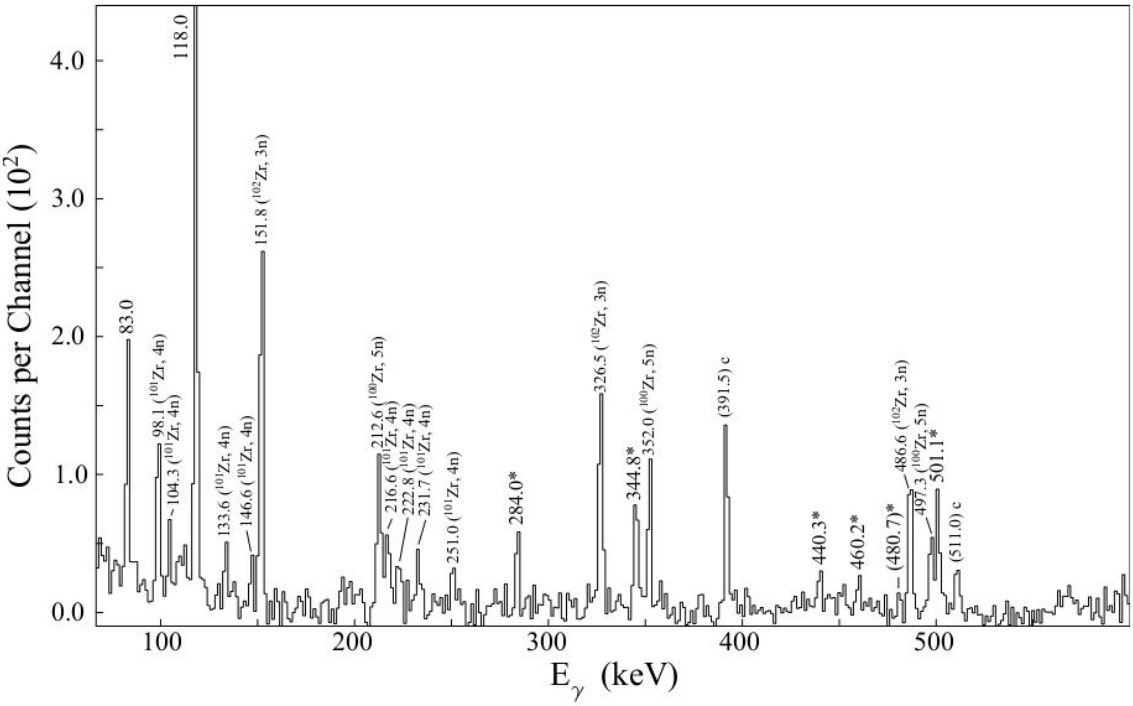

Figure 4. 4. 3. Partial γ ray spectrum by triple gating on 283.5, 251.4 and 633.2 keV transitions in ^{147}Ce. New transitions are labeled with an asterisk. The 391.5-keV peak labeled with a letter c comes from the coincidence of the 630.5-keV transition in ^{102}Zr partner which is mixed with the 633.2-keV γ transition. The 511.0-keV peak labeled with a letter c is caused by the annihilation of electrons and positrons.

transitions in band (1). All the other transitions in band (1) and the correlated 118.0 and 283.5 keV transitions can be seen. Fig. 4. 4. 3 is a coincidence spectrum by triple gated on the 283.5, 251.4 and 633.2 keV transitions. The 344.8 and 480.7 keV transition in band (2), 284.0 and 460.2 keV in band (3) and the 501.1 and 440.3 keV interband linking transitions can be seen. Bands (4) and (5) were previously reported in the ^{252}Cf SF. For band (6), two new 438.8 and 488.7 keV transitions are observed in the present work as well as a 68.5 keV linking transition. It should be noted that a 437.2 keV transition is

observed to feed the 333.0 keV level in β decay work [75]. This transition is considered to differ from the the 438.8 keV transition in the current work because of the 1.6 keV energy deviation.

The $5/2^-$ ground state assignment comes from β decay work. The 118.0 level was

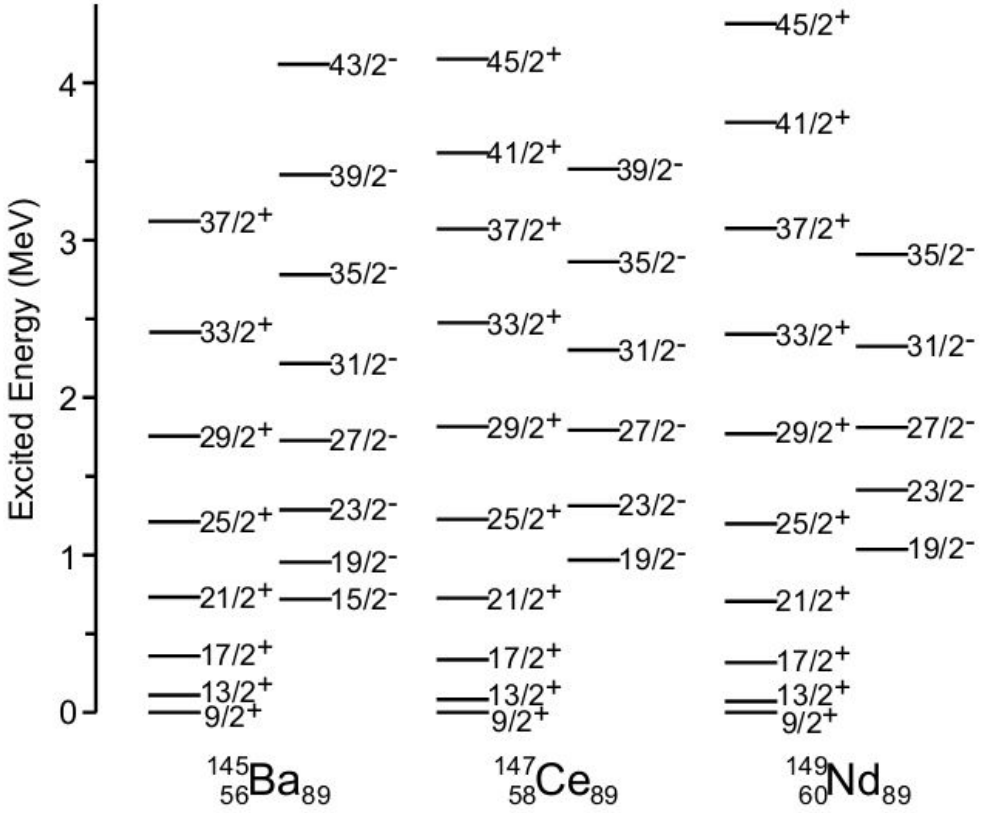

Figure 4. 4. 4. Comparison of the levels of s=-i octupole bands in ^{145}Ba [80], ^{147}Ce (current work) and ^{149}Nd [74].

assigned to $5/2^-$ or $3/2^-$ in ^{147}La β decay work [75], since the ^{147}La ground state was assigned to $3/2^+$ in ^{147}Ba β decay work [76, 77]. This assignment contradict the assignment from previous ^{248}Cm and ^{252}Cf SF work of $7/2^-$ [78, 79]. But Zhu *et al.* reassigned the ^{147}La ground state to $5/2^+$ in ^{252}Cf SF experiment [71]. If Zhu's assumption is correct, the 118.0 keV level with the current 7/2- assignment is accessible in ^{147}La β

decay. The 401.5 keV level was assigned as $5/2^+$ in ^{147}La β decay work. In previous ^{248}Cm and ^{252}Cf SF and the current work [78, 79], this level is tentatively assigned as $9/2^+$. The β decay from the ground state of ^{147}La to the 401.5 keV level of ^{147}Ce would be a second forbidden transition in this spin and parity assignment. However, the current spin and parity assignments of the positive band (1) agree with the systematics of the neighboring N=89 ^{145}Ba and ^{149}Nd nuclei. Hence, there might be a low energy transition lying between the 83.0 and the 283.5 keV ones so that it is not observed in ^{248}Cm and ^{252}Cf SF. As shown in Fig. 4. 4. 4, the levels of the s=i octupole bands in ^{145}Ba, ^{147}Ce and ^{149}Nd have very similar patterns. Their positive parity bands built on the $9/2^+$ level are proposed to arise from the $\nu i_{13/2}$ shell [73]. Therefore, the opposite parity bands (1) and (2) are likely to form an octupole band structure with simplex number s=i. The structure of band (3) is unknown. It could be the beginning of the positive parity members of the s=-i band or be a 3 quasiparticle state at high energy. Another possibility is a coupling of the neutron single particle to the β or γ vibration, since these two kinds of vibrational mode were observed in the ^{146}Ce core.

The B(E1)/B(E2) ratio for the 2703.1 keV level (31/2-) is $0.72(8) \times 10^{-6}$fm^{-2} and is $0.95(12) \times 10^{-6}$fm^{-2} for the 3264.0 keV level (35/2-). The average B(E1)/B(E2) value for s=+i octupole structure decreases from ^{144}Ce (6.12), ^{146}Ce (1.70), ^{148}Ce (0.82), ^{150}Ce (0.04), to ^{152}Ce (0.023×10^{-6}fm^{-2}) in the even even Ce isotopes and that in ^{147}Ce (0.84) lies between ^{146}Ce and ^{148}Ce. The comparison shows that the octupole deformation of ^{147}Ce lies between the neighboring Ce isotopes. This is consistent with systematics.

The energy displacement between the opposite parity bands in ^{147}Ce is calculated by the equation

$$\delta E(I) = E(I^-) - \frac{(I+1)E(I-1)^+ + IE(I+1)^+}{2I+1}$$

and is shown in Fig. 4. 4. 5 with comparison to those of ^{145}Ba and ^{149}Nd. It can be seen from the figure that the similar down sloping δE variations with increasing spins in these nuclei. So ^{145}Ba almost reaches stable octupole deformation about 35/2 $\hbar$. Meanwhile, ^{147}Ce and ^{149}Nd do not reach stable octupole deformation. The result shows that the

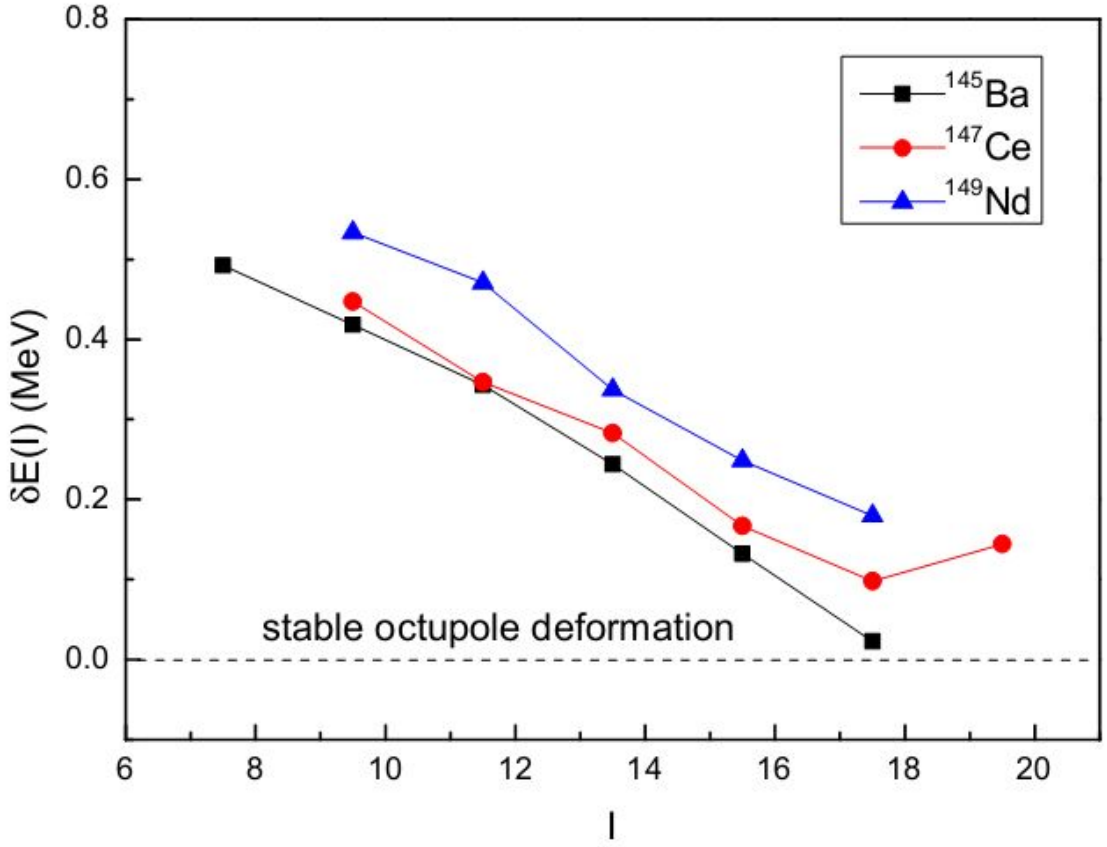

Figure 4. 4. 5. Comparison of δE(I) vs. I in ^{145}Ba, ^{147}Ce, ^{149}Nd. Note that there are some corrections on Fig. 3 of Ref. [73].

octupole correlations become more unstable as proton number goes far from the Z=56 stable octupole deformation center. It is interesting that δE increases at 39/2 $\hbar$ in ^{147}Ce. This upturn might be related to the backbending of the positive band (1) at high energy.

The behavior of δE agree with the B(E1)/B(E2) ratio result and systematics. On the other hand, the rotational frequency ratio of the opposite parity bands indicate the ^{145}Ba, ^{147}Ce, ^{149}Nd do not reach stable octupole deformation, as shown in Fig. 4. 4. 6.

RASM calculations were carried out in Ref. [73]. The results reproduce the opposite parity bands quite well and proposed an $i_{13/2}$ [660]1/2 configuration for the octupole band.

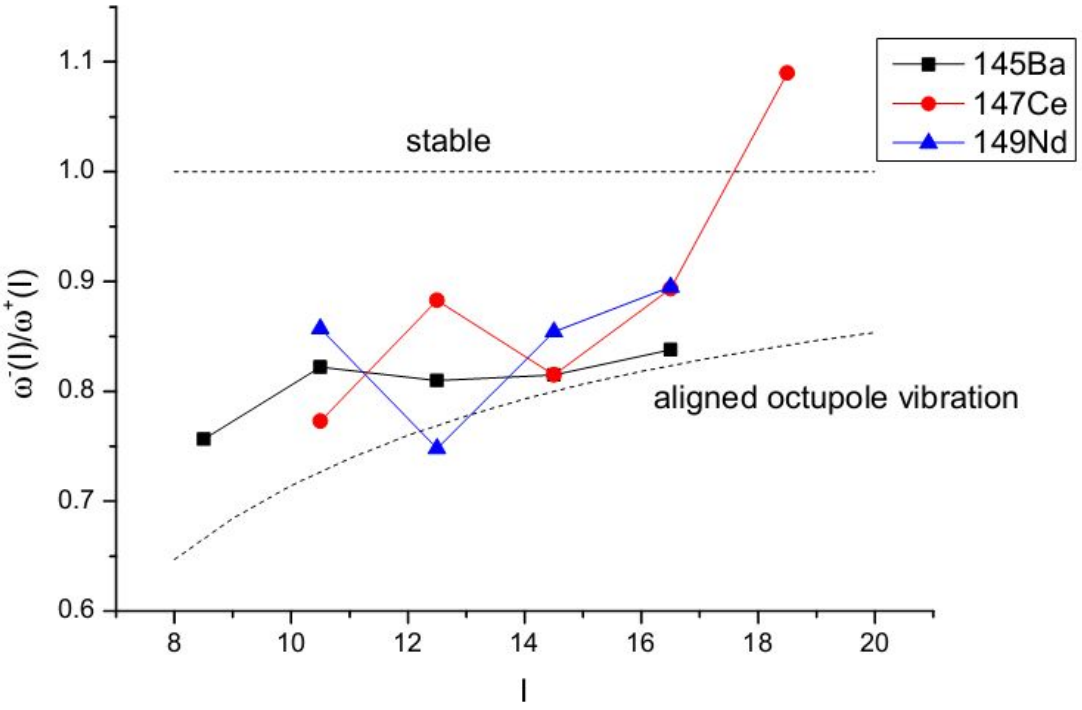

Figure 4. 4. 6. Comparison of rotational frequency ratio vs. I in ^{145}Ba, ^{147}Ce, ^{149}Nd.

^{148}Ce

The level scheme of ^{148}Ce obtained in the present work is shown in Fig. 4. 4. 7. In the previous ^{252}Cf SF studies [60, 81, 68], the ground state band was extended up to 22^+ and s=±1 octupole correlated bands were identified. Those octupole bands reported previously are not included in the current level scheme in Fig 4. 4. 7 for the sake of

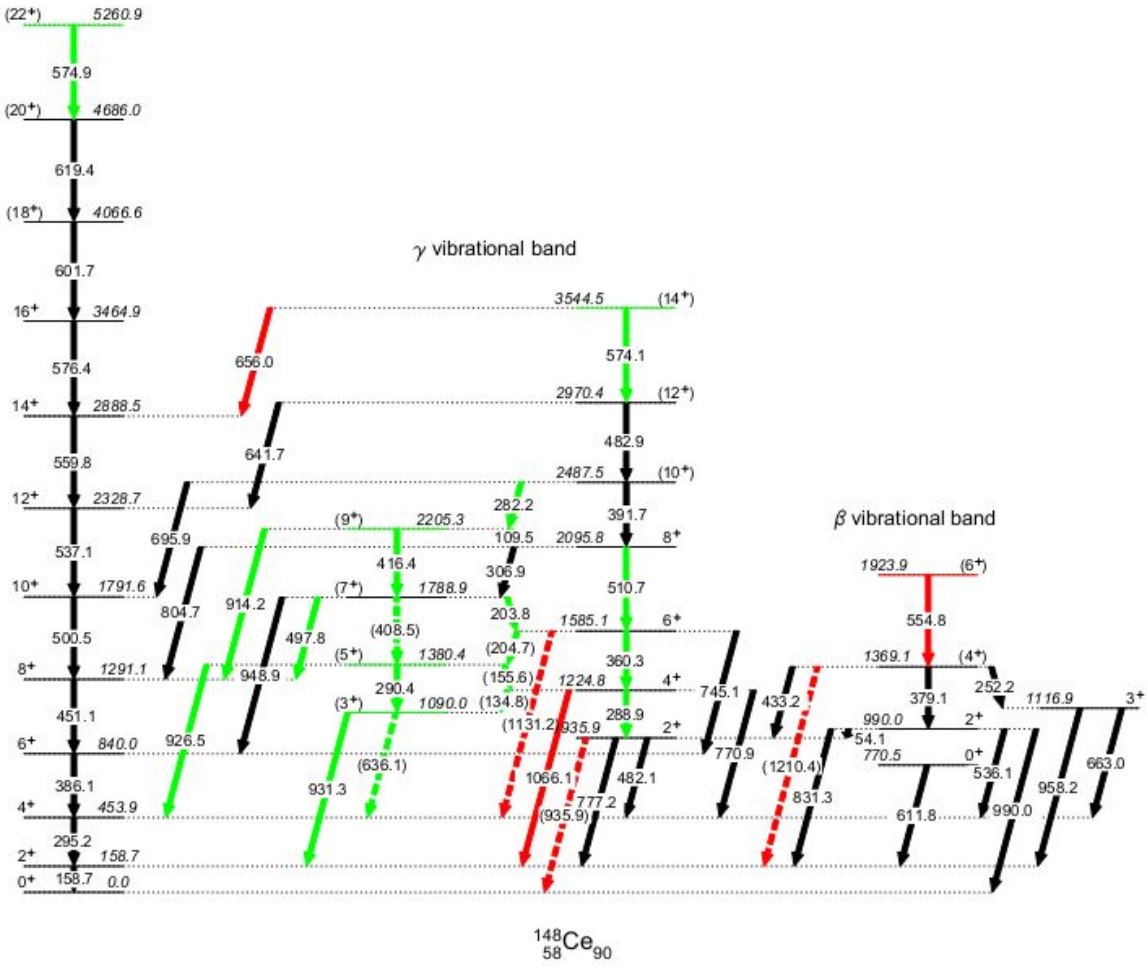

Figure 4. 4. 7. Partial level scheme of ^{148}Ce. New transitions in Ref. [4] are labeled in green. New transitions in the current work are labeled in red.

simplicity. Nathan added one more transition to the ground state band and established an 1γ vibrational band in his Ph. D. thesis [4], as shown in blue in Fig 4. 4. 7. Angular correlations of some cascades were also used to determine the spins and parities of the 1116.9, 1224.8 and 1585.1 keV level [4]. Details can be found in Ref. [4]. The 0^+, 2^+ and 4^+ levels in the 1β vibrational band were previously reported in ^{148}La β decay work [82] but not as a β band structure. These levels and the corresponding γ transitions are confirmed in the current work. A new 554.8 keV transition in this band was identified in

the current work. The possible E2 transition from the 935.9 keV (2^+) level to the ground

Table 5. The γ ray relative intensities of ^{148}Ce. Some of the values come from Ref.[4, 60].

E_γ (keV)	Intensity	E_i (keV)	E_f (keV)	E_γ (keV)	Intensity	E_i (keV)	E_f (keV)
54.1	<0.1	990.0	935.9	554.8	0.1	1923.9	1369.1
109.5	0.1	2205.3	2095.8	559.8	8.0	2888.5	2328.7
134.8		1224.8	1090.0	574.1	0.4	3544.5	2970.4
155.6	<0.2	1380.4	1224.8	574.9	0.5	5260.9	4686.0
158.7	100	158.7	0.0	576.4	6.3	3464.9	2888.5
203.8	0.4	1788.9	1585.1	601.7	3.9	4066.6	3464.9
204.7	<0.6	1585.1	1380.4	611.8	0.2	770.5	158.7
252.2		1369.1	1116.9	619.4	2.0	4686.0	4066.6
282.2	0.2	2487.5	2205.3	636.1	<0.1	1090.0	453.9
288.9	0.3	1224.8	935.9	641.7	1.0	2970.4	2328.7
290.4	0.6	1380.4	1090.0	656.0	0.2	3544.5	2888.5
295.2	82	453.9	158.7	663.0	2.2	1116.9	453.9
306.9	3.2	2095.8	1788.9	695.9	2.1	2487.5	1791.6
360.3	0.4	1585.1	1224.8	745.1	4.0	1585.1	840.0
379.1	0.7	1369.1	990.0	770.9	3.3	1224.8	453.9
386.1	63	840.0	453.9	777.2	1.0	935.9	158.7
391.7	2.1	2487.5	2095.8	804.7	2.1	2095.8	1291.1
408.5	<1.9	1788.9	1380.4	831.3	0.6	990.0	158.7
416.4	0.2	2205.3	1788.9	914.2	0.3	2205.3	1291.1
433.2		1369.1	935.9	926.5	0.2	1380.4	453.9
451.1	39	1291.1	840.0	931.3	0.4	1090.0	158.7
482.1		935.9	453.9	935.9	<0.4	935.9	0.0
482.9	1.5	2970.4	2487.5	948.9	5.0	1788.9	840.0
497.8	<2	1788.9	1291.1	958.2	9.1	1116.9	158.7
500.5	30	1791.6	1291.1	990.0	1.0	990.0	0.0
510.7		2095.8	1585.1	1066.1	0.4	1224.8	158.7
536.1		990.0	453.9	1131.2	<0.6	1585.1	453.9
537.1	16	2328.7	1791.6	1210.4	<1.1	1369.1	158.7

state is not observed in this ^{100}Zr fission partner double gate. The possible E2 transition from 990.0 keV (2^+) level to the 770.5 keV (0^+) level is not observed in the 379.1 and 611.8 keV double gate. The γ ray intensities are listed in Table 5. The result combines the previous ^{252}Cf SF work in Ref. [4, 60] and new measurements in the current work.

Table 6. The γ ray branching ratio of ^{148}Ce. Part of values come from Ref. [82].

level energy (keV)	transition energy (keV)	branching ratio	pattern
935.9	482.1	13(1)	$2^+ \rightarrow 4^+_{gs}$
	777.2	100(3)	$2^+ \rightarrow 2^+_{gs}$
990.0	54.1		$2^+ \rightarrow 2^+$
	536.1	5.3(6)	$2^+ \rightarrow 4^+_{gs}$
	831.3	55(3)	$2^+ \rightarrow 2^+_{gs}$
	990.0	100(3)	$2^+ \rightarrow 0^+_{gs}$
1369.1	379.1	100(10)	$4^+_{1\beta} \rightarrow 2^+$
	433.2	28.2(14)	$4^+_{1\beta} \rightarrow 2^+$

Internal conversion is included for the strong 158.7, 295.2 keV E2 transitions in the yrast band. The intensities of the 482.1 and 536.1 keV transitions can not be measured due to the high background from the 482.9 keV and 537.1 keV ones, respectively. The 433.2 keV transition intensity cannot be measured but can be deduced from the branching ratio in Ref. [82].

The ownership of the 2^+ levels in the β and γ vibrational band is uncertain. Both 935.9 and 990.0 keV 2^+ levels do not decay to the 770.5 keV 0^+ level. Thus, these two 2^+ level could be switched in these bands. The branching ratios of the 935.9 (2^+), 990.0 (2^+) and 1369.1 keV (4^+) levels are listed in Table 6. The intensity ratio comes from the ^{148}La β decay work. In this table, the 935.9 and 990.0 keV levels have similar

$I(2^+ \rightarrow 4^+_{gs})/I(2^+ \rightarrow 2^+_{gs})$ intensity ratios. Nevertheless, according to the Alaga rules [40], the $B(E2,2^+ \rightarrow 4^+_{gs})/B(E2,2^+ \rightarrow 2^+_{gs})$ ratio of a $2^+_{1\beta}$ level should be much larger that of the $2^+_{1\gamma}$ one. On the other hand, the B(E2) ratio of the 1369.1 keV level is B(E2,433.2)/B(E2,379.1) = 0.14(2). This value show some evidence that the 990.0 keV level is more likely to be the 2^+ level of the 1β vibrational than the 935.9 keV one. Also the 1224.8 keV $4^+_{1\gamma}$ level does not decay to the 990.0 keV level to likewise support the 990.0 keV 1β assignment. Moreover, if the 990.0 keV level is assigned to the 1β band, the energy spacing between the 4^+ and 2^+ levels in 1β band agrees better with the systematics in the neighboring ^{146}Ce, ^{150}Nd, ^{152}Sm nuclei. However, since the experiment evidence is not sufficient enough and the mixing among the ground state band, the 1β vibrational band and the 1γ vibrational band is unknown, more theoretical work is needed

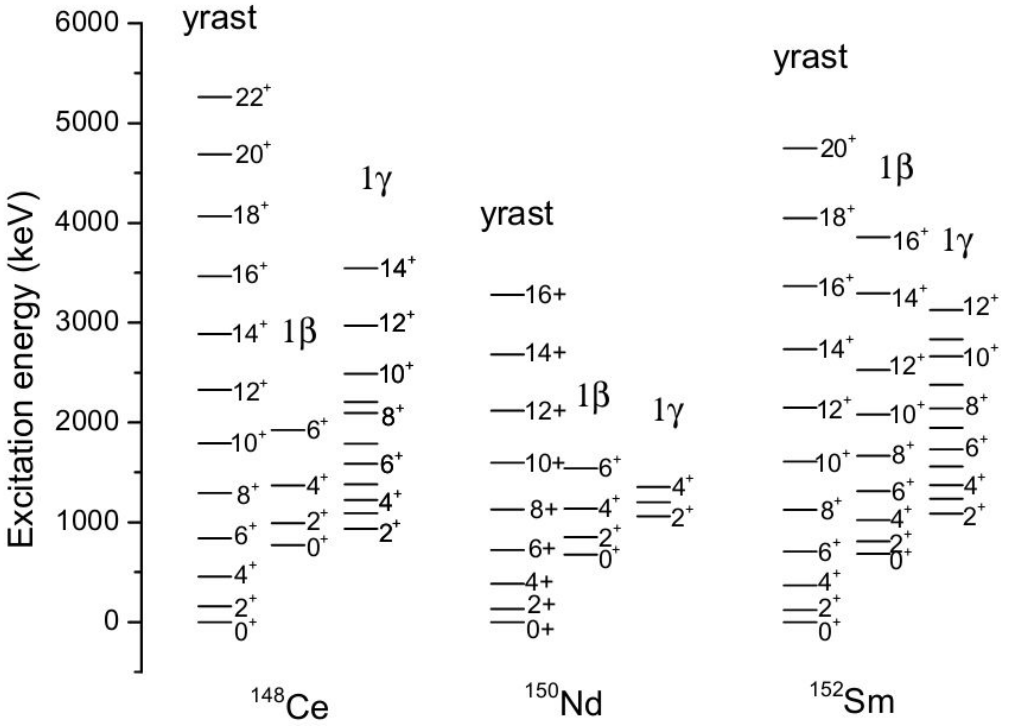

Fig. 4. 4. 8. Comparison of the ground state band, the 1β vibrational band and the 1γ vibrational band in ^{148}Ce (current work), ^{150}Nd [84, 87, 88] and ^{152}Sm [89].

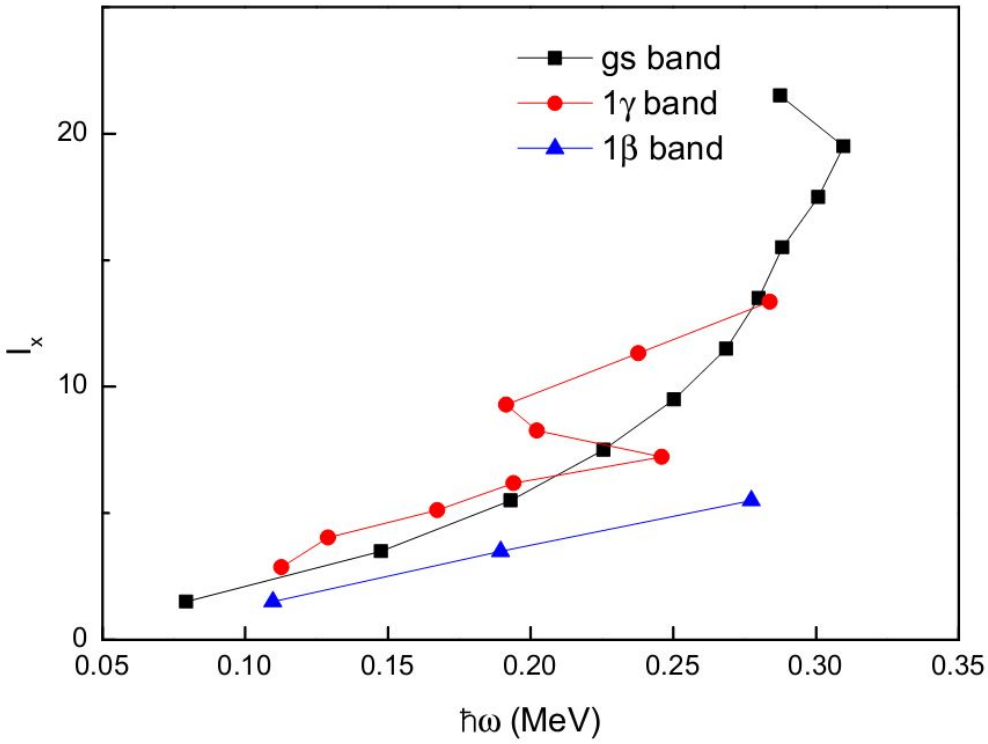

Fig. 4. 4. 9. Angular momentum alignment vs. rotational frequency of the ground state band, the 1β vibrational band and the 1γ vibrational band in ^{148}Ce.

to study the 2^+ level assignments of the 1β and 1γ band.

The level scheme of ^{148}Ce is similar to those in ^{150}Nd and ^{152}Sm (see in Fig. 4. 4. 8). These nuclei lie in the region between spherical and rigid deformed shapes. Note that according to the finite-range liquid-drop model (FRLDM) calculation [83], ^{148}Ce has deformation parameters ε2=0.19, ε3=0.05, ε4=-0.05. The ^{150}Nd and ^{152}Sm nuclei were proposed to have X(5) dynamical symmetry, which corresponds the critical point of phase transition between spherical vibrator and axially deformed rotor [84, 85]. ^{148}Ce was also proposed for a X(5) symmetric nucleus in Ref. [86]. However, the octupole correlation in ^{148}Ce might interfere with the X(5) symmetry and weaken it compared to ^{150}Nd and ^{152}Sm.

The aligned angular momentum vs. rotation frequency is shown in Fig 4. 4. 9. For the ground state band, a small upbending begins at about ħω~0.29 MeV. Then another bending occurs at ħω~0.31 MeV. These bending phenomena may originated from the alignment of a pair of $h_{11/2}$ protons or a pair of $i_{13/2}$ neutrons. The behavior of the γ band is more irregular. A pronounced backbending occurs at ħω~0.22 MeV roughly. This backbending in the γ band might be caused by the alignment of a pair of neutrons or admixture of octupole correlation. However, as discussed above, similar X(5) symmetry refers to an unstable γ vibration and might be quenched at higher spin.

4.5 Identification of new transitions, levels and mass assignments of $^{143\text{-}153}$Pr

Studies of nuclear energy levels over long isotopic chains reveal structural changes as a function of N to provide important tests of nuclear models. Spontaneous fission provides a good approach to study nuclei over long isotopic chains [60], and specifically, to investigate the high spin states and the possible octupole correlations for neutron rich Pr isotopes around the A=150 mass region. Historically, levels of several Pr isotopes have been identified from ^{252}Cf and ^{248}Cm SF [90-93]. Only ^{151,153}Pr were reported to have possible octupole correlations between parity-doublet bands [91].

In SF, the new transitions in a certain isotope are generally identified by gating on some known transitions in this isotope observed in β-decay or by gating on known transitions in the partner isotopes. Usually, this procedure gives unique identifications. However, in some cases, when the γ-spectrum is complex, the overlapping of transition energies in different isotopes can lead to a wrong mass identification of the bands.

The mass assignments of the previously reported levels assigned to ^{151,152,153}Pr [91, 93] have recently been called into question [94]. The γ-ray transitions and levels in ^{151,153}Pr [91] reported in the previous work were assigned to ^{152,154}Pr respectively in Ref. [94]. The two bands proposed to be in ^{152}Pr in Ref. [93] were assigned to ^{151,153}Pr separately [94]. In this paper, we provide new analysis in both ^{252}Cf SF and ^{238}U+^{9}Be induced fission data [15] with full fragment mass and Z identification to give reliable assignments of the levels and transitions in these Pr isotopes. New level schemes of $^{145,147\text{-}153}$Pr and new transitions $^{143\text{-}146}$Pr are presented in the present work. The question of octupole correlations in their band structures requires further studies.

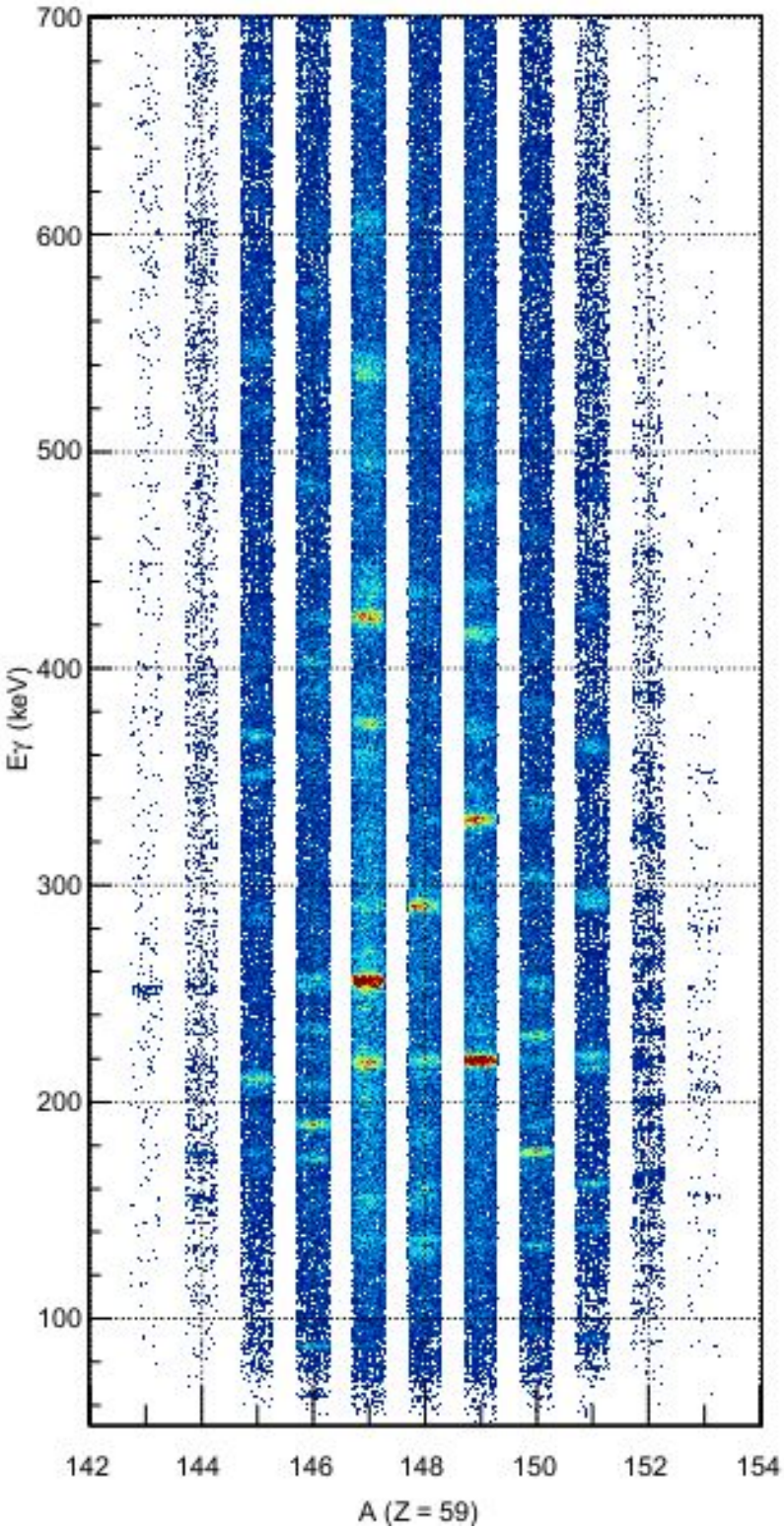

Figure 4. 5. 1. Doppler corrected γ-ray energy as a function of the mass number (A) of the Pr (Z=59) fragment identified in VAMOS++.

Fig. 4. 5. 1 shows a two dimensional spectra of A vs 'singles' E for the Pr isotopes. Using such a data set also allows one to view directly the evolution of the various transitions as a function of mass number. Note that the yield is maximized at ^{147}Pr and ^{149}Pr. This phenomenon may be due to the odd-even effect.

^{143}Pr

The A- and Z- gated γ-ray spectrum on ^{143}Pr is shown in Fig. 4. 5. 2. Three new transitions 251(1),445(1) and 554(1) keV were identified. Other transitions are not labeled.

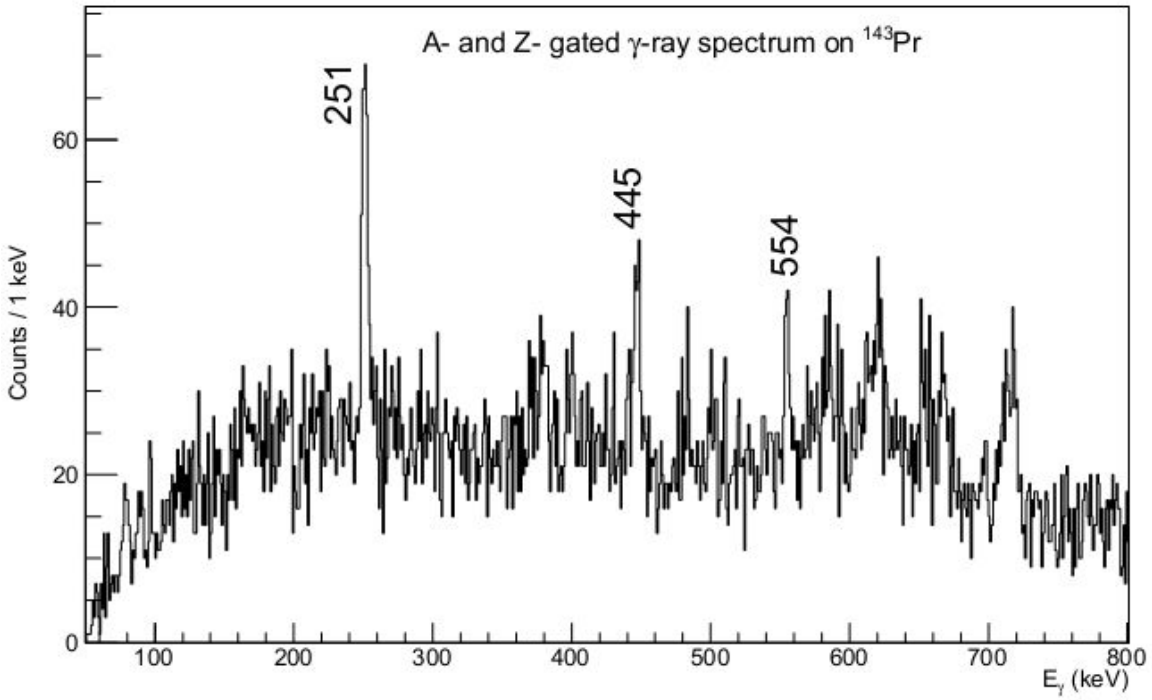

Figure 4. 5. 2. Partial ^{143}Pr A- and Z- gated γ-ray spectrum obtained from ^{238}U +^{9}Be induced fission data.

^{144}Pr

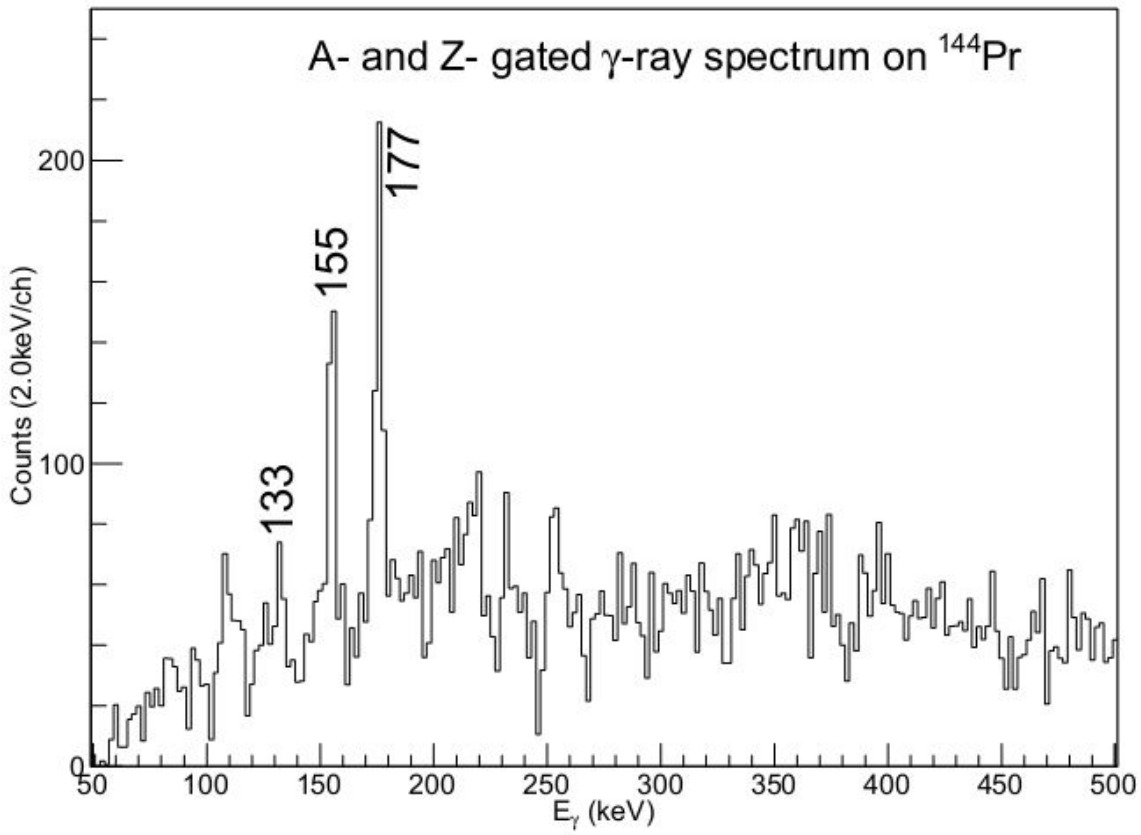

Fig. 4. 5. 3. Partial ^{144}Pr mass- and Z- gated γ-ray spectrum obtained from ^{238}U + ^{9}Be induced fission data.

The mass- and Z- gated γ-ray spectrum on ^{144}Pr is shown in Fig. 4. 5. 3. The 132.2 keV peak could be the 133.5 keV transition identified in ^{144}Ce-decay [95]. Other labeled transitions are newly identified. It should be pointed out that the unbiased "singles" nature of the data allows the identification of low multiplicity transitions seen in beta decay. In addition two new transitions 155(1) and 177(1) keV were also identified. Due to the complexity of the spectrum and lack of coincidences in this odd-odd nucleus, other transitions above 200 keV are not labeled and no level scheme is presented.

^{145}Pr

The new level scheme of ^{145}Pr is shown in Fig. 4. 5. 4. A new band was identified with 3/2+ band head. The mass- and Z- gated γ-ray spectrum on ^{145}Pr is shown in Fig. 4. 5. 5(a). The 207.6, 211.6, 284.5 and 492.2 keV peaks were previously identified in ^{145}Ce β-decay [96]. The 350.9 keV peak could be an overlap of the 350.9 keV transition (decay from 350.9 keV level to 0 keV level) and another 350.9 keV transition (decay from 540.1 keV level to 188.8 keV level) identified in β-decay [96]. Fig. 4. 5. 2(b) and (c) are projections on 211.6 and 546 keV transitions. In these spectrum, the coincident 204.0, 207.6, 284.5, 368.8, 492.2, 546.3 and 672.3 keV transitions can be seen. From the energy spacing of the 211.6, 368.8, 546.3 and 672.3 keV transitions and the intensities shown in Fig. 4. 5. 5(a), these-rays are possibly E2 transitions in a rotational band. Thus, spins and

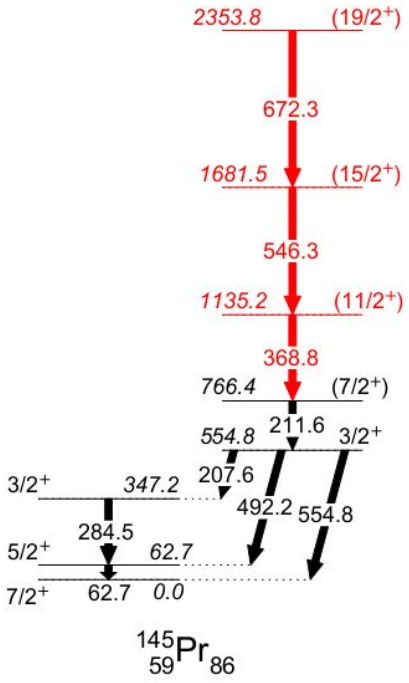

Fig. 4. 5. 4. The new level scheme of ^{145}Pr in the present work. Transitions and levels previously reported in β decay work are labeled in black. New ones in the current work are labeled in red.

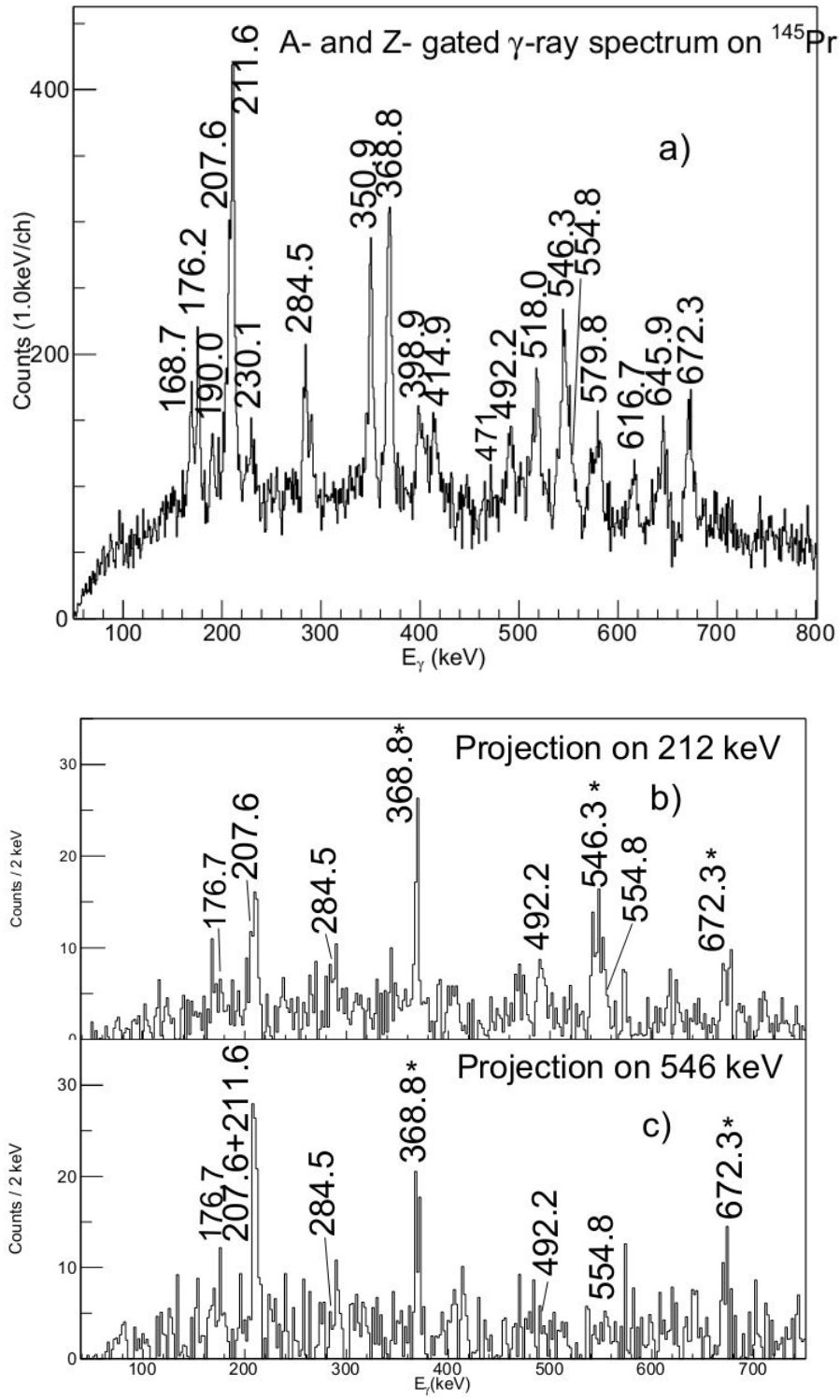

Fig. 4. 5. 5. Partial ^{145}Pr mass- and Z- gated γ-ray spectra obtained from ^{238}U + ^{9}Be induced fission data. Part (a) is single γ-ray spectrum. Part (b) is a projection spectrum on 211.6 keV and part (c) is a projection on 546.2. keV.

parities of levels in this band are tentatively assigned. It should be pointed out that in the beta decay measurements the 211.6 is weak whereas in the present work it is very intense, showing the complementarity of the in beam and decay work. There is coincidence evidence in the A/Z gated data for a 350-415-471 possibility feeding a 168 keV transition. It is not definitive that this cascade feeds into the 207-211 cascades, so it is not placed in the level scheme. The A/Z gated γ data includes a 176.7 keV transition which is in coincidence with the 207-211-284-368-546 keV cascade, but it is not clear where to place it.

^{146}Pr

The mass- and Z- gated γ-ray spectrum on ^{146}Pr is shown in Fig. 4. 5. 6(a). The 87.2 keV transition could be the one previously identified in ^{146}Ce β-decay [97]. Fig. 4. 5. 6(b) is a projection on 188.9 keV transition. In this spectrum, the coincident 87.2, 173.9 and 484.6 keV transitions can be seen. With the given data it is not possible to build a level scheme.

^{147}Pr

The new level scheme for ^{147}Pr is shown in Fig. 4. 5. 7. In this case, the 2.7, 25.2, 218.5, 243.7 and 138.7 keV transitions were previously observed in the β-decay of ^{147}Ce [98, 99]. The ground state, 2.7, 27.9 keV levels were tentatively assigned to $5/2^+$, $3/2^+$ and $5/2^+$ respectively [98]. The 246.4 keV level was tentatively proposed to have a positive parity without any spin assignment [98]. The A/Z gated γ-ray spectrum is shown in Fig. 4. 5. 8, where evidence for a high spin band is seen. A new band is assigned to ^{147}Pr by

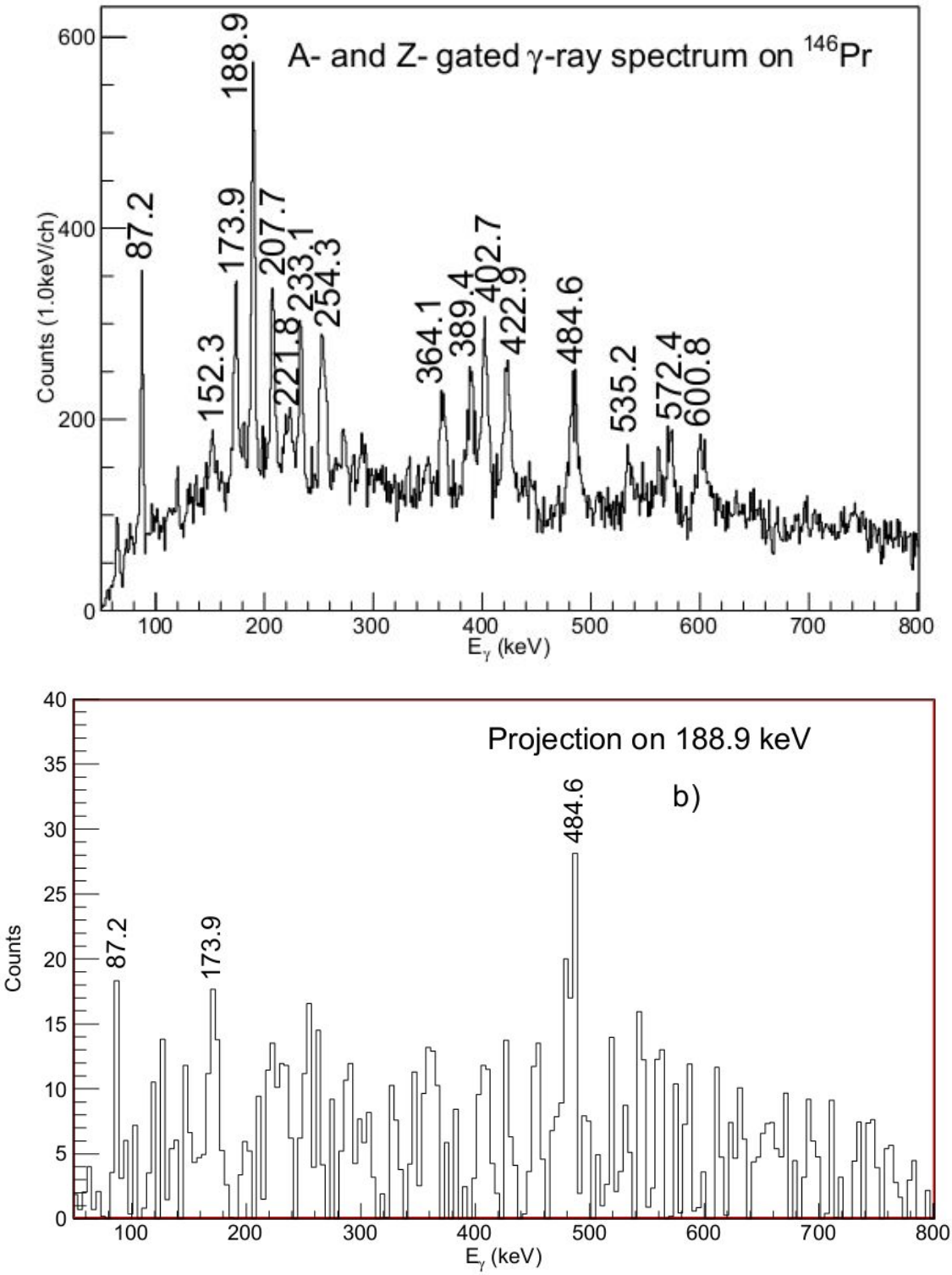

Fig. 4. 5. 6. Partial ^{146}Pr mass- and Z- gated γ-ray spectra obtained from ^{238}U + ^{9}Be induced fission data. Part (a) is a single γ-ray spectrum. Part (b) is a projection spectrum on 188.9 keV.

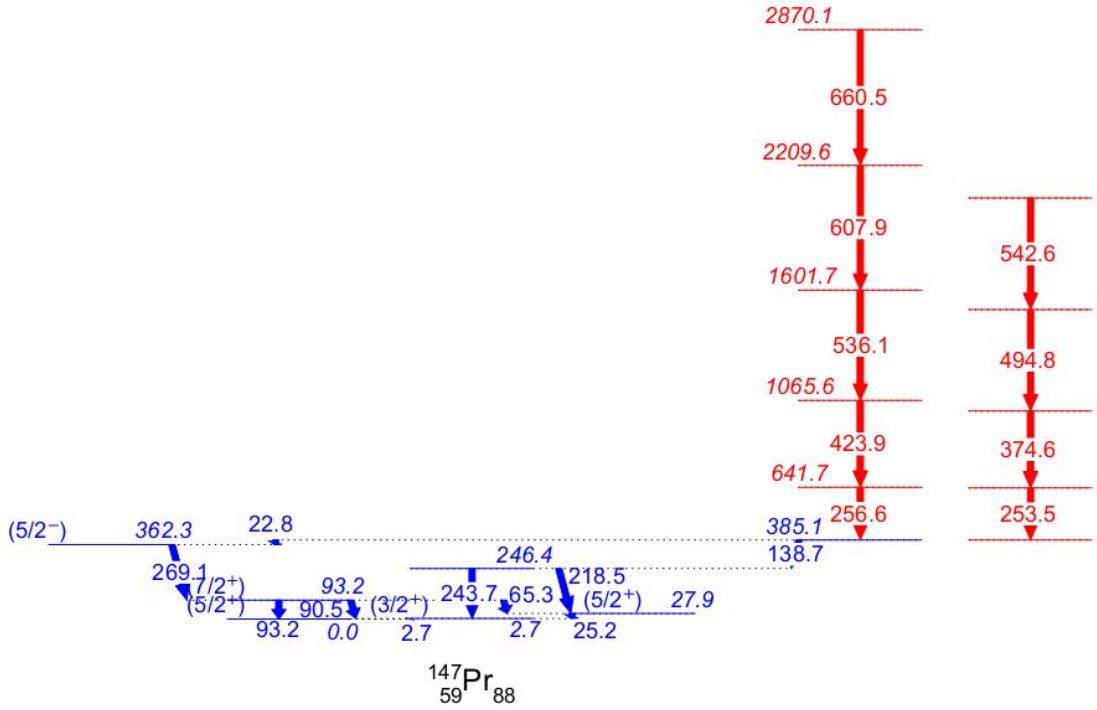

Fig. 4. 5. 7. The new level scheme of ^{147}Pr in the present work. Transitions and levels previously reported in β-decay work are labeled in blue. New ones in the current work are labeled in red.

observing the γ-rays in coincident with the 138.7, 218.5 and 243.7 keV transitions. The A/Z gated γ spectrum is shown in Fig. 4. 5. 8, where evidence for a high spin band is seen. A new band is assigned to ^{147}Pr by observing the γ-rays in coincidence with the138.7, 218.5 and 243.7 keV transitions. A partial coincident γ-ray spectrum is shown in Fig. 4. 5. 9. In this spectrum with gate on a previously known transition and the strongest transition in Fig. 4. 5. 8, one can clearly see the 218.5 and 243.7 keV known transitions, 256.6, 423.9, 536.1, 607.9 and 660.5 keV new transitions and the Y partner transitions. These new transitions are confirmed in the mass-Z gated spectrum on ^{147}Pr (Fig. 4. 5. 5). The 2.7 and 25.2 keV transitions are not observed in the current work because of the low

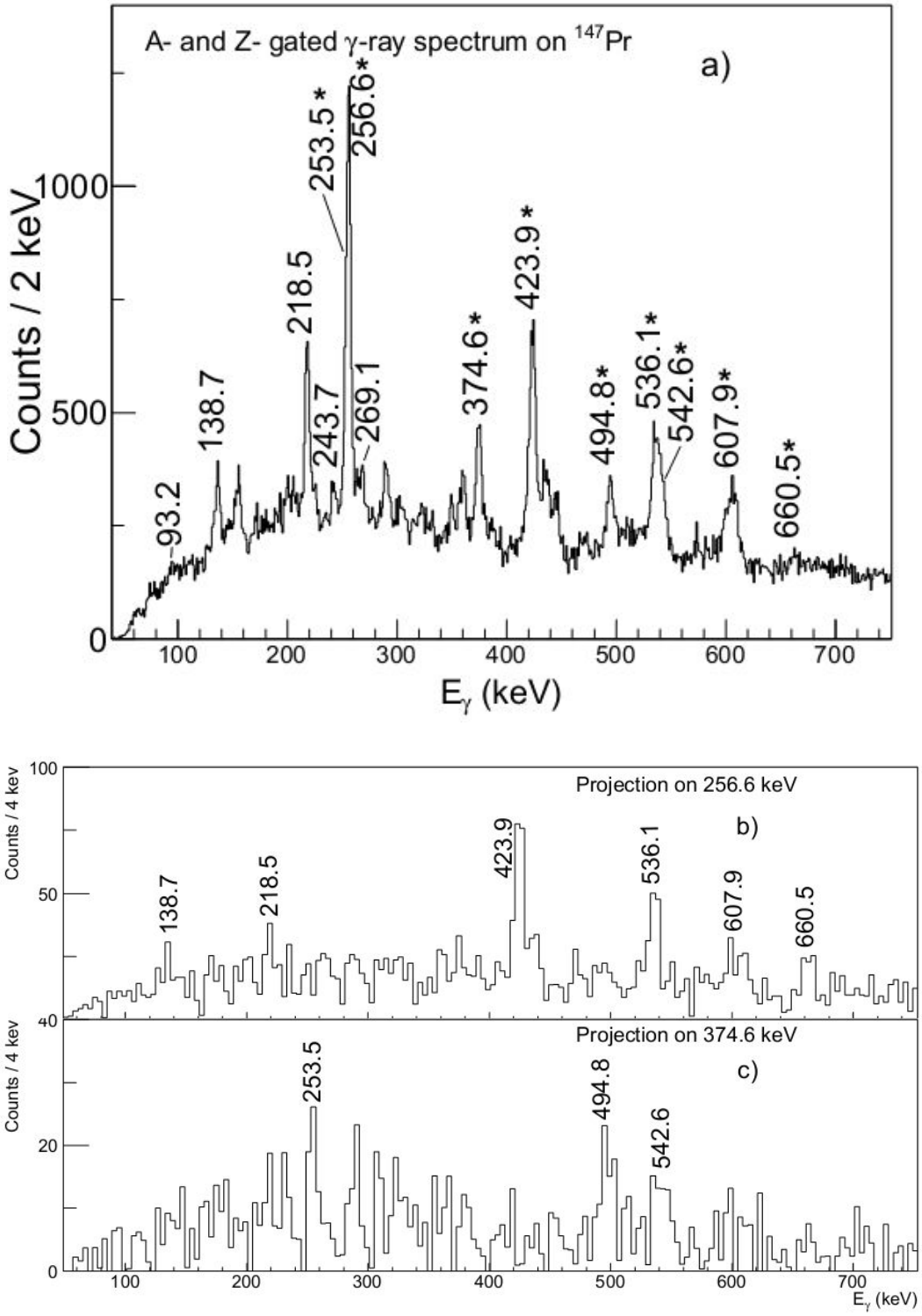

Fig. 4. 5. 8. (a) Partial ^{147}Pr mass- and Z- gated γ-ray spectra obtained from ^{238}U + ^{9}Be induced fission data. New transitions are shown with asterisks. (b) is a projection spectrum on 256.6 keV and (c) is a projection spectrum on 374.6 keV.

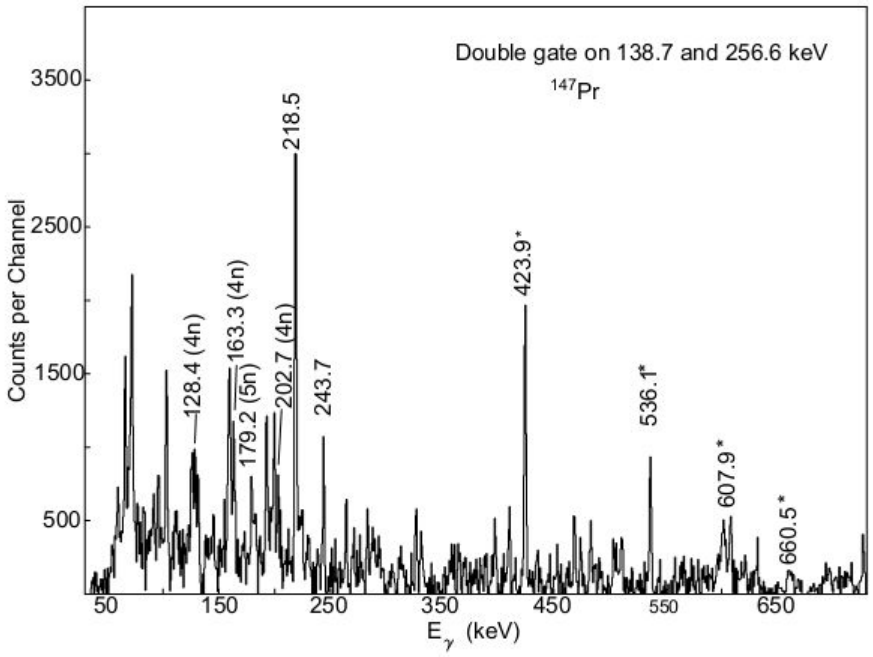

Fig. 4. 5. 9. Partial γ-ray coincidence spectrum by gating on 138.7 and 256.6 keV transitions in ^{147}Pr from ^{252}Cf SF data. New transitions are marked with asterisk. In the spectrum, transitions in Y fission partners are indicated with neutron evaporation numbers.

efficiency of the detectors at low energy region. The time gated data also indicate some lifetime of the 385.7 keV level. However, since no lifetime of this level was reported by Mantica *et al.* in β-decay work, there might be a very low energy transition between the 138.7 and 256.6 keV transitions. The 138.7 keV transition is very small in the prompt A/Z gated spectrum due to a possible lifetime for the corresponding state. Such a loss of intensity has already been found in the case of the neutron rich Zr isotopes [13]. The projection of 374 keV transition of A/Z gated data show evidence for a 253-374-495-542 cascade as seen in Fig. 4. 5. 8(c). This cascade is also confirmed by the ^{252}Cf SF data, but not in coincidence with any other transitions reported in ^{147}Ce β-decay in Ref. [98, 99].

Thus, level energy of this cascade is not placed in the level scheme. Other transitions identified in the Fig. 9 could not be placed in the level scheme.

^{148}Pr

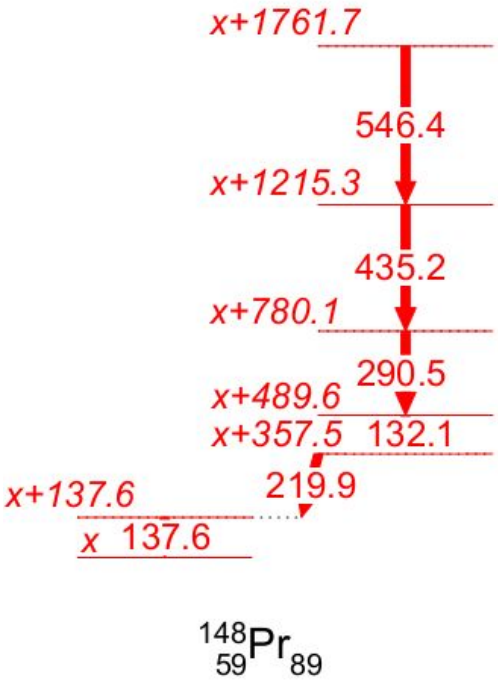

Figure 4. 5. 10. The new level scheme of ^{148}Pr in the current work.

The new level scheme for ^{148}Pr is shown in Fig. 4. 5. 10. In this case, all transitions are newly identified. The new transitions are seen in the mass-Z gated spectrum of ^{148}Pr (Fig. 4. 5. 11). None of transitions from the β-decay of ^{148}Ce [99-101] are observed in this work. A partial coincident γ-ray spectrum is shown in Fig. 4. 5. 12. In this spectrum with gate on 132.1 and 290.5 keV transitions one can clearly see the 137.6, 219.9, 435.2 and 546.4 keV new transitions and the Y partner transitions. The order of these new transitions are placed due to the intensity and the similarity to ^{150}Pr. The three lowest energy transitions of 66, 72 and 102 keV in this gate in Fig. 4. 5. 12 are seen in the

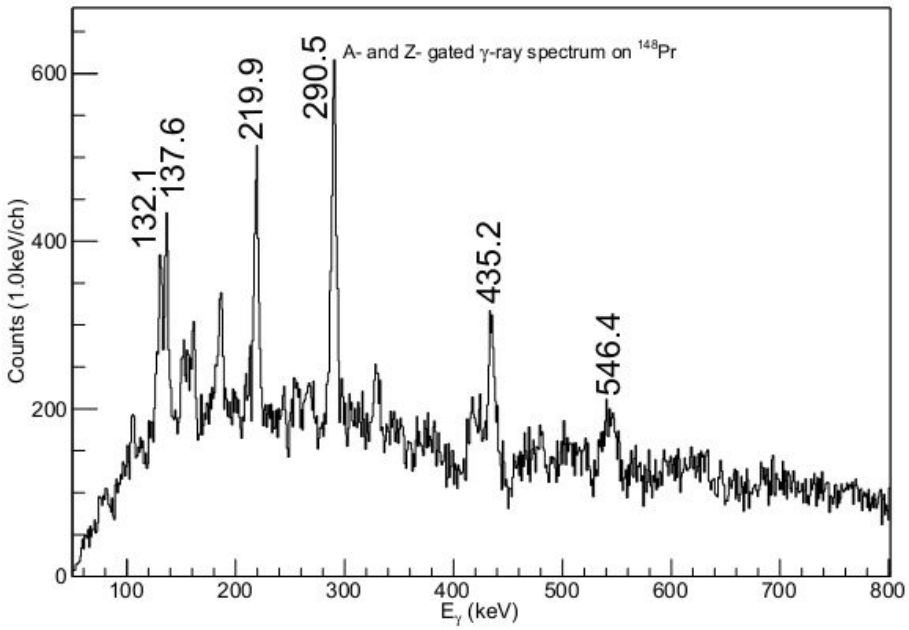

Figure 4. 5. 11. Partial ^{148}Pr mass- and Z- gated γ-ray spectra obtained from ^{238}U + ^{9}Be induced fission data.

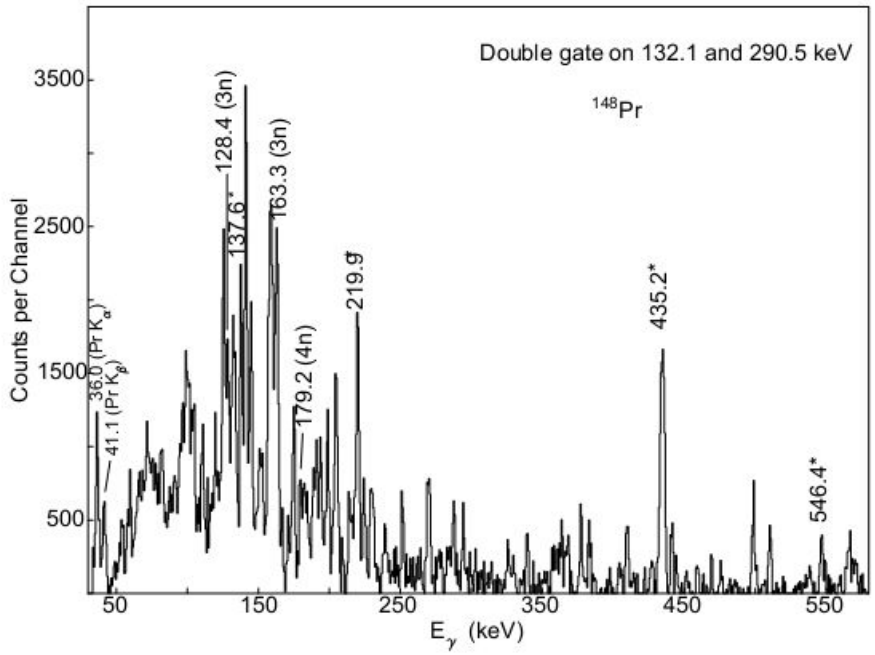

Fig. 4. 5. 12. Partial γ-ray coincidence spectrum by gating on 132.1 and 290.5 keV transitions in ^{148}Pr from ^{252}Cf SF data. New transitions are marked with asterisk. In the spectrum, transitions in Y fission partners are indicated with neutron evaporation numbers.

256.6-423.9 keV gated spectrum, so are not in ^{147}Pr.The new transitions are also confirmed in the mass-Z gated spectrum on ^{148}Pr (Fig. 4. 5. 11). The A-Z gated spectrum contains 5-10% contamination from adjacent Z nuclei, e.g. 158 keV for ^{148}Ce and for adjacent M ^{149}Pr has 330 keV transition. For even A Pr mass-Z gated spectra, intensities of the γ-rays from this small contribution are comparable with some of the Pr ones. Such components from Ce and Nd are subtracted from ^{148}Pr data. In ^{252}Cf SF data, the intensity ratio of 137.6/132.1 and 219.9/132.1decrease about 80% as the time coincidence window decreases from 500ns to 8ns. In the contrast, the ratio of the 132.1, 290.5, 435.2 and 546.4 keV transition intensities remain almost the same. Thus, the 219.9 and 137.6 keV transitions are placed at the bottom and a lifetime is proposed for the level which the 132.1 keV transition feeds. This is consistent with the non observation of the 219.9 keV transition in coincidence with 290.5 keV in the prompt gamma ray spectrum obtained using the A, Z gate. In addition spectra obtained in coincidence with 219.9 keV suggest the existence of another band consisting of 219.9 and 329 keV transitions.

^{149}Pr

The new level scheme for ^{149}Pr is shown in Fig. 4. 5. 13. In this case, the 58.5 and 86.5 keV transitions were previously observed in the β-decay of ^{149}Ce [102, 103]. The band (1) in Fig. 4. 5. 13 was previously assigned by our group [90]. In Fig. 4. 5. 14, previously reported band (1) transitions and new transitions in band (2) and (3) are seen in the mass-Z gated spectrum. The mass/Z gated spectrum was important in guiding our γ ray coincidence spectra analysis to identify new band (3). These two bands (2) and (3) are established by in the present work by observing the coincidence between the γ rays in

these bands and the 58.5 or 86.5 keV transitions in ^{252}Cf SF data. A partial coincident γ-ray spectrum is shown in Fig. 4. 5. 15 (a). In this spectrum with a gate on two new transitions in band (3) one can clearly see the 86.5 keV transition, three other new transitions and Y partner transitions. The 179.2 keV transition labeled in the spectrum is a new one in ^{100}Y. The work including the new level scheme of ^{100}Y will be published later.

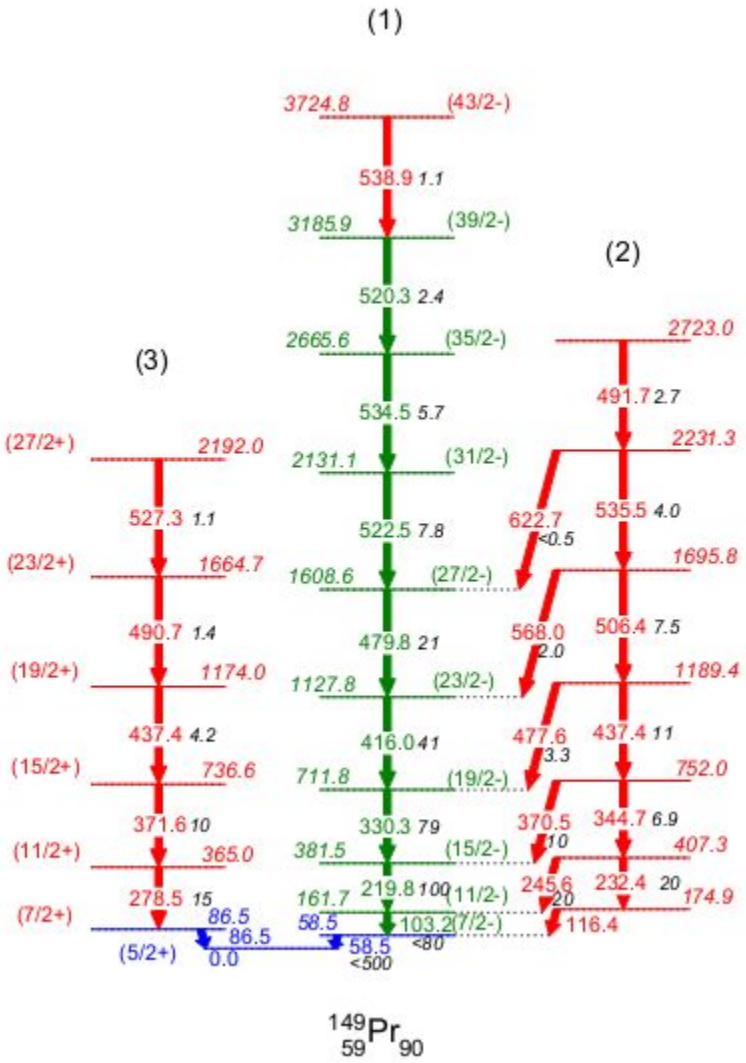

Fig. 4. 5. 13. The new level scheme of ^{149}Pr in the present work. Transitions and levels previously reported in β-decay work are labeled in blue. Those reported by Hwang [90] are labeled in green. New ones are labeled in red.

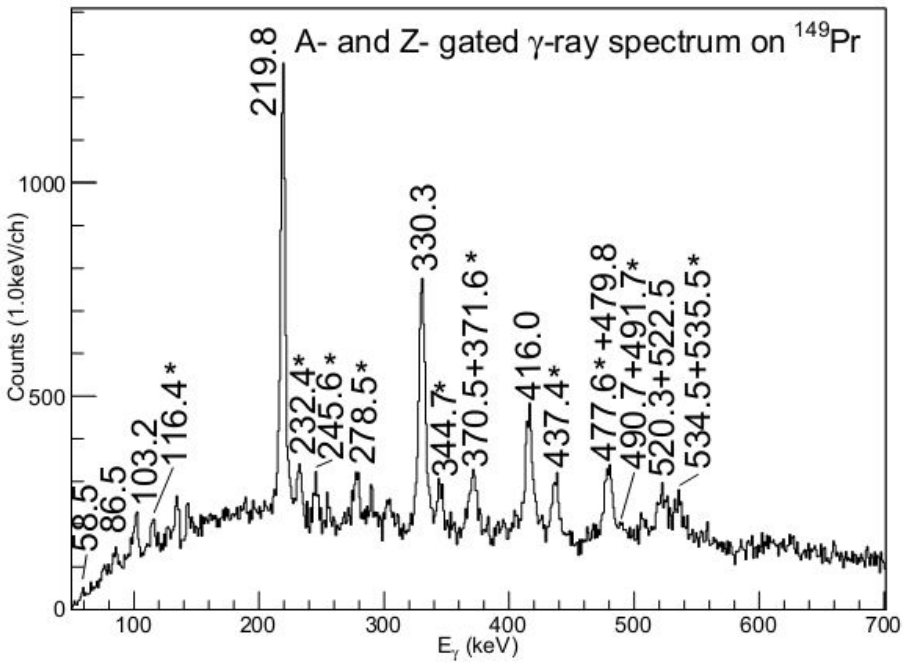

Figure 4. 5. 14. Partial ^{149}Pr mass- and Z- gated γ-ray spectra obtained from ^{238}U + ^{9}Be induced fission data. New transitions are labeled with an asterisk.

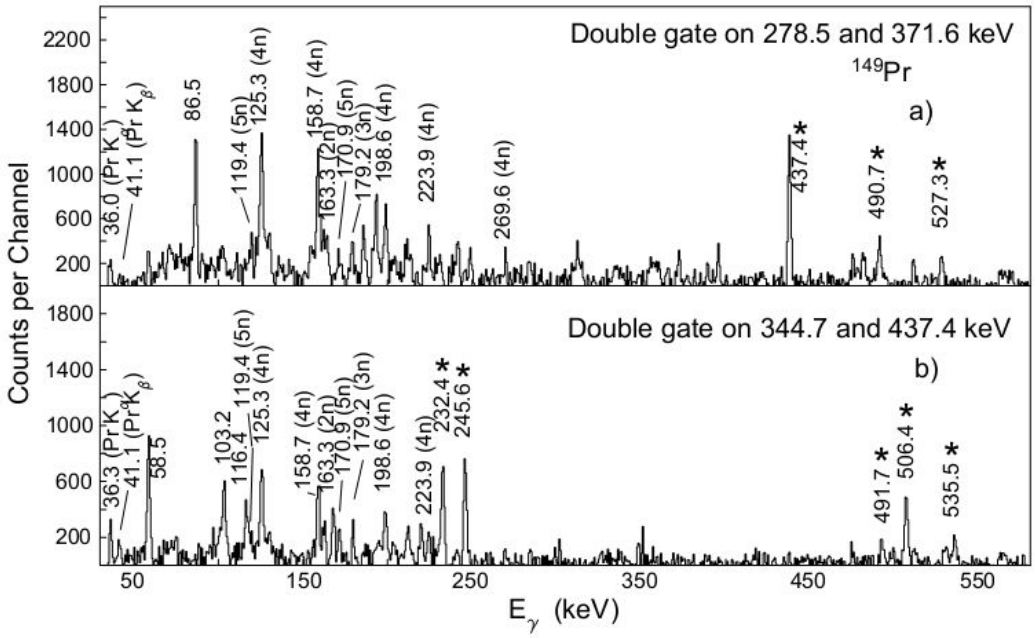

Fig. 4. 5. 15. Partial γ-ray coincidence spectrum by gating on a) 132.1 and 290.5 keV transitions and b) 344.7 and 437.4 keV transitions in ^{149}Pr from ^{252}Cf SF data. New transitions are marked with an asterisk. In the spectrum, transitions in Y fission partners are indicated with neutron evaporation numbers.

Another partial coincident γ-ray spectrum is shown in Fig. 4. 5. 15(b). In this spectrum with gate on two new transitions in band (2) one can clearly see the 58.5, 103.2 keV transitions, six other new transitions and Y partner transitions. By gating on these new transitions and analyzing the relative γ-transition intensities, these two new bands areproposed for ^{149}Pr.

Spins and parities of levels in band (1) were tentatively assigned in Ref. [92]. by an internal conversion coefficient measurement and theoretical calculations. Those results are adopted in this paper. Based on the regular energy spacings and γ-ray intensities, the new level at 3724.8 keV is assigned to $43/2^-$.

The total internal conversion coefficient of the 86.5 keV transition in ^{149}Pr has been measured from the intensity ratio between the 86.5 and 278.5 keV transitions in the coincident spectrum gated on 371.6 and 437.4 keV transitions above them. The value obtained was 1.63(22), and in agreement with the theoretical calculated value of 1.96 [104] for a M1 transition (E2=3.58).

A quasiparticle-rotor model (QPRM) calculation [92] and a combination of quasiparticle phonon model (QPM) + particle-rotor model (PRM) calculation [105] suggests a π5/2[413] configuration for the ^{149}Pr ground state level. The lowest three exited level energies at 86.5, 365.0, 736.6 of band (2) in ^{149}Pr are also reasonably consistent with the QRPM calculations of $7/2^+$, $11/2^+$ and $15/2^+$ for the states at 87, 342 and 708 keV, respectively in Ref. [92]. Therefore, the spins and parities of exited states in band (2) are tentatively assigned as 7/2+, 11/2+, 15/2+, 19/2+, 23/2+ and 27/2+ in the present work.

^{150}Pr

The new level scheme for ^{150}Pr is shown in Fig. 4. 5. 16. Bands (1) and (4) were previously assigned to ^{150}Pr by our group [90, 91] from the SF work of ^{252}Cf. In this earlier work, the relative yield ratios of partner Y isotopes were measured [91]. The transitions previously assigned to ^{150}Pr along with several new ones are shown in the mass-Z gated spectrum (Fig. 4. 5. 17). Fig. 4. 5. 18 (a) shows a coincidence spectrum double-gated on the new 190.2 and 254.6 keV transitions. Fig. 4. 5. 18 (b) shows a

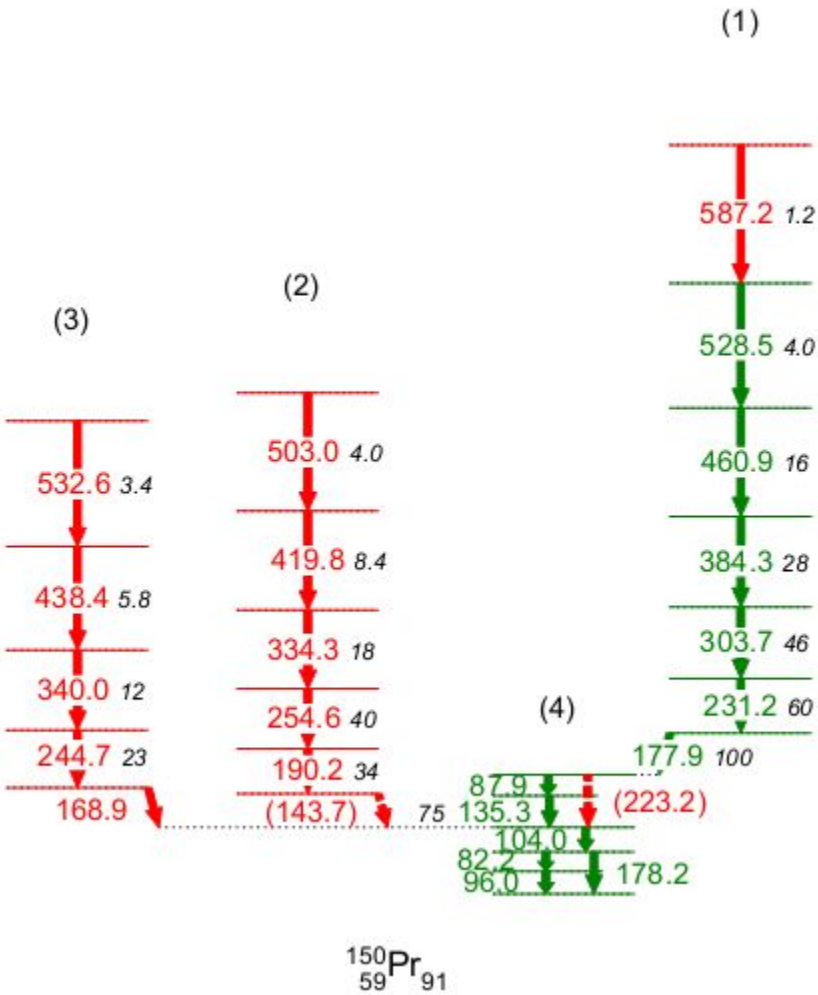

Fig. 4. 5. 16. The new level scheme of ^{150}Pr in the present work. Transitions and levels previously reported by Hwang [90, 91] are labeled in green. New ones are labeled in red.

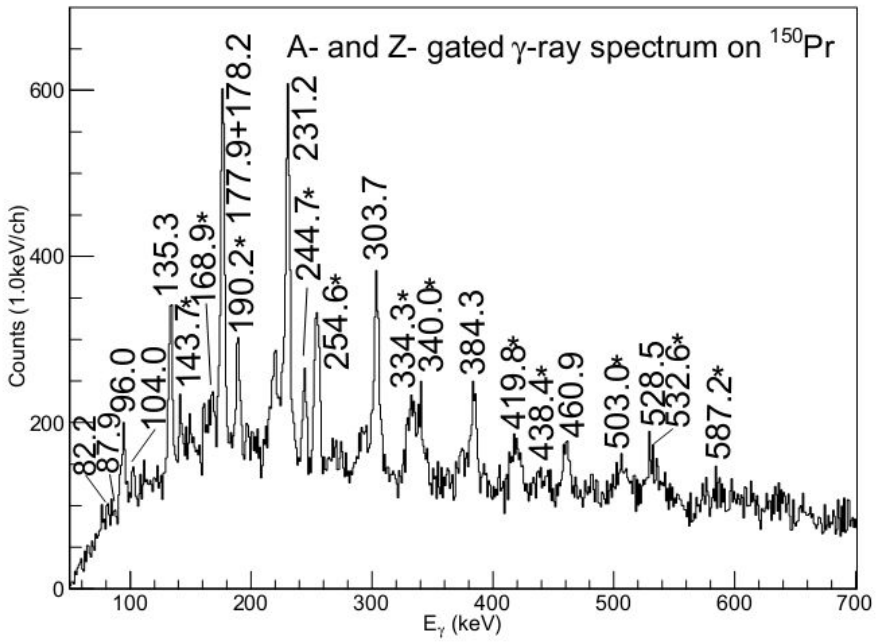

Figure 4. 5. 17. Partial ^{150}Pr mass- and Z- gated γ-ray spectra obtained from ^{238}U + ^{9}Be induced fission data. New transitions are labeled with an asterisk.

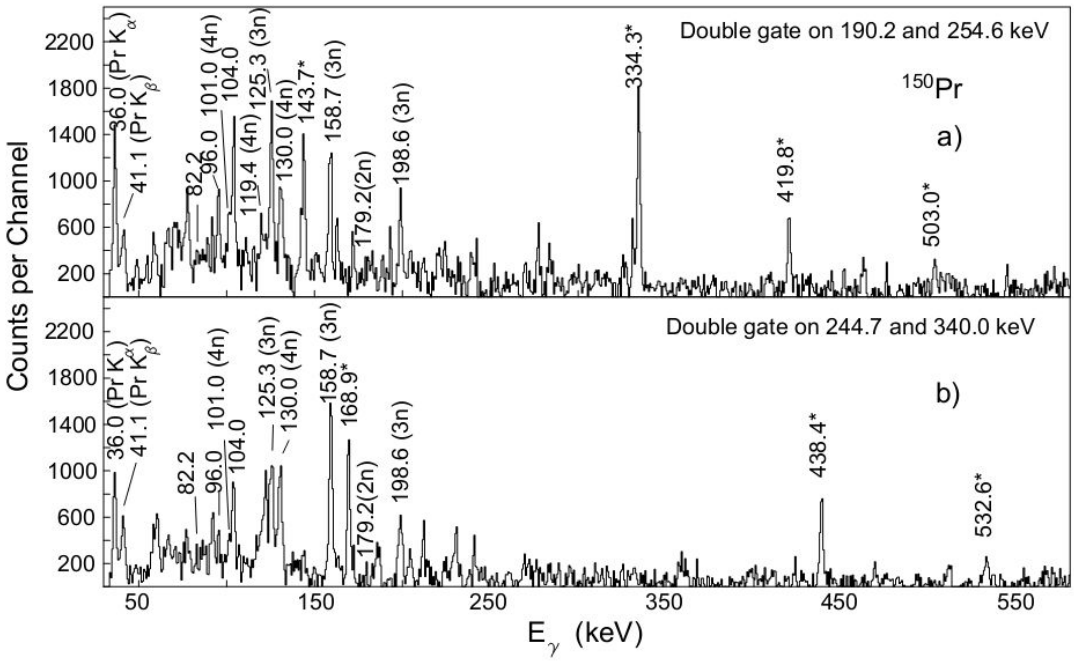

Figure 4. 5. 18. Partial γ ray coincidence spectra by a) gating on 190.2 and 254.6 keV transitions, and b) by gating on 244.7 and 340.0 keV transitions in ^{150}Pr from ^{252}Cf SF data. New transitions are marked with asterisk. In the spectrum, transitions in Y fission partners are indicated with neutron evaporation numbers.

coincidence spectrum double gated on the new 244.7 and 340.0 keV transitions. The previously known γ-transitions of 96, 82.2 and 104.0 keV of ^{150}Pr and the γ-transitions in the partner Y isotopes can be seen in these spectra. Therefore, these new transitions are assigned to ^{150}Pr in the present work. The new 334.3, 419.8 and 503.0 keV transitions are coincident with the new 190.2 and 254.6 keV transitions in Fig. 4. 5. 18 (a). Also, the new 438.4 and 532.6 keV transitions are coincident with the new 340.7 and 244.7 keV transitions in Fig. 4. 5. 18 (b). By using these coincidence relationships in multiple gates, bands (2) and (3) were found as shown in Fig. 4. 5. 16. The 143.7 keV transition was dashed because the intensity is weaker than that of the 190.2 keV one.

^{151}Pr

The new level scheme for ^{151}Pr is shown in Fig. 4. 5. 19. The ^{151}Pr mass and Z gated spectra obtained from ^{238}U + ^{9}Be induced fission are shown in Figs. 4. 5. 20(a) and (b). Bands (1) and (2) in Fig. 4. 5. 19 were assigned previously to ^{151}Pr by our group [91]. In this earlier work, the relative yield ratios of partner Y isotopes were measured. However, bands (1) and (2) were assigned separately to ^{152}Pr and ^{154}Pr, respectively, by Malkiewicz [94].The previously reported γ-transitions in bands (1) and (2) [91] are confirmed from the mass and Z gated spectrum in Fig. 4. 5. 20(a). In the present work, the 204.2 and 41.9 keV transitions are replaced with the new 214.6 and 52.3 keV transitions in bands (1) and (2) of Fig. 4. 5. 19. Also, a possible new 143.1 keV transition is added. Previously, bands (3) and (4) were assigned to ^{152}Pr by our group [93].

Then band (3) was assigned to ^{151}Pr and band (4) to ^{153}Pr from the SF work of ^{248}Cm and ^{252}Cf [94]. Now band (3)and band (4) in Fig. 4. 5. 19 are assigned to ^{151}Pr in the

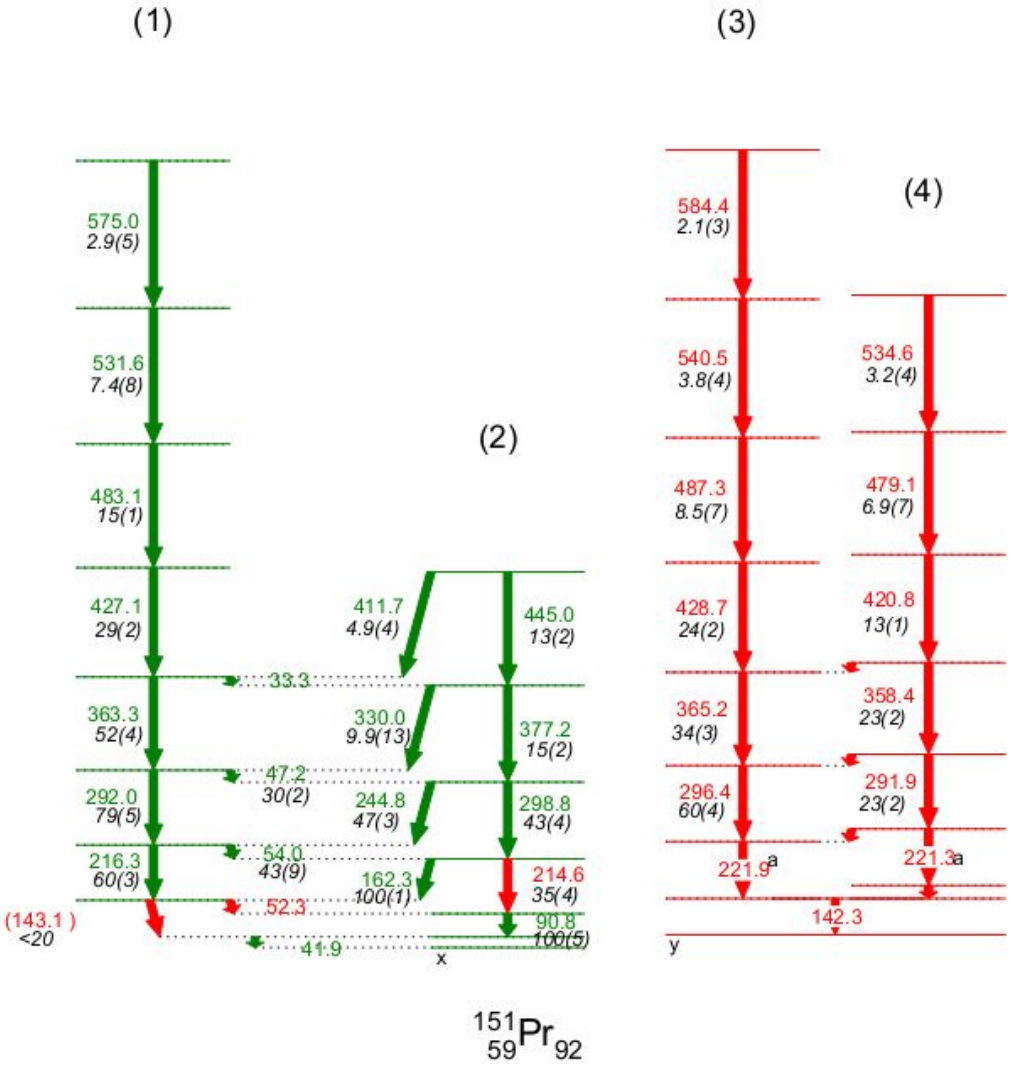

Fig. 4. 5. 19. The new level scheme of ^{151}Pr in the present work. Transitions and levels previously reported by Hwang [91] are labeled in green. New ones are labeled in red. a: the 221.9 + 221.3 keV transitions have the relative intensity of 100.

present work because the 142.3, 221.3+221.9, 296.4, 291.9, 365.2 and 358.4 keV transitions are seen in the ^{151}Pr mass and Z gated spectra in Figs. 4. 5. 20 (a) and (b). The 221.3 and 221.9 keV transitions were reported earlier as one 221.9 keV transition by our group [93]. Later, the 142.3 keV transition in Ref. [93] was separated into 142.1 and 141.6 keV transitions in Ref. [94]. The 221.9 keV transition in Ref. [93] was separated

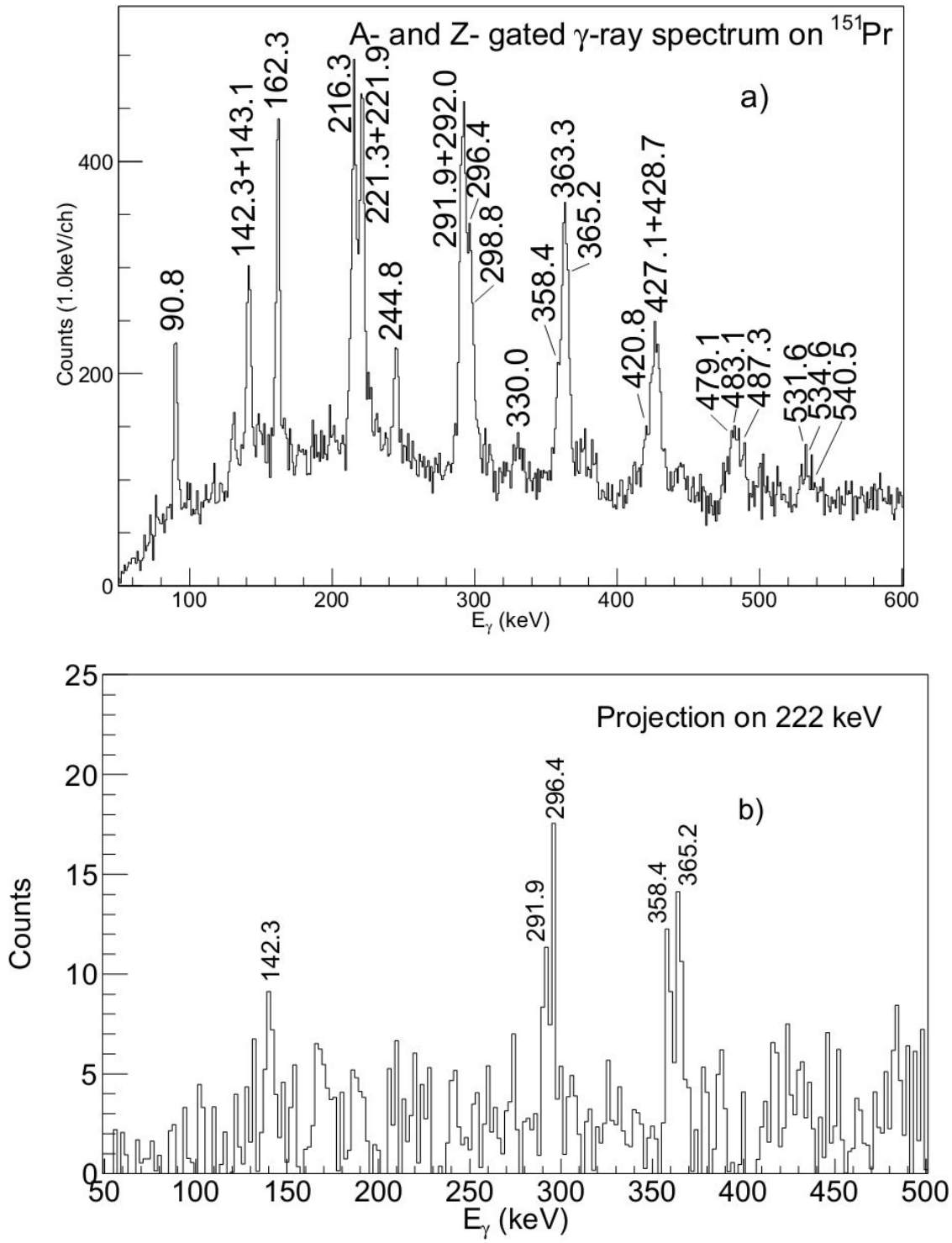

Figure 4. 5. 20. Partial ^{151}Pr mass- and Z- gated γ-ray spectra obtained from ^{238}U + ^{9}Be induced fission data. Part (a) is a single γ-ray spectrum. Part (b) is a projection spectrum on 222 keV.

into 221.8 and 221.0 keV transitions in Ref. [94]. In this paper, a shift of about 0.6 keV of the 221.9 keV peak has been confirmed by comparing the gates between bands (3) and (4), for example, double gates on 296.4 and 356.2 keV in band (3), 291.9 and 358.4 keV in band (4), triple gates on 296.4,356.2 and 428.7 keV in band (3), 291.9, 358.4 and 420.8 keV in band (4). But no visible energy difference of the 142.3 keV transition is seen when comparisons are set between any of the gates in bands (3) and (4). Thus, two different 221.9 and 221.3 keV transitions are proposed but there is only one 142.3 keV transition in the level scheme. In the present work all of bands (1), (2), (3) and (4) are definitely assigned to ^{151}Pr, as shown Fig. 4. 5. 19. Further analysis about the mass assignment will be presented in the ^{152,153}Pr and discussion sections. Previously, conversion coefficient measurements established the 47.2 and 54.0 keV transitions as E1 and the 90.8 keV one as M1 [91]. The value of the 90.8 keV one was obtained from the 90.8 and 292.0 keV transition intensities in the coincidence spectrum gated on 216.3 and 363.3 keV in Ref. [91]. This measurement did not include the contribution of the 47.2 one. If this contribution is taken into account, the internal conversion value will increase by a factor of ~20%, which will make it closer to the theoretical M1 value.

Fig. 4. 5. 21(a) is a coincidence spectrum from ^{252}Cf SF data by gating on 216.3 and 292.0 keV transitions showing the new 52.3 and 143.1 keV transitions. The peak around 41 keV is an overlap of a 41.9 keV γ transition and 41.0 keV Pr X-ray. Therefore, the energy of the 41.9 keV transition has a relative large uncertainty and might range from 39 to 42 keV. The 143.1 keV transition is much weaker than the 90.8 keV one and was dashed in the level scheme. Fig. 4. 5. 21(b) is a coincidence spectrum from ^{252}Cf SF data triple gated on 298.8, 377.2 and 445.0 keV transitions. The interference from another

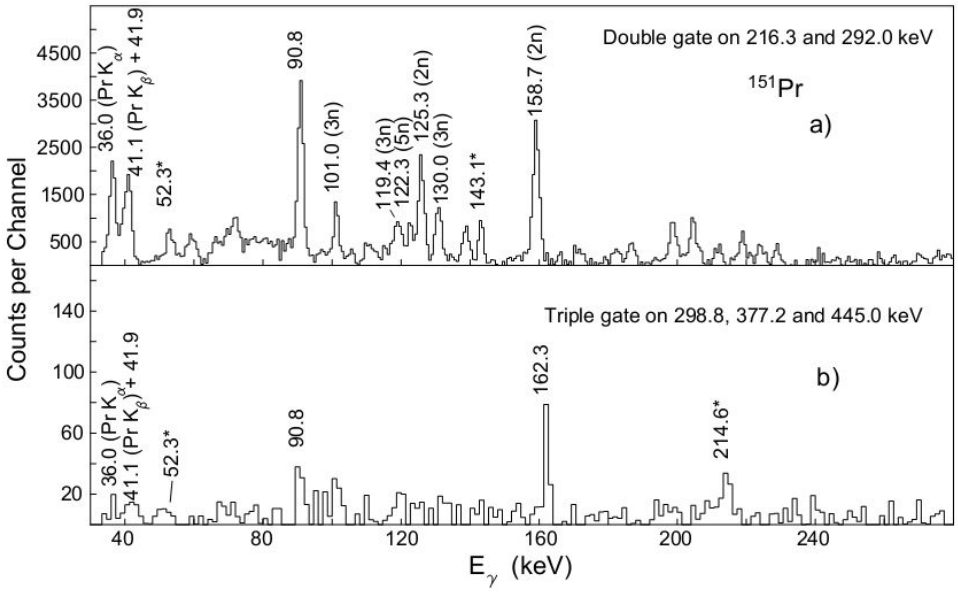

Figure 4. 5. 21. Partial γ-ray coincidence spectra (a) by gating on 216.3 and 292.0 keV transitions, and (b) by gating on 298.8, 377.2 and 445.0 keV transitions in ^{151}Pr from ^{252}Cf SF data. Transitions in Y fission partners are indicated with neutron evaporation numbers. New transitions have an asterisk.

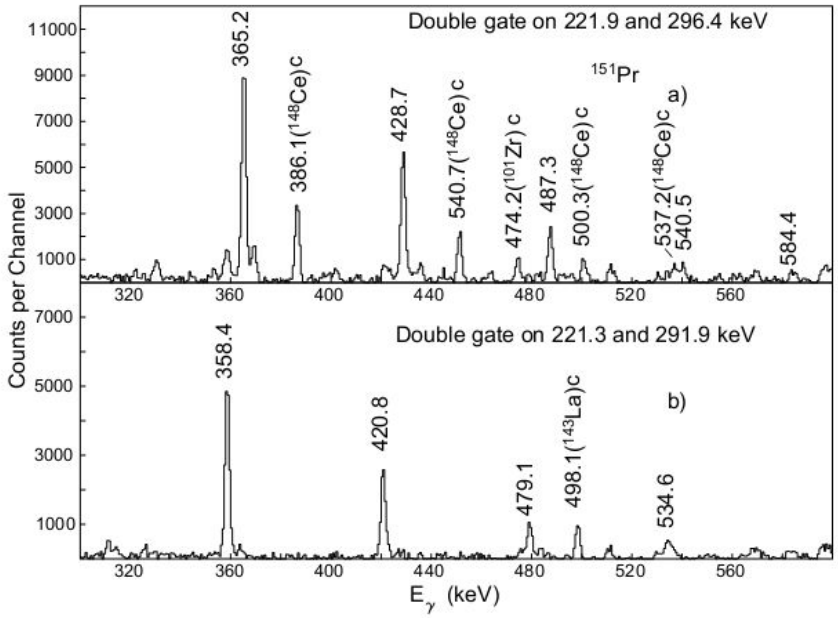

Figure. 4. 5. 22. Partial γ-ray coincidence spectra (a) by gating on 221.9.3 and 296.4 keV transitions, and (b) by gating on 221.3 and 291.9 keV transitions in ^{151}Pr from ^{252}Cf SF data. Contamination transitions are labeled with a letter c.

strong transition of 216.3 keV in ^{151}Pr was eliminated from this gate in order to give the evidence for the 214.6 keV one. The 204.2 keV transition is not seen compared to 214.6 keV in this gate, which suggest some contamination at 204.2 keV in the spectrum of the previous work (Ref. [91]). Thus, the 204.2 keV transition is replaced by the 214.6 one in the present work.

The analysis result for γ transition intensities are also labeled in the level scheme. The intensities have been separated into two parts. The intensities of transitions in band (1) and band (2) are normalized to the 162.3 keV transition and that in band (3) and band (4) are normalized to the summation of 221.9 and 221.3 keV transition intensities.

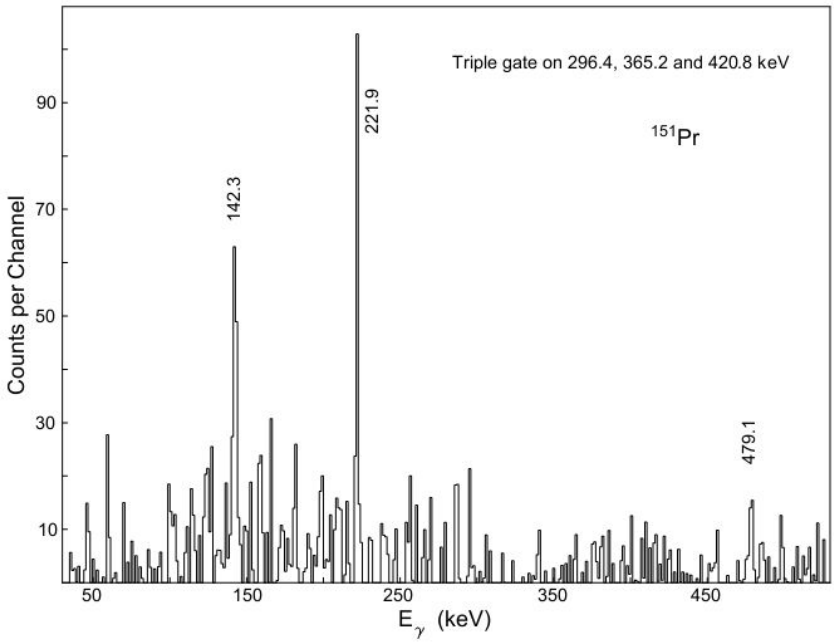

Figure 4. 5. 23. Partial γ-ray coincidence spectrum by gating on 296.4, 365.2 and 420.8 keV transitions.

Fig. 4. 5. 22(a) is a coincidence spectrum from ^{252}Cf SF data by gating on 221.9 and 296.4 keV transitions. The 365.2, 428.7, 487.3, 540.5 and 584.4 keV transitions in band 3 can be seen. The contamination transitions in this spectrum mainly come from the

coincidence of the 223.0 keV transition depopulating the 320.8 keV level in ^{101}Zr and the 295.4 keV transition depopulating the 454.1keV level in fission partner ^{148}Ce. Thus, contamination transitions in ^{101}Zr and ^{148}Ce can be seen. Fig. 4. 5. 23(b) is a coincidence spectrum from ^{252}Cf SF data by gating on 221.3 and 291.9 keV transitions. The 358.4, 420.8, 479.1and 534.6 keV transitions in band 4 can be seen. The contamination transitions in this spectrum mainly come from the coincidence of the 220.6 keV transition depopulating the 511.0 keV level in ^{105}Nb and the 291.3 keV transition depopulating the ground state in its fission partner ^{143}La. Thus, the labeled contamination transition in ^{143}La can be seen.

The present level scheme of ^{151}Pr contains a very low energy unobserved transition between the 142.3 and 221.3 keV ones in band (4) and other three very low energy transitions linking band (4) and band (3), which were not proposed in the previous work [93]. The four fold ^{252}Cf SF data gives the evidence of these low energy transitions. In Fig. 4. 5. 23 a coincidence spectrum gating on the 296.4 and 365.2 keV transitions in band (3) and a 420.8 keV transition in band (4), shows the 142.3 keV transition in band (3) and 479.1 keV transition in band (4). This spectrum confirms the coincidences among the 142.3, 221.9, 296.4, 365.2, 420.8 and 479.1 keV transitions. Similarly, the coincidences among the 142.3, 221.9, 296.4, 291.9, 358.4, 420.8 and 479.1 keV transitions are confirmed from the four fold ^{252}Cf SF data. The data indicate the existence of a very low energy transition between the 142.3 and 221.9 keV ones to lift up the whole band (4). The ^{252}Cf SF data also provide some weak evidence of a 59 keV transition lying below the 142.3 keV one, which is not placed in the level scheme.

We suggest that all four bands arise from the odd-proton being in the 1/2+[420]

Nilsson orbital. The signature splitting for both band pairs is that characteristic of a j=1/2 orbital, where the particle j value is completely decoupled from the spheroidal shape. The same pattern of doublets, however, could come from the odd-proton in the $1/2^{+}$[420] Nilsson orbital, where on the prolate side the wave function will be a mixture of g7/2 and d5/2, which will give rise to cancelling signature-splitting effects. The parities of the bands are not determined, but combined bands (1) and (2) are of the same parity, and bands (3) and (4) of the opposite parity. These opposite parity bands arise from doubling due to some octupole shape terms (pear shape) in nuclear shape due to Y3,0 mixing between orbitals of the same K and opposite pairing near the Fermi energy. The level scheme of Fig. 4. 5. 13 for ^{149}Pr is similar to that of ^{151}Pr except that one of the four bands is not observed. With only a small shift in the decoupling parameter one of the bands could be unpopulated, leaving only one band cascading by E2 transitions.

^{152}Pr

The new level scheme for ^{152}Pr is shown in Fig. 4. 5. 24. All levels and transitions are newly established in the present work except for the 114.8 and 98.1 keV transitions, which are identified by ^{152}Ce β- decay [106]. Fig. 4. 5. 25 is specific ^{152}Pr mass- and Z-gated single γ spectrum from ^{238}U + ^{9}Be induced fission data, showing the evidence for the mass assignment for these three new bands. All the strong transitions in these three bands can be seen. Also the 221.3, 221.9, 358.4 and 365.3 keV transitions are not seen in mass 152 gated Fig. 4. 5. 25 like they are in mass 151 gated Figs. 4. 5. 20 (a), (b). Thus, the 142.3-221.9-296.4 (^{151}Pr) and 142.3-221.3-292.0 keV cascades do not belong as previously reported in ^{152}Pr but in ^{151}Pr and the latter does not belong to ^{153}Pr as recently

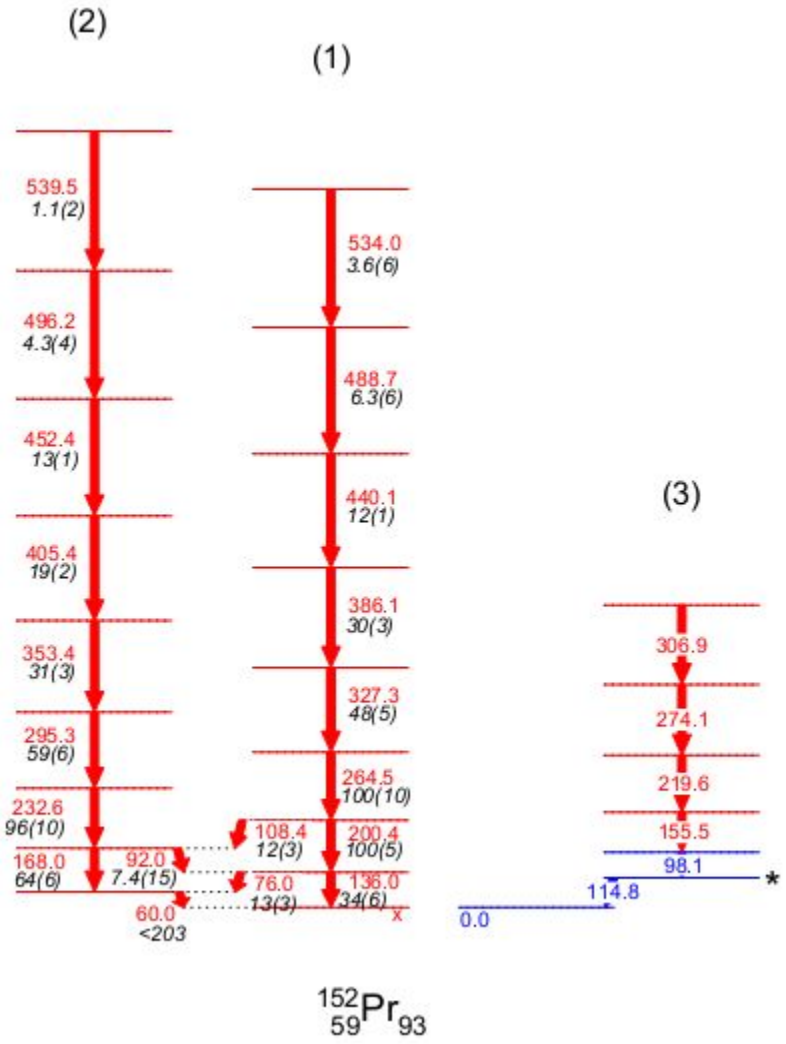

Fig. 4. 5. 24. The new level scheme of ^{152}Pr in the present work. Transitions and levels previously reported in β decay work [106] are labeled in blue .New ones are labeled in red. * This level is an isomer with a 4.1 μs lifetime according to the measurement in Ref. [106].

reported [94]. The position of the 162.3 keV transition in ^{151}Pr (100 relative intensity) is labeled in Fig. 4. 5. 25. The absence of the 162.3 keV peak indicates band (1) assigned to ^{151}Pr in this work does not belong to ^{152}Pr as recently reported by Malkiewicz [94] and the current ^{151}Pr M/Z gated spectrum is a clean Z gate. Those facts gives further evidence for the mass assignment for the four bands in ^{151}Pr in the present work. Further analysis

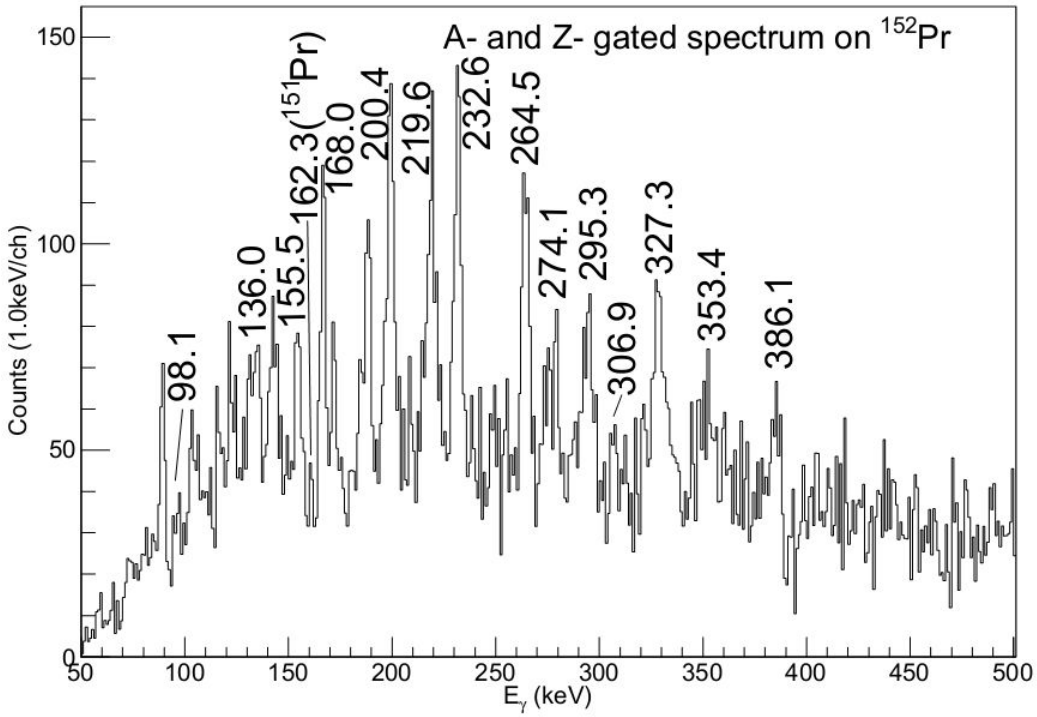

Fig. 4. 5. 25. Partial ^{152}Pr mass- and Z- gated γ-ray spectrum from ^{238}U + ^{9}Be data. Note the absence of the 114.8 keV isomeric transition.

of the mass assignments will be reported in the ^{153}Pr and discussion sections.

Fig. 4. 5. 26 (a) shows a coincidence spectrum from the ^{252}Cf SF data by double gating on 264.5 and 327.3 keV transitions. The 136.0, 200.4, 386.1, 440.1, 488.7 and 534.0 keV transitions in band (1) and 60.0, 76.0, 92.0, 108.4 keV linking transitions between band (1) and band (2) can be seen. Fig. 4. 5. 22 (b) shows a coincidence spectrum from the ^{252}Cf SF data by triple gating on 232.6, 295.3 and 353.4 keV transitions, where 168.0, 405.4, 452.4, 496.2 and 539.5 keV transitions in band (2) and 60.0, 76.0, and 92.0 linking transitions between band (1) and band (2) can be seen. Fig. 4. 5. 22 (c) shows a coincidence spectrum from ^{252}Cf SF data by triple gating on 219.6, 274.1 and 306.9 keV transitions, where 98.1 and 155.5 keV transitions in band (3) can be seen. The 114.8 keV transition is not observed in the current work since the electronic

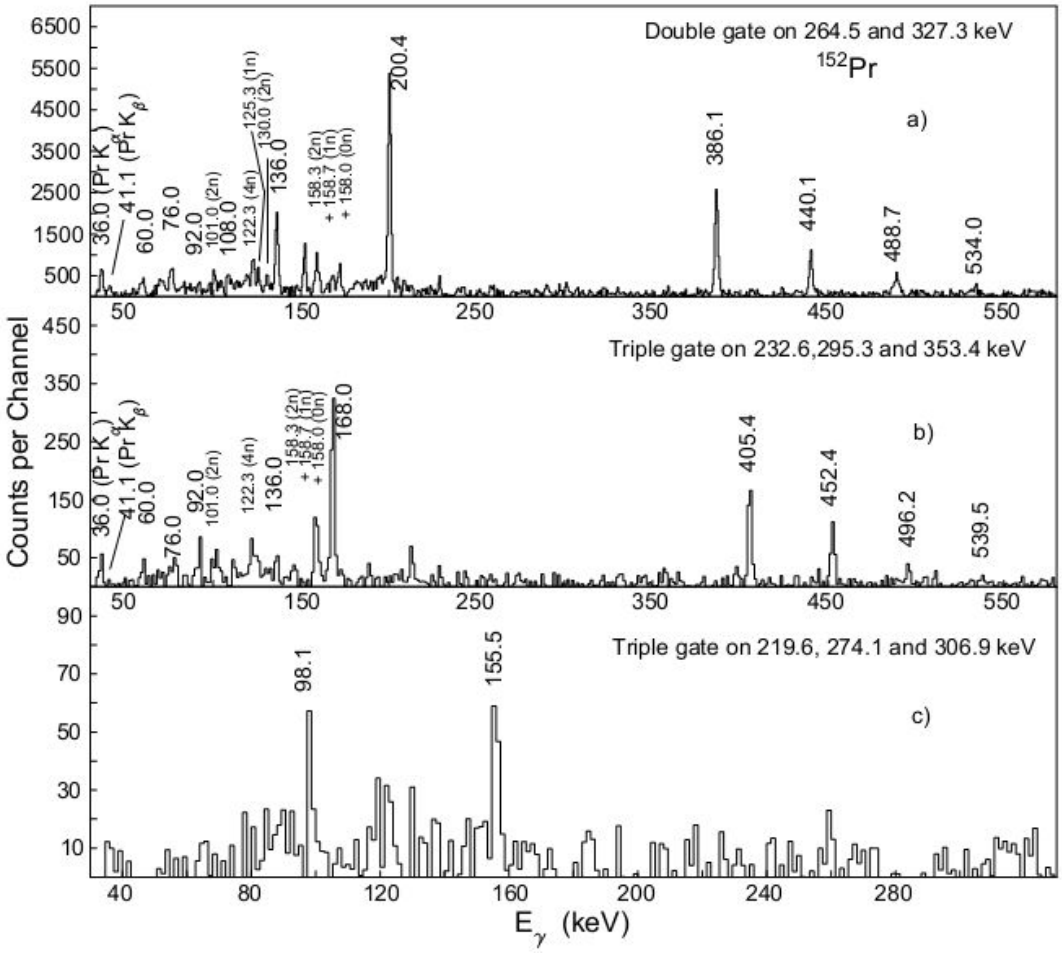

Fig. 4. 5. 26. Partial γ-ray coincidence spectra (a) by gating on 264.5 and 327.3 keV transitions, (b) by gating on 232.6, 295.3 and 353.4 keV transitions, and (c) by gating on 219.6, 274.1 and 306.9 keV transitions in ^{152}Pr from ^{252}Cf SF data. Transitions belonging to Y fission partner are indicated with neutron evaporation numbers.

coincidence time window for the ^{252}Cf fission experiment is about 1 μs (several ns for VAMOS++ and EXOGAM), which is relatively smaller than the 4.1 μs life time [106] of the 114.8 keV level. The result for γ transition intensities are also given in the level scheme.

^{153}Pr

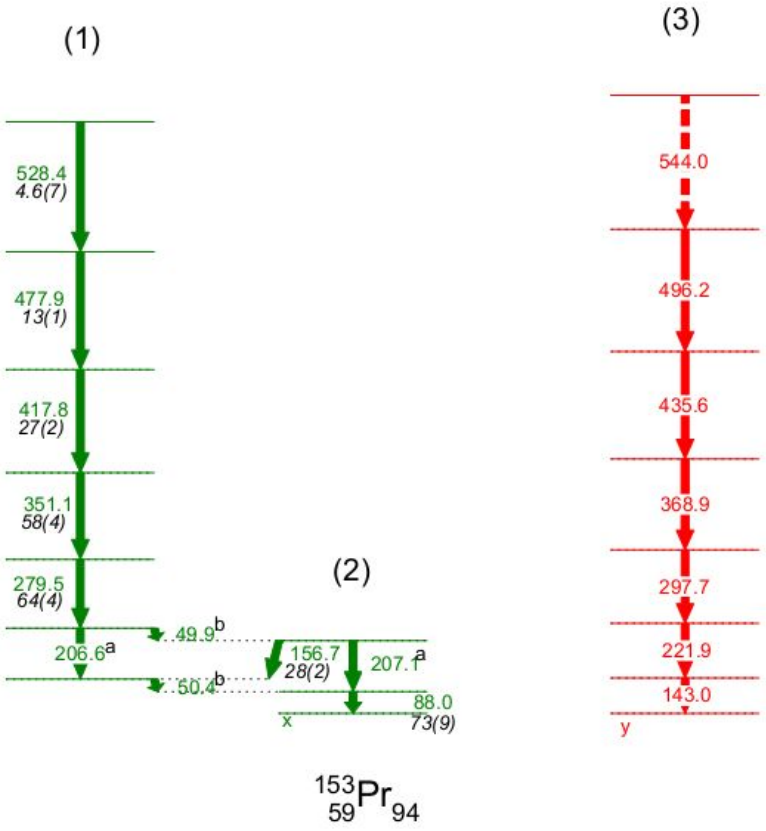

Fig. 4. 5. 27. The level scheme of ^{153}Pr in the present work. Transitions and levels previously reported by Hwang [91] are labeled in green. New ones are labeled in red. a: The 206.6+207.1 keV transitions have the relative intensity of 100. b: The 49.9+50.4 keV transition have the relative intensity of<127.

The new level scheme for ^{153}Pr is shown in Fig. 4. 5. 27. Band (1) transitions in this figure were assigned previously to ^{153}Pr by our group [91], but were assigned, recently, to ^{154}Pr from the SF work of ^{248}Cm and ^{252}Cf [94]. In the earlier work, the relative yield ratios of partner Y isotopes were measured [91]. The ^{153}Pr mass and Z gated spectra obtained from ^{238}U + ^{9}Be induced fission are shown in Fig. 4. 5. 28. The previously reported γ-transitions of 88.0, 156.7, 206.6, 279.5, 351.1, 417.8 and 477.9 keV transitions

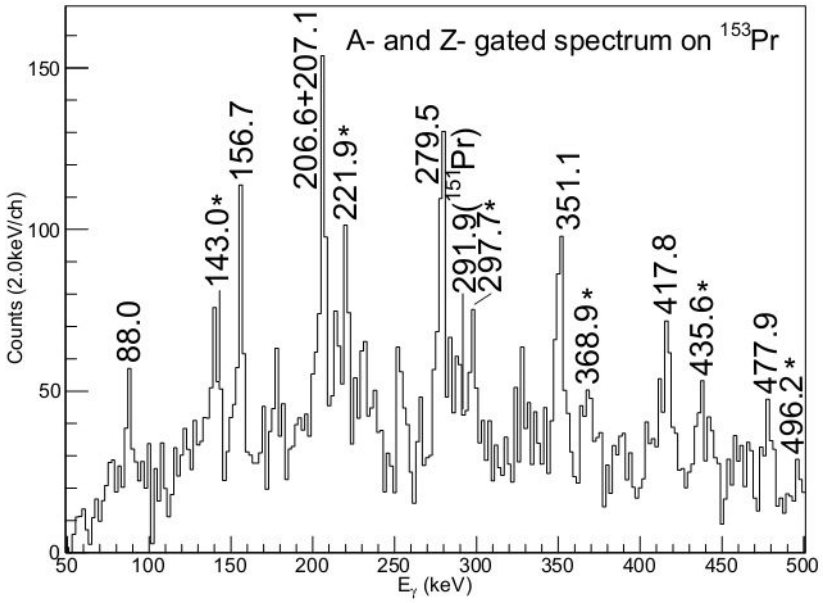

Fig. 4. 5. 28. Partial ^{153}Pr A- and Z- gated γ-ray spectrum from ^{238}U + ^{9}Be data. Note the absence of the 114.8 keV isomeric transition. New transitions are labeled with an asterisk.

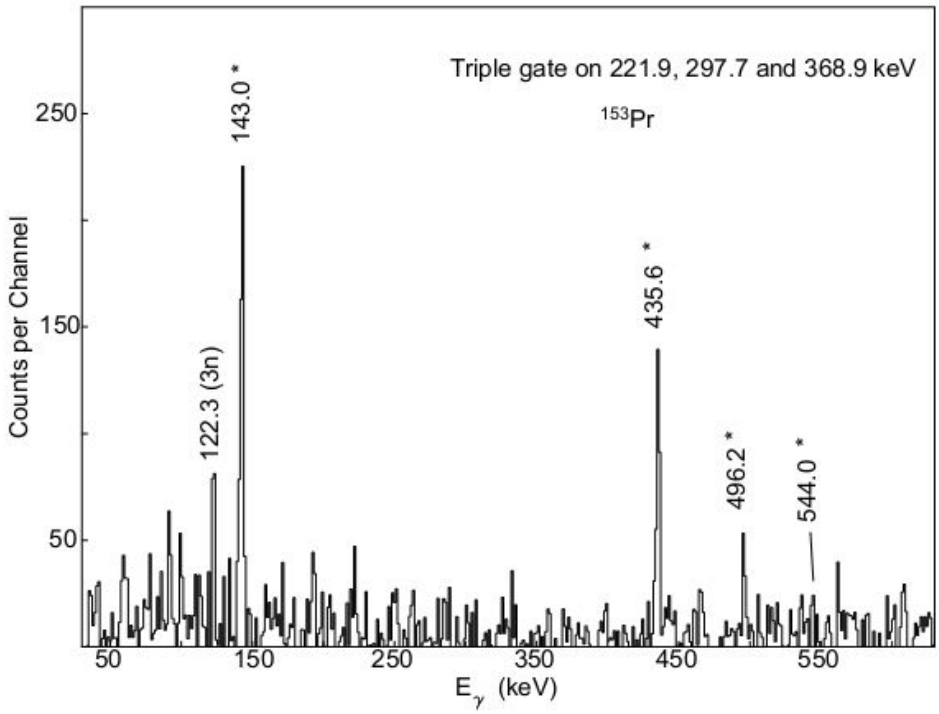

Fig. 4. 5. 29. Partial γ-ray coincidence spectra by gating on 221.9, 297.7 and 368.9 keV transitions in ^{153}Pr from ^{252}Cf SF data. Transitions belonging to Y fission partner are indicated with neutron evaporation numbers.

in ^{153}Pr [91] are confirmed from the mass and Z gated spectrum in Fig. 4. 5. 28. The 142.3, 221.3 and 292.2 keV cascade previously assigned to ^{153}Pr by Malkiewicz et al [94] is not confirmed by the mass and Z gated spectrum in Fig. 4. 5. 28 because the 292.2 keV transition is not observed in the spectrum. Instead, a new cascade with 143.1, 221.9 and 297.7 keV transition can be seen in the spectrum. Further analysis about the mass assignment will be reported in the discussion part.

The previously assigned 51.7, 227.8 and 277.7 keV transitions are not placed in Fig. 4. 5. 27 because these transitions are not clearly seen in our work. Furthermore, the 227.8 keV transition is not observed in the 206.6 and 969.1 keV (a fission partner ^{95}Y transition [107]) double gate and the 206.6 and 417.8 keV double gate. Thus, the previously reported 13/2 level and its three transitions are tentatively deleted from the level scheme. The results for γ transition intensities are shown in the level scheme. Previously conversion coefficient measurements established the 50.4 keV transition as E1 and the 88.0 keV one as M1 [91]. Fig. 4. 5. 29 shows a coincidence spectrum from ^{252}Cf SF data by gating on the 221.9, 297.7 and 368.9 keV transitions. In this gate, four other γ-ray transitions in band (3) can be seen. This gate might contain some components from the 141.1 (1683.0 to 1542.1 keV level) -222.0-298.1-369.5-423.9 keV cascade in ^{152}Nd. However, the 423.9 keV transition in ^{152}Nd is not clearly seen in the mass/Z gated spectra on ^{153}Pr as the 435.6 keV one. Moreover, the 122.3 keV fission partner transition in ^{96}Y in Fig. 4. 5. 25 also provide evidence for these ^{153}Pr transitions.

Discussion

To further verify the mass assignments obtained above, the relative yield curves of

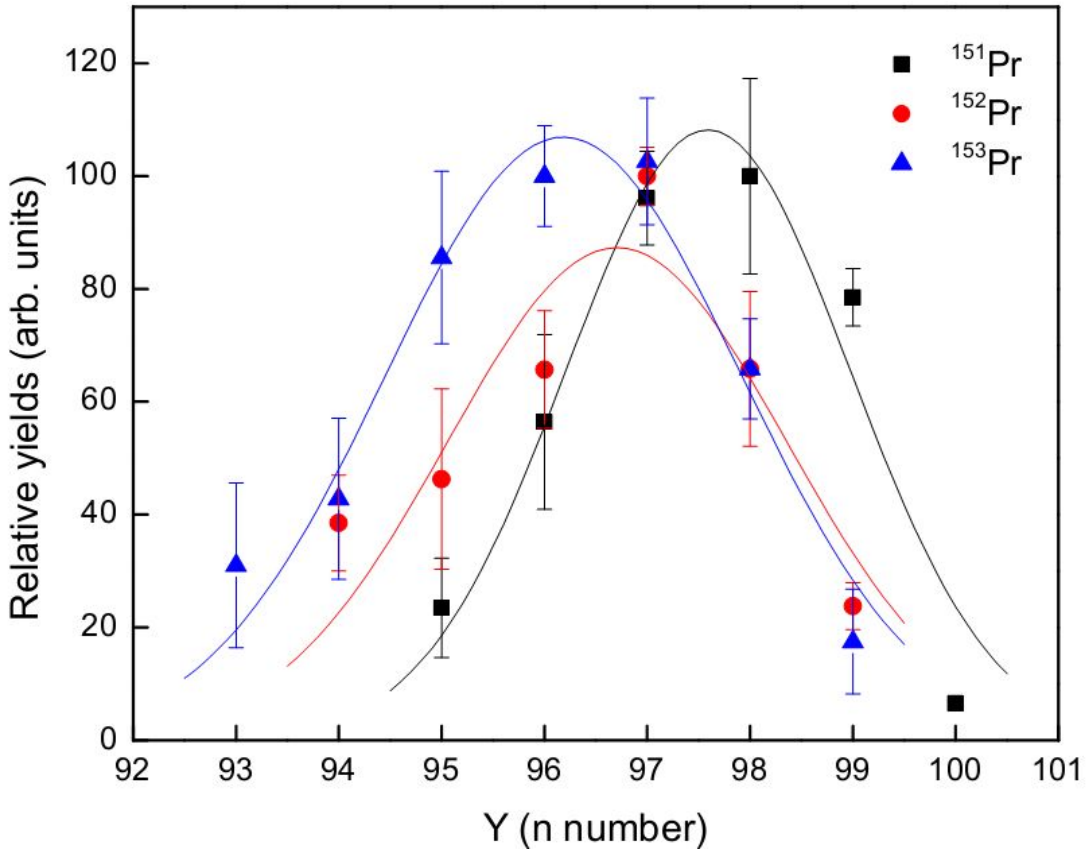

Fig. 4. 5. 30. Relative yield curves of yttrium by gating on transitions in ^{151}Pr (black square symbol), ^{152}Pr (red circular symbol) and ^{153}Pr (blue triangular symbol) from ^{252}Cf SF data. Each Pr gate yield set are normalized to the highest Y yield for comparison. The gaussian fittings for Pr gate are also shown as lines in the same colors.

the yttrium partner isotopes coincident with ^{151,152,153}Pr were measured. Fig. 4. 5. 30 is a set of Y yield curves measured by double or triple gating on transitions in $^{151\text{-}153}$Pr. The intensity summations of all the observable transitions which directly feed the ground state were used as a representative of the respective Y yields. The ^{97}Y isotope has an isomeric state at a level energy of 667.5 keV (1.17s). Therefore, the intensity summation of two transitions (668.6 and 989.9 keV), which feed the 667.5 keV state, was used instead. In the ^{252}Cf binary spontaneous fission, a pair of correlated partners is produced and followed by neutron emission after fission. The yield is generally maximized at the 3n or

4n channel. In Fig. 4. 5. 30, the highest yields were populated at around $^{98, 97, 96}$Y for $^{151, 152, 153}$Pr respectively, which are all 3n reaction channels for these Pr isotopes. Further gaussian fitting analysis for the curves indicate that the fitting peaks for the ^{151,152,153}Pr are located at the respective 3.4, 3.3 and 2.8n channel. These yield distribution curves of the Y partner isotopes support the mass assignments of levels in ^{151,152,153}Pr in the present work.

For odd A Pr isotopes in the present study, the strongest bands, including the possible new band in ^{145}Pr, the new band in ^{147}Pr, bands (1) in ^{149,151,153}Pr, are not similar except for ^{151}Pr and ^{153}Pr. This phenomenon is reasonable because the neighboring Ce and Nd isotopes imply a transition region from spherical to rigid deformed. As discussed in section 4. 4, the critical point is located at about N=90. In our previous work, the negative band in ^{149}Pr was interpreted as a $h_{11/2}$ band [90] and the 58.5 keV band-head was assigned to $11/2^-$. This assignment might be questionable because ^{149}Pr with N=90 may not be nearly spherical. Later in Ref. [92], the ground state in ^{149}Pr was assigned to $5/2^+$ with 49% of 5/2[413] and 43% of 3/2[422] calculated components. The 58.5 keV level was assigned to $7/2^-$ with 81% of 1/2[550] component. Then in Ref. [105], calculation predicted 58% of 5/2[413] and 21% of 3/2[411] for the ground state and 77% of 1/2[550] for the 58.5 keV state. The calculation in Ref. [92] can reproduce levels in bands (1) and (3) in ^{149}Pr at low spin but not the bending at high spin.

In the previous reported transitions in ^{151}Pr from β decay [108], the 38.9 (38.9 to 0), 40.6 (402.6 to 362.0), 142.1, 362.1 (362.0 to 0), 363.7 (402.6 to 38.9) and 428.8 (467.7 to 38.9) keV transitions have the similar energy to the transitions obtained in the present work. The 38.9 and 142.1 keV transitions are possible to be the same transition observed

in the present work.

Table 7. Comparison of the E2 transitions energies in bands 1, 2 and 3 in ^{149,151,153}Pr and the transition energy difference.

band 1 E2 energy			band 2 E2 energy			band 3 E2 energy		
^{149}Pr	^{151}Pr	^{153}Pr	^{149}Pr	^{151}Pr	^{153}Pr	^{149}Pr	^{151}Pr	^{153}Pr
103							142	143
220	216	207	232	215	207		222	222
330	292	280	345	299		279	296	298
416	363	351	437	377		372	365	369
480	427	418	506	445		437	429	436
523	483	478	536			491	487	496
535	532	528	492			527	541	544
520	575						584	
539								
band 1 ΔE2 energy			band 2 ΔE2 energy			band 3 ΔE2 energy		
117							80	79
110	76	73	113	84			74	76
86	71	71	92	78		93	69	71
64	64	67	69	68		65	64	67
43	56	60	30			54	58	60
12	49	50	-44			36	54	48
-15	43						43	
19								

A comparison of the proposed E2 transition energies and transition energy spacings in bands (1), (2) and (3) in ^{149,151,153}Pr is shown in Table 7. The similarity of the transition energies indicates similar structures of the nuclei. Moreover, bands (1) and (3) in ^{151,153}Pr are almost identical both in transition energy (less than 10 keV) and intensity up to very high spins. Such identical bands was also observed in ^{152,154,156}Nd, ^{153,155,157}Pm,

^{156,158,160}Sm, ^{155,157,159}Eu, ^{160,162,164}Gd, respectively. The ΔE2 energy shrinks somewhat more in ^{149}Pr and bending takes place at high spin. In contrast, the ΔE2 energies are similar and do not shrink much in ^{151,153}Pr, which indicates a relative more rigid rotor in these nuclei. An internal conversion measurement in Ref. [91] implied E1 interband transitions between band (1) and band (2) in ^{151}Pr. Therefore, there could be a small octupole deformation in ^{151}Pr. Bands (1) and (3) in ^{151}Pr and ^{153}Pr are quite similar while the coupled bands (2) and (4) in ^{151}Pr are not observed in ^{153}Pr. Therefore, ^{151}Pr and ^{153}Pr may have similar deformation and the same configuration for the respective bands. However, ^{151}Pr may lie on the verge of octupole deformation. If octupole deformation exists in ^{151}Pr, the band (3) in ^{149}Pr could be an ocupole band too. Note that ocupole correlations were reported in ^{147}La and ^{151}Pm. The TRS calculations by the Peking University group provide some evidence for octupole shape in ^{149}Pr but not for ^{151,153}Pr. However, such calculation cannot reproduce the 58.5 keV isomer (~20ns) in ^{149}Pr [90, 92] and 35.1 keV isomer (~50μs) in ^{151}Pr [94, 108]. These isomers both decay to the ground state by E1 transitions.

For even A Pr isotopes, their energy spacings indicate an increasing trend of deformation as N increases. This is consistent with systematics. In ^{150}Pr, band (1) does not show any trend of bending at the current observed levels (up to $\hbar\omega \approx 0.29$ MeV). This fact indicate the bending in ^{149}Pr at $\hbar\omega \approx 0.27$ MeV is probable caused by the alignment of a pair of neutrons. Since the configuration of the bands in ^{149,150}Pr is unknown, this speculation need further work. The behaviors of the dynamic moments of inertia of bands (1) and (3) in ^{150}Pr are quite different, while band (2) seems to lie between those. Thus, there might be shape coexistence and structure change between bands (1) and (2) in ^{150}Pr.

The configuration for ^{152}Pr is unknown. The available orbitals for Z=59 are $3/2^-[541]$, $1/2^+[420]$ and $3/2^+[422]$ [93, 94]. The available orbitals for N= 93 are $3/2^-[521]$ and $5/2^+[642]$ [93, 109].

More work on both experiment and theory is needed to understand the nuclear structure of $^{143\text{-}153}$Pr well.

4.6 New Transitions and Mass Assignments of ^{156,157}Pm

About 30 γ ray transitions in ^{156}Pm were identified in ^{156}Nd β decay work [110, 111]. But many of them were reported with no coincidence and not placed in the level scheme. Hwang *et al.* reported a rotational band in ^{156}Pm from ^{252}Cf SF data [112]. No transitions identified in β decay were confirmed in the latter work. For ^{157}Pm, no excited states were reported previously. In the current work, ^{252}Cf SF and ^{238}U+^{9}Be induced fission data have been combined to identify transitions in ^{156,157}Pm. The transitions and levels previously assigned to ^{156}Pm by Hwang *et al.* [112] are now assigned to ^{157}Pm by using the mass identification of the ^{238}U+^{9}Be data. New levels and transitions of ^{156,157}Pm are established. The ^{156}Pm transitions identified in the β decay work are still not observed in the current data.

^{156}Pm

The level scheme of ^{156}Pm obtained in the current work in shown in Fig. 4. 6. 1. All the transitions are newly identified. Note that 1) the ground state of ^{156}Pm was assigned to spin 4; 2) a 150.3 keV isomeric state with <5s lifetime and spin 1 was reported in ^{156}Nd β decay. Since no transitions identified in ^{156}Nd β decay can be seen in the current data, it is uncertain whether transitions in this level scheme decay to the ground state or the 150.3 keV isomer.

The mass- and Z- gated γ ray spectrum on ^{156}Pm is shown in Fig. 4. 6. 2. In this spectrum, the 91.9, 109.5, 172.5, 182.6, 119.0, 135.4, 254.4, 318.8, 384.3, 450.6, 236.1, 307.1 and 376.3 keV transitions in the level scheme can be seen. From the energy spacing

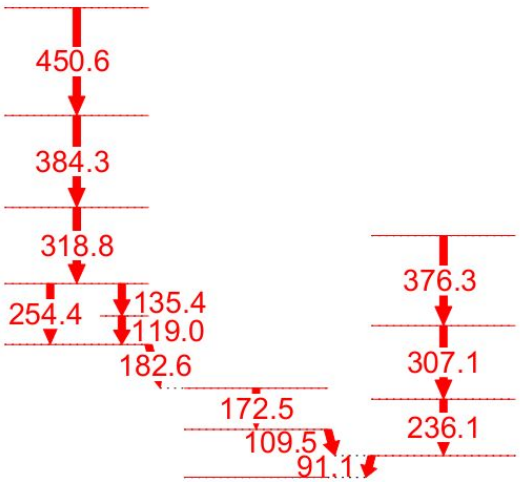

Figure 4. 6. 1. The level scheme of ^{156}Pm. All transitions are new.

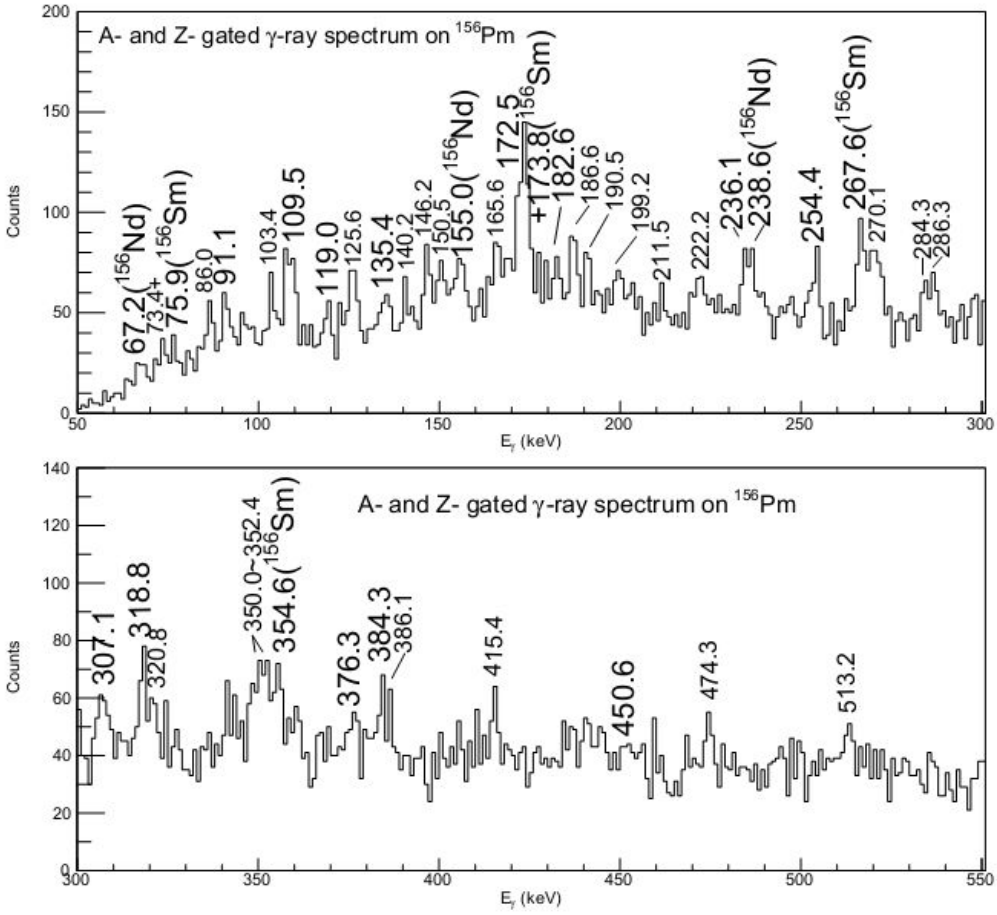

Figure 4. 6. 2. Mass- and Z- gated γ- ray spectrum on ^{156}Pm from ^{9}Be+ ^{238}U induced fission. Transitions not placed in the level scheme are labeled with smaller fonts.

and intensities in Fig. 4. 6. 2, the 254.4, 318.8, 384.3 and 450.6 keV transitions seem to form a band structure. Similarly, the 236.1, 307.1 and 376.3 keV transition seem to form another band. It is somewhat strange that the 182.6 keV transition is weaker than the 254.4 and 172. 5 keV ones in Fig. 4. 6. 2. However, the placement of the 182.6 keV transition is confirmed in the ^{252}Cf SF coincidence data. There are many transitions labeled in Fig. 4. 6. 2. with smaller font not placed in the level scheme of ^{156}Pm. Their coincidence are not observed in the ^{252}Cf SF data. The 85.6, 103.6, 124.7, 139.4, 165.4, 264.1 and 304.8 keV transitions previously assigned to ^{156}Pm by Hwang *et al.* [112] are also seen in Fig. 4. 6. 2. They are considered to be transitions leaking through the ^{155,157}Pm mass gate in the present work. There are some other peaks both seen in the ^{156,157}Pm mass gates. They might be the ones leaking through the ^{157}Pm mass gate too. Furthermore, transitions from ^{156}Nd, ^{156}Sm are also seen in Fig. 4. 6. 2. One can see that the ^{156}Sm leaking transitions are stronger than that in ^{156}Nd. Besides the possible transitions leaking from the ^{157}Pm, ^{156}Nd, ^{156}Sm, the 73, 146, 150, 186, 211, 222, 270, 284, 286, 320, 351, 415, 513 keV transitions might be ones from ^{156}Pm and not placed in the level scheme. Further discussion is included in the ^{157}Pm part. However, mass/Z gated spectra from ^{155}Pm is needed to eliminate some other possible contaminated transitions in the ^{156}Pm mass/Z gated spectrum. Despite the 150 keV one, none of the transitions seen in this spectrum have the same energy with those identified in ^{156}Nd β decay. The 150.5 keV peak in Fig 4. 6. 2 is considered to be a transition different from the 150.3 keV one observed in ^{156}Nd β decay because the latter one is a E3 transition.

Partial γ ray coincidence spectra are shown in Fig. 4. 6. 3. Part a) is a double gate on 318.8 and 384.3 keV transitions. This spectrum has some contamination from the 384.1

keV transition in ^{145}La in coincidence with the Compton background of 318.8 keV to give rise to 172.0, 183.1, 238.1 and 366.0 keV transitions which are strong in ^{145}La. In this spectrum, the coincident 91.1, 109.5, 119.0, 135.4, 172.5, 182.6, 254.4 and 450.6 keV transitions can be seen. The 182.5 keV transition is clearly seen and strong in this spectrum, which is not consistent with the intensities shown in ^{156}Pm A/Z gated spectrum in Fig. 4. 6. 2. Strong transitions in the ^{91,92,93}Rb ^{252}Cf SF partner are also seen. Part b) is a double gate on 236.1 and 307.1 keV transitions. In this spectrum, the coincident 91.1 and 376.3 keV transitions can be seen as well as the ^{91,92,93}Rb ^{252}Cf SF partner transitions.

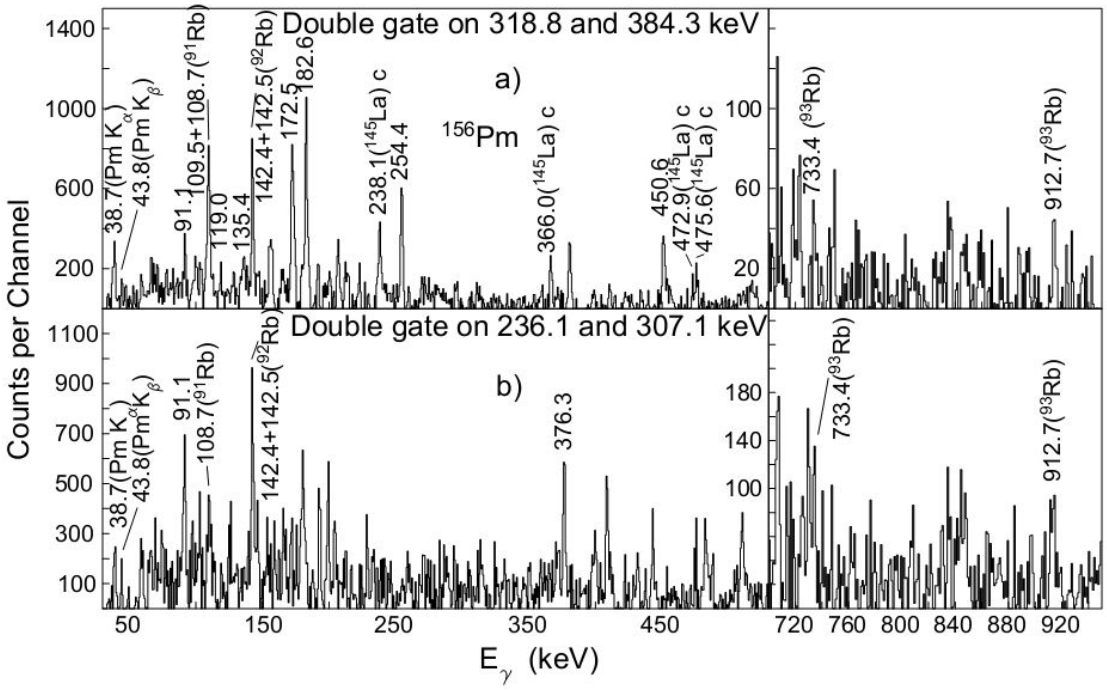

Figure 4. 6. 3. Partial γ coincidence spectra by a) double gating on 318.8 and 384.3 keV and b) 236.1 and 307.1 keV transitions in ^{156}Pm.

^{157}Pm

The new level scheme of ^{157}Pm is shown in Fig. 4. 6. 4. The previous ^{156}Pm transitions of 85.6, 103.6, 124.7, 139.4, 165.4 keV reported in Ref. [112] are all assigned

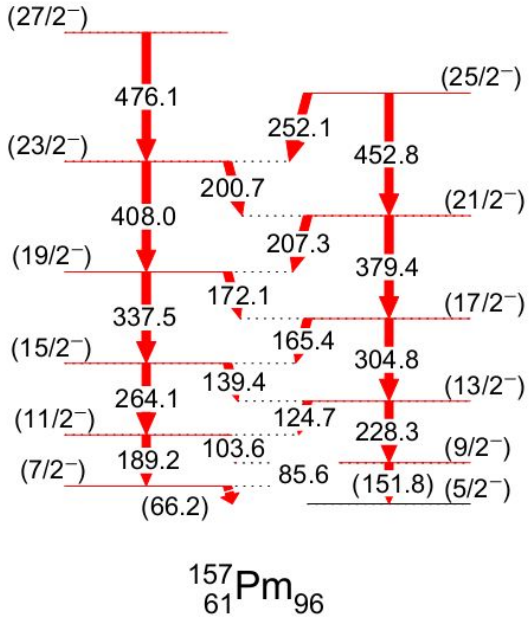

Figure 4. 6. 4. The level scheme of ^{157}Pm.

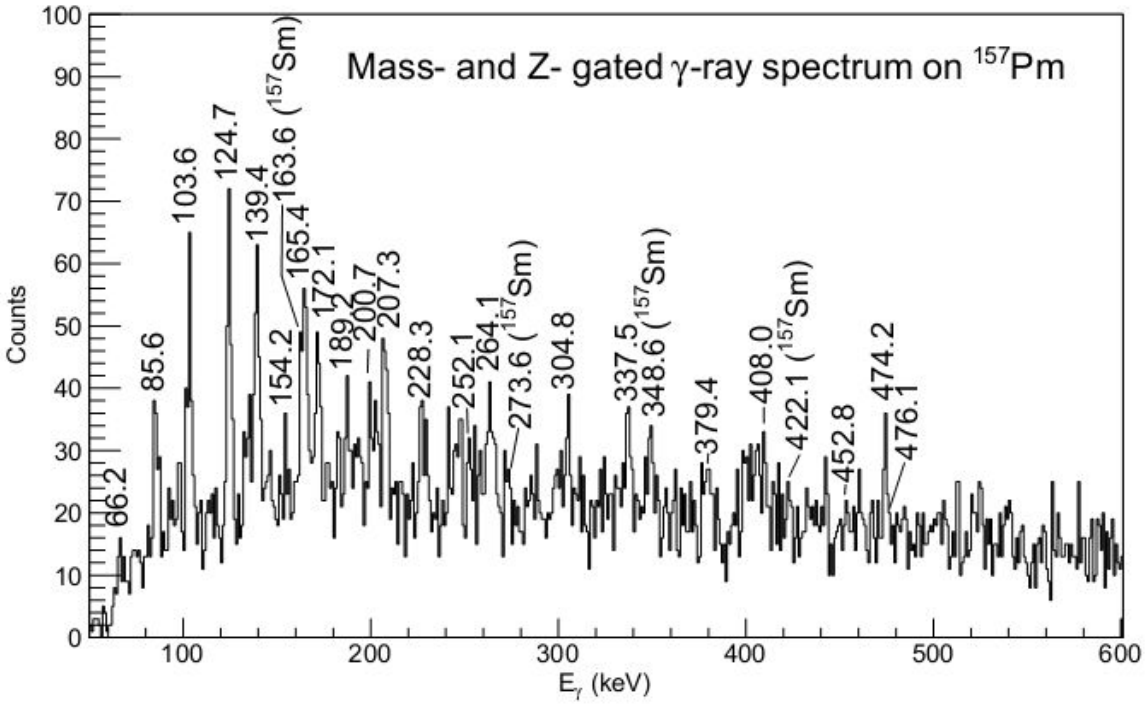

Figure 4. 6. 5. Mass- and Z- gated γ- ray spectrum on ^{157}Pm from ^{9}Be+ ^{238}U induced fission.

to ^{157}Pm in the present work. The levels are established up to 27/2-. According to the systematics, the ground state is tentatively assigned to 5/2- with 5/2[532] configuration in the present work. The 7/2- level may decay to the 5/2- ground state through a 66.2 keV transition. The evidence, as discussed later, is not fully convincing.

Fig. 4. 6. 5 shows the mass/Z gated ^{157}Pm spectrum. In this spectrum, all the transitions placed in the ^{157}Pm level scheme can be seen. Note that these transitions are also seen in the mass/Z gated ^{156}Pm spectrum in Fig. 4. 6. 2. Their intensities in the ^{156}Pm mass/Z gate are about half of those in the ^{157}Pm mass/Z gate. Thus, transitions might be leaking through the 157 mass gate to 156, or both ^{156,157}Pm have these transitions. However, the other ^{156}Pm transitions are not clearly seen in the ^{157}Pm mass/Z gate in Fig. 4. 6. 5, which means the ^{157}Pm spectrum of Fig. 4. 6. 5 is a clean mass gate but not clean Z gate. Some transitions in ^{157}Sm are also seen in the ^{157}Pm mass/Z gated spectrum. These transitions were previously reported by our group in ^{252}Cf SF work. The 474.2 keV transition is not placed in the ^{157}Pm level scheme. The 66.2 keV transition is tentatively assigned as a transition from the 7/2- state to the 5/2- ground state. The 474.2 keV peak has some tail on the right as shown in Fig. 4. 6. 5. This tail is considered to be the 476.1 keV one.

Partial γ ray coincidence spectra are shown in Fig. 4. 6. 6. Part a) is a double gated spectrum on the 38.7 keV Pm x ray and the 103.6 keV transition in ^{157}Pm. In this spectrum, the correlated 85.6, 124.7, 139.4, 165.4, 172.1, 200.7, 207.3, 252.1, 264.1, 304.8, 337.5, 379.4, 452.8, 476.1 keV transitions can be seen. The ^{91,92,93}Rb fission partner transitions are also seen in the spectrum. The background in the 66.2 keV region is high and it is hard to be certain of this transition. Part b) is a double gated spectrum on

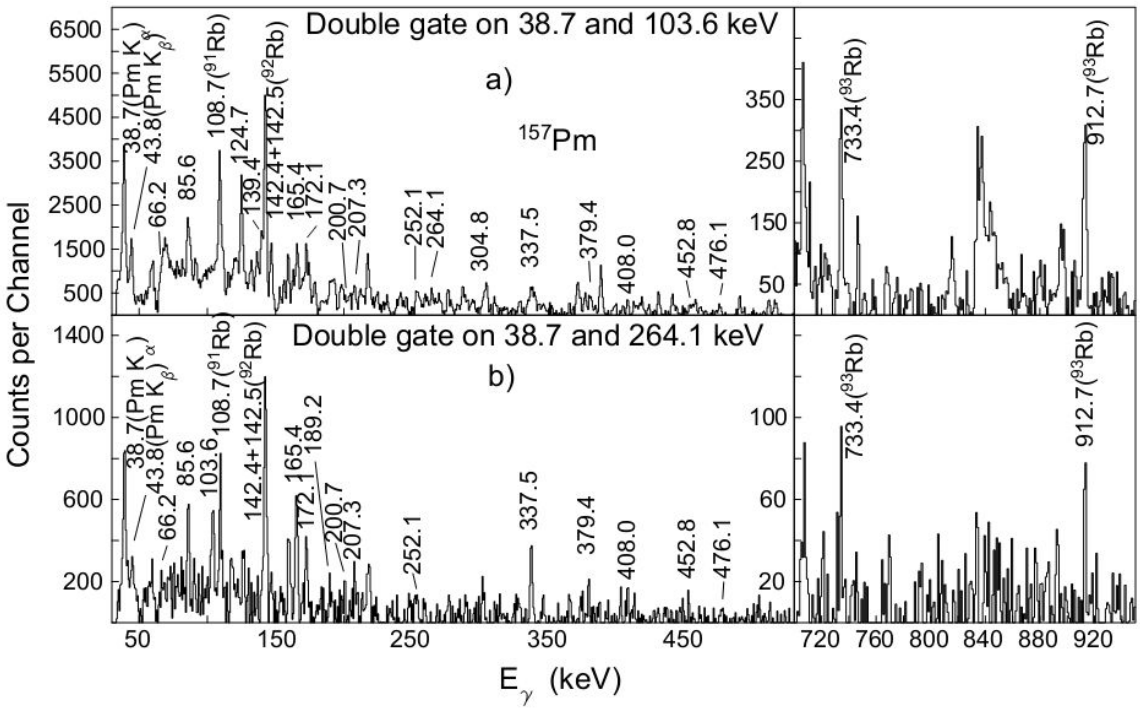

Figure 4. 6. 6. Partial γ ray coincidence spectra by a) gating on 38.7 keV Pm x ray and the 103.6 keV in ^{157}Pm and b) gating on 38.7 keV Pm x ray and 264.1 keV transition in ^{157}Pm.

the 38.7 keV Pm x ray and the 264.1 keV transition in ^{157}Pm. In this spectrum, the correlated 85.6, 103.6, 165.4, 172.1, 189.2, 200.7, 207.3, 252.1, 337.5, 379.4, 452.8, 476.1 keV transitions can be seen. This spectrum also show some evidence for a correlated 66.2 keV transition. However, due to the high contamination in the low energy region, not much evidence can be seen in other γ coincidence spectra. The ^{91,92,93}Rb fission partner transitions are also seen in this spectrum, which confirm that this gate belongs to a Pm isotope.

The 5/2[532] configuration band in ^{157}Pm is identical to those in ^{153,155}Pm. These bands have very similar level energies (shown in Fig. 4. 6. 7) and kinematic (J1) and dynamic (J2) moments of inertia (shown in Fig. 4. 6. 8). Note that the 7/2- level of ^{157}Pm is assumed to be at 66.2 keV in Fig. 4. 6. 7. There is also some similarity in the adjacent

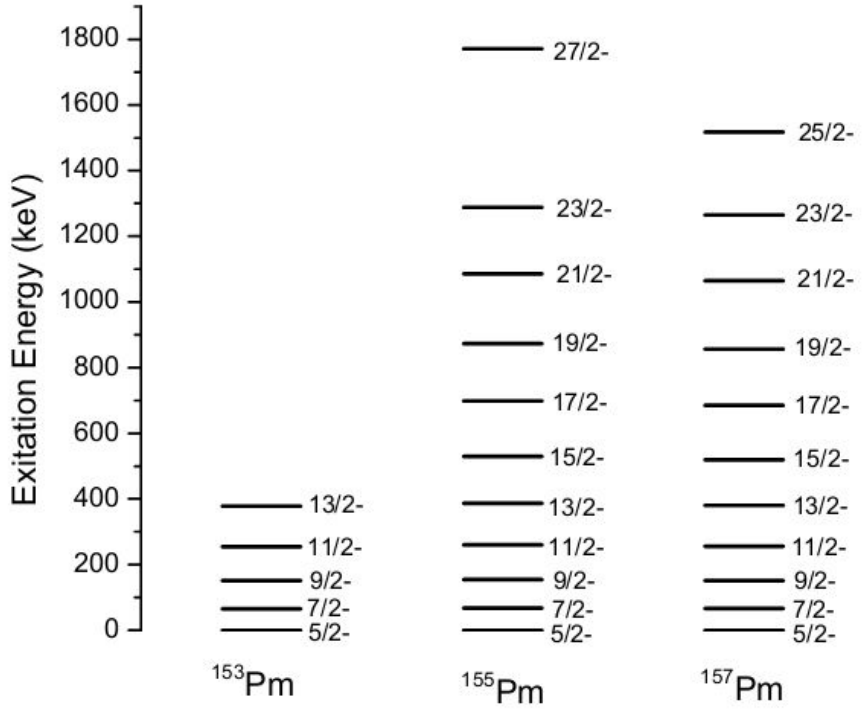

Figure 4. 6. 7. Comparison of 5/2[532] band levels in ^{153,155,157}Pm [112, 113].

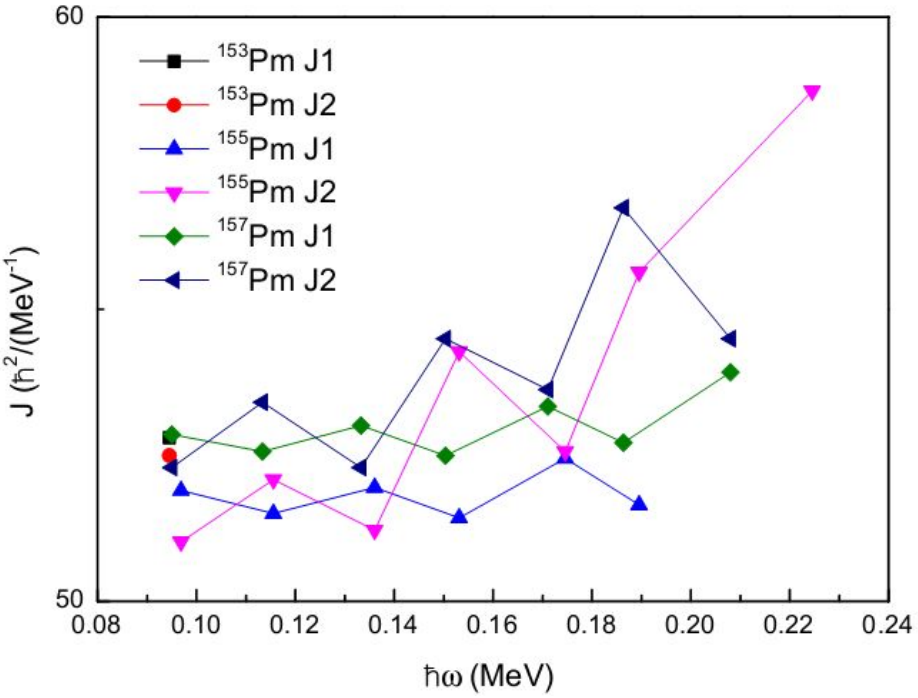

Figure 4. 6. 8. Moment of inertia of the 5/2- band in ^{153,155,157}Pm. Note only one point for ^{153}Pm.

odd A Eu isotopes 5/2[532] bands. Such identical bands at normal deformation was interpreted as effective decoupling mechanism which is the cancellation between paring and deformation parameter [114, 115]. Moreover, the J values of ^{153}Pm are almost the same as those in ^{157}Pm and are somewhat larger than those in ^{155}Pm. Note that the β_2 values for ^{153,155,157}Pm are 0.270, 0.279, 0.289 respectively according to the calculations in Ref. [54]. Thus, it is possible that the pair coupling in ^{153}Pm is weaker, or there is small octupole correlation in ^{153}Pm. Note that an octupole parity doublet was reported in ^{151}Pm. It is also seen that the J_1 and J_2 have small differences and do not change much with the rotation frequency in these nuclei, which shows behavior like expected for a rigid rotor. However, the J values are roughly 75% of a rigid body at low spin.

4. 7 Possible proton two-quasiparticle band in ^{158}Sm

The neutron-rich nuclei with A≈150 change discretely from spherical to large stable prolate deformed shapes as A increases. Static octupole deformation centered around Z=56 and N=88 also occurs in this region. In these well-deformed nuclei, multi-quasiparticle (qp) K-isomeric structures appear systematically. This kind of structure of qp states and the rotational bands built on them are of current interest. Historically, two qp states in ^{156,158,160}Sm and ^{152,154,156}Nd have been studied by γ-ray spectroscopy following β-decay [116, 117] and spontaneous and induced fission [118-122]. Lifetimes have been measured for some qp states and physical quantities have been compared systematically for the rotational bands built on them. A two qp state with υ5/2[642] ⊗ υ5/2[523] configuration was found in ^{158}Sm [118, 121]. A rotational negative parity band was established up to 18^-. In this work, a comparison between a new analysis of ^{158}Sm levels and theoretical calculations gives evidence for a proton two qp band close in energy to the neutron two qp level as theoretically predicted [120, 123].

The partial level scheme of ^{158}Sm obtained in the present work is shown in Fig. 4. 7. 1. Three bands are labeled on top with numbers (1),(2),(3). We only show the levels of the yrast band (1) up to 498.4 keV because we mainly discuss the structure of the negative parity bands in this paper. In the earlier experiments on the prompt γ-rays from the spontaneous fission of ^{252}Cf, band (1) was established [124, 125] and expanded [118, 121] to spin 16^+. In this work, we have confirmed all the previously observed transitions and a new 692.7 keV γ transition has been found to feed the 16^+ level. The 1279 keV band head of band (2) was identified by Zhu *et al.* [118] with three possible M1

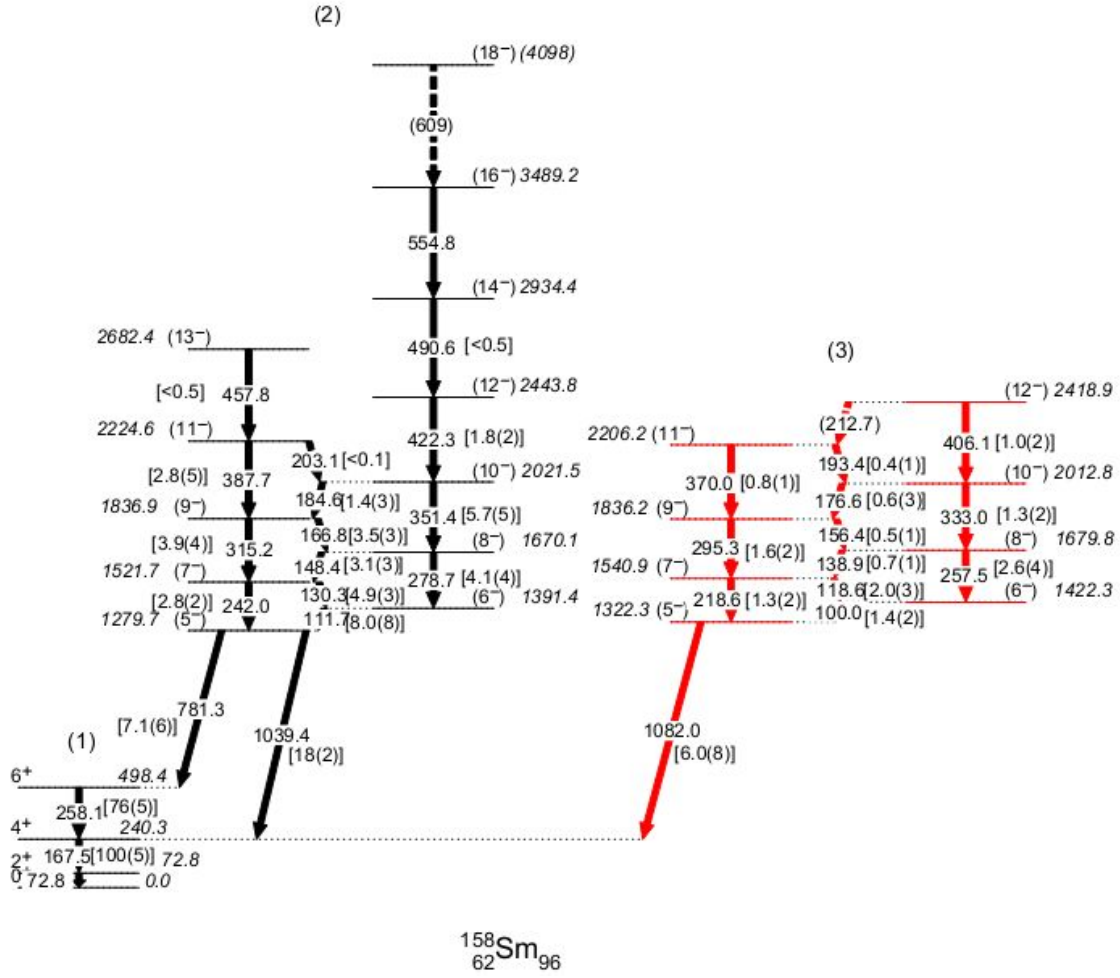

Figure 4. 7. 1. The level scheme of ^{158}Sm. Band (2) from Ref. [121] is included for comparison. New transitions and levels are labeled in red.

transitions on top. Simpson *et al.* [121] expanded this band up to 4098 keV (18^-) level with 16 γ-ray transitions. Gauthein *et al.* [120] measured the lifetime of the 1279 keV (5^-) level by using the delayed γ-ray spectroscopy of ^{252}Cf SF fragments. The value obtained was 115ns. Simpson *et al.* [121] used a similar technique which gave a half life of 83(12)ns. Recently, our group measured this half life to be 72(6)ns [126]. Based on theoretical calculation [120-122, 127], this level was assigned to 5^- with a υ5/2[642] ⊗ υ5/2[523] configuration. Note that Simpson *et al.* identified a second 5^- and 7^- level band

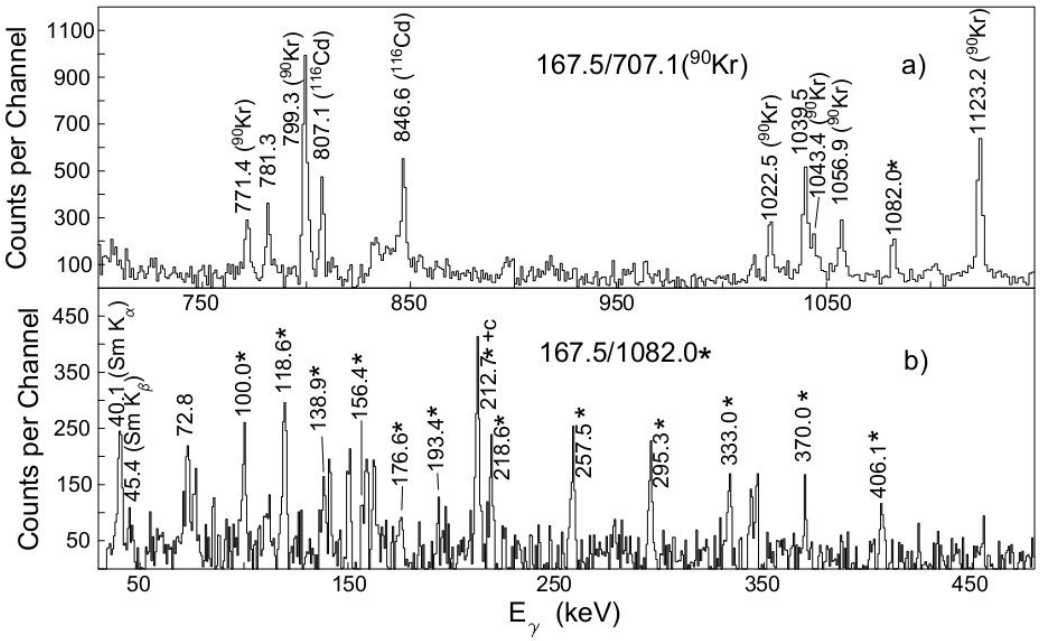

Figure 4. 7. 2. Partial γ-ray coincidence spectrum a) by gating on 167.5 keV transitions in ^{158}Sm and 707.1 keV transition in ^{90}Kr fission partner, and (b) by gating on 167.5 and 1082.0 keV transitions in ^{158}Sm from ^{252}Cf SF data. The 212.7 keV transition has a strong contaminated component.

in ^{156}Sm in their Fig. 9 [121].

All the levels and transitions in band (3) are newly identified in the present work. In contrast to band (2), only one interband transition between band (3) and band (1) has been found. However, because of the high contamination in the low energy region, we are not able to measure the lifetime of the new 1322.3 keV state.

Fig. 4. 7. 2a) shows a coincidence spectrum double gated on the 167.5 and 707.1 keV transition in ^{90}Kr (4n channel) fission partner. In this gate, we focus on the high energy region. One can see the 771.4, 799.3, 1022.5, 1043.4, 1056.9, 1123.2 keV γ-ray transitions in ^{90}Kr. These transitions are all correlated with the 707.1 keV one. The new

1082.0 keV transition is labeled with an asterisk in this gate. The peak height is about 1/3 of the 1039.5 one established earlier. This peak is not observed in the 258.1 and 707.1 keV double gate, which means this 1082.0 keV γ-ray transition directly feeds the 240.3 keV level. The 807.1 and 846.6 keV contamination transitions in ^{116}Cd in this spectrum come from the coincidence of the 167.0 ($10^+ \rightarrow 8^+$) and 706.0 ($4^+ \rightarrow 2^+$) keV transitions of the $10^+ \rightarrow 8^+ \rightarrow 6^+ \rightarrow 4^+ \rightarrow 2^+ \rightarrow 0^+$ cascade in ^{116}Cd.

Fig. 4. 7. 2b) shows a coincidence spectrum double gated on the 167.5 and 1082.0 keV transition. In this gate, we focus on the low energy region. In addition to the known γ-ray at 72.8 keV in ^{158}Sm and the 40.1 and 45.4 keV x-rays in Sm, new γ-ray transitions at 100.0, 118.6, 138.9, 156.4, 176.6, 193.4, 212.7, 218.6, 257.5, 295.3, 330.0, 370.0, 406.1 keV are observed. The 212.7 keV peak has some unknown strong contamination which makes the intensity larger than the others. The 257.5 keV peak may also contain some contamination of the 258.1 keV yrast transition from background coincidence with the 167.5 keV yrast transition.

Transition intensities and their errors in the new band (3) are labeled with parentheses. The intensities of 167.5 and 258.1 keV γ-rays in the yrast band and 781.3 and 1039.4 keV interband γ-rays from band (2) to band (1) as well as those in band (2) observed in Ref. [121] are also remeasured for comparison. Internal conversion electrons are included to correct the intensities in the yrast band but not for the negative parity bands. We note that the intensity of the 1039.4 keV γ-ray measured in the previous work (6.1) [118] is significantly different from the current work (18). The reason might be the statistics, since the previous experiment [118] only collected two orders of magnitude fewer triple γ coincidence events compared to the current work.

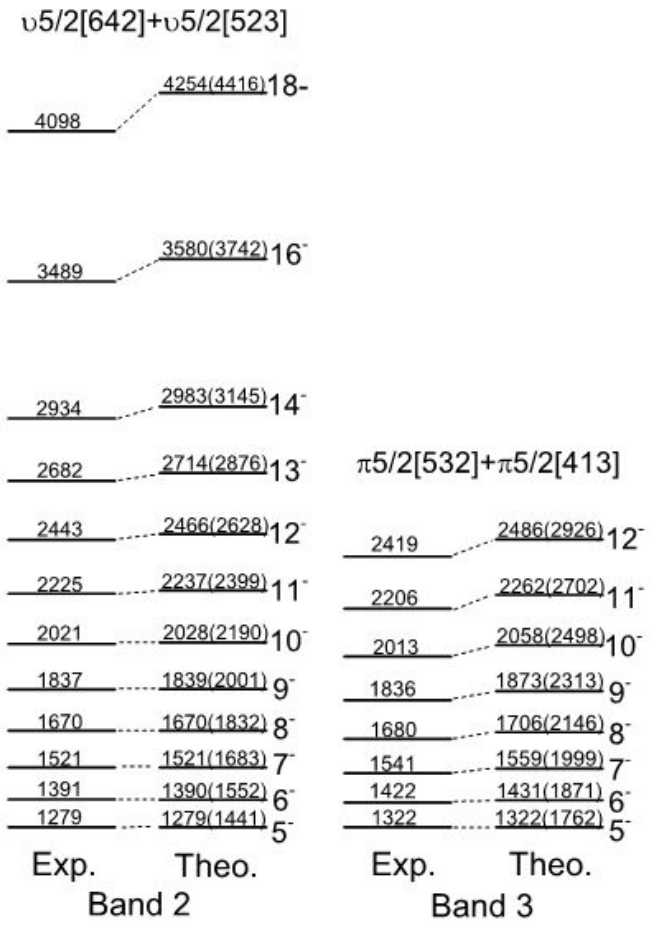

Figure 4. 7. 3. Comparison of level energies of ^{158}Sm with PSM calculations in Ref. [123]. The band head energies have been taken as references.

The possible transition from the 1322.3 keV bandhead level to the 6^+ level is not observed. Thus, if only the decay pattern is considered, this level also could have 3^-, 4^-, 2^+ or 3^+ spin and parity rather than 5^-. Gautherin *et al.* [120] made a Hartree-Fock-Bogoliubov (HFB) calculation to predict the two lowest proton and neutron 2qp states at 1.3~1.4 MeV(less than 100 keV separation) with υ5/2[642] ⊗ υ5/2[523] and π5/2[532] ⊗ π5/2[413] configurations respectively. Simpson *et al.* [121] predicted the proton 5^- 2qp state at an energy 346 keV higher than the neutron 5^- 2qp state using the quasiparticle plus rotor model(QPRM). Yang *et al.* [123] calculated the rotational bands on these two

configurations with the projected shell model(PSM) method. The results are shown in Fig. 4. 7. 3. For comparison we have normalized the theoretical band head energies to the experimental ones. For band (3), as the energies increase, there is seen small differences increasing between the experimental excitations and the theoretical calculations, in contrast to the case of band (2), where very good reproductions were achieved at all energies. The deviations between the experiment and the theory in band (3), however, are within the errors of the theoretical calculations. Such deviations may also be related to the missing of octupole correlations in the PSM calculation. Note that Simpson *et al.* [121] attributed their deviation to the missing of octupole deformation in PRM calculations. However, the rotational bands are well reproduced by the calculation. Thus, the 1322 keV level is tentatively assigned to 5^- in the current work. The intraband transition energies in band (3) are similar to those in band (2) and in other rotational bands built on 5^- 2qp states in ^{156}Nd and ^{156}Sm (almost identical to ^{156}Nd).

In conclusion, high-spin states of neutron-rich ^{158}Sm have been reinvestigated. A new band has been observed and compared to the known ones. The new level energies have been compared with theoretical calculations. The band head has been tentatively assigned to a 5^- proton two qp state with a $\pi 5/2[532] \otimes \pi 5/2[413]$ configuration.

CHAPTER 5

CONCLUSIONS

In summary, a four fold γ coincidence hypercube with high statistics has been built by using the raw data obtained in the previous ^{252}Cf SF experiment with Gammasphere. The new data have been combined with the previous triple coincidence data to analyze the properties of neutron rich nuclei. An international collaboration with a group in GANIL, France has provided the sharing of our data and their ^{238}U +^{9}Be induced fission γ-γ data with full fragment mass and Z identification.

The new level schemes of ^{96,100}Y have been established. γ ray coincidences have been identified in our ^{252}Cf SF data and transitions in ^{100}Y have been confirmed in the mass-Z gate from ^{238}U +^{9}Be induced fission data. The ^{96}Y level scheme shows some features of spherical shape at low spin. The band structures in ^{100}Y are similar to pairing free ones. Two new bands in ^{100}Y may have 4^{+} π5/2[422] ⊗ υ3/2[411] and 5^{+} π5/2[422] ⊗ υ5/2[413] configurations and form a pseudo spin doublet. This speculation needs more theoretical analysis.

The new level schemes of ^{107}Nb have been established. Gamma ray coincidences have been identified in ^{252}Cf SF data and transitions in ^{107}Nb have been confirmed in the mass-Z gate from ^{238}U +^{9}Be induced fission data. The π5/2+[422] band is similar to the neighboring odd A Nb isotopes. More work is needed to identify the possible 1γ vibrational band.

The new level schemes of ^{118,119}Ag have been established. More calculations are needed to confirm the shape of these nuclei. The ^{118}Ag shows larger signature splitting than ^{114,116}Ag, which may be related to principal axis rotation or evolution of the γ value. The ^{119}Ag might have a magnetic rotation band.

The new level schemes of ^{147,148}Ce have been established. An octupole band in ^{147}Ce has been reported. An 1γ vibrational band and an 1β vibrational band in ^{148}Ce were established. The work on ^{147}Ce has been published in physical review c [73]. The work on ^{148}Ce need further support through theoretical calculations.

The new transitions in $^{143\text{-}146}$Pr have been identified and new level schemes of $^{145,147\text{-}153}$Pr have been established. The γ ray coincidences have been identified in ^{252}Cf SF data and transitions have been confirmed in the mass-Z gates from ^{238}U +^{9}Be induced fission data. This part of the present dissertation clarifies the previous questions by Malkiewicz *et al.* [94] of the mass assignments of levels in $^{151\text{-}153}$Pr. Assignments of levels in ^{151,153}Pr by our group [91] have been confirmed. Levels assigned to ^{152}Pr by our group [93] have been assigned to ^{151}Pr. Systematics imply increasing deformation with the increasing neutron number in Pr isotopes from $^{147\text{-}153}$Pr. The ^{149,151}Pr may have octupole bands. More work is needed to assign the configurations of the bands in these Pr nuclei. The work will be submitted to Physical Review C.

The new level schemes of ^{156,157}Pm have been established. The γ ray coincidences have been identified in ^{252}Cf SF data and transitions have been confirmed in the mass-Z gates from ^{238}U +^{9}Be induced fission data. Levels of ^{156}Pm previously assigned by our group [112] have been reassigned to ^{157}Pm. The 5/2-[532] band in ^{157}Pm is identical to those in ^{153,155}Pm.

A new level scheme of ^{158}Sm has been established. The new band in ^{158}Sm is proposed to be a two proton quasiparticle band in agreement with theoretical predictions. Levels have been compared with theoretical calculations. This work has been published to Physical Review C.

REFERENCES

[1] Fujia Yang and Joseph H. Hamilton, *Modern Atomic and Nuclear Physics*, revised Edition, (2010).

[2] R. B. Firestone, V.S. Shirley, C.M. Baglin, S.Y.F. Chu, and J. Zipkin, *Table of Isotopes*, 8th Edition, John Wiley & Sons, Inc., New York (1996, 1998, 1999).

[3] D. C. Radford, *Nucl. Instrum. Methods Phys. Res. A* **361**, 297 (1995).

[4] N. T. Brewer, Measurements from the Prompt and Delayed Radiation of Fission Fragments: Deformation Properties of Neutron Rich Nuclei, Ph.D. thesis, 2013.

[5] http://www.phy.anl.gov/gammasphere/doc/index.html. http://nucalf.physics.fsu.edu/~riley/gamma.

[6] S. J. Zhu, Summer School in Lanzhou, 2010.

[7] S. H. Liu, Nuclear structure studies of neutron-rich nuclei produced in the spontaneous fission of 252Cf: triaxiality near A=110; spherical shapes and octupole correlations beyond 132Sn, Ph.D. thesis, 2010.

[8] A. V. Daniel *et al.*, *Nucl. Instrum. Methods Phys. Res. B* **262**, 399 (2007).

[9] H. W. Taylor *et al.*, *Nuclear Data Tables A* **9**, 1 (1971).

[10] J. K. Hwang *et al.*, *Phys. Rev. C* **57**, 2250 (1998).

[11] J. K. Hwang *et al.*, *Phys. Rev. C* **67**, 054304 (2003).

[12] M. Rejmund *et al.*, *Nucl. Inst. Meth. Phys. Res. A* **646**,184 (2011).

[13] A. Navin *et al.*, *Phys. Lett. B* **728**, 136 (2014).

[14] J. Simpson *et al.*, *Acta Physica Hungarica, New Series, Heavy Ion Physics* **11**, 159 (2000).

[15] A. Navin *et al.*, 5th Int. Conf. on "**Fission and prop-erties of neutron-rich nuclei, Sanibel 2012**", eds. J. H. Hamilton & A. V. Ramayya, World Scientific, 2013.

[16] G. Jung *et al.*, *Nuclear Physics A* **352**, 1 (1981).

[17] F. K. Wohn *et al.*, *Phys. Rev. C* **36**, 1118 (1987).

[18] J. K. Hwang *et al.*, *Phys. Rev. C* **58**, 3252 (1998).

[19] T. A. Khan *et al.*, *Z. Phys. A* **283**, 105 (1977).

[20] U. Hager *et al.*, *Nuclear Physics A* **793**, 20 (2007).

[21] K. Baczynska *et al.*, *J. Phys. G: Nucl. Part. Phys.* **37,** 105103 (2010).

[22] B. Cheal *et al.*, *Phys. Lett. B* **645**, 133 (2007).

[23] J. G. Wang *et al.*, *Phys. Lett. B* **675**, 420 (2009).

[24] H. J. Li *et al.*, *Phys. Rev. C* **88**, 054311 (2013).

[25] A. Guessous *et al.*, *Phys. Rev. Lett.* **75**, 2280 (1995).

[26] A. Guessous *et al.*, *Phys. Rev. C* **53**, 1191 (1996).

[27] L. M. Yang *et al.*, *Chin. Phys. Lett.* **18**, 24 (2001)

[28] R. Q. Xu et al., *Chin. Phys. Lett.* **19**, 180 (2002).

[29] H. Hua *et al.*, *Phys. Rev. C* **69**, 014317 (2004).

[30] H. B. Ding *et al.*, *Chin. Phys. Lett.* **24**, 1517 (2007).

[31] X. L. Che *et al.*, *Chin. Phys. Lett.* **21**, 1904 (2004).

[32] S. J. Zhu *et al.*, *Int. J. Mod. Phys. E* **18**, 1717 (2009).

[33] X. L. Che *et al.*, *Chin. Phys. Lett.* **23**, 328 (2006).

[34] E. Y. Yeoh *et al.*, *Phys. Rev. C* **83**, 054317 (2011).

[35] H. B. Ding *et al.*, *Phys. Rev. C* **74**, 054301 (2006).

[36] L. Gu *et al.*, *Chin. Phys. Lett.* **26**, 092502 (2009).

[37] L. Gu *et al.*, *Chin. Phys. Lett.* **27**, 062501 (2010).

[38] Y. X. Luo *et al.*, *J. Phys. G: Nucl. Part. Phys.* **31**, 1303 (2005).

[39] Y. X. Luo *et al.*, *Phys. Rev. C* **69**, 024315 (2004).

[40] A. Bohr, and B. R. Mottelson, *Nuclear Structure* v. 1,2 (1969).

[41] J. Hill, IS-4351, *Iowa State University Res. Rept.*, p.10 (1979).

[42] B. Fogelberg *et al.*, *Phys. Lett. B* **36**, 334 (1971).

[43] Z. Janas, *Nuclear Physics A* **552**, 340 (1993).

[44] H. Penttila *et al.*, *Z. Phys. A* **338**, 291 (1991).

[45] J. K. Hwang *et al.*, *Phys. Rev. C***65**, 054314 (2002).

[46] M. -G. Porquet *et al.*, *Eur. Phys. J. A* **18**, 25 (2003).

[47] M. -G. Porquet *et al.*, *Eur. Phys. J. A* **15**, 463 (2002).

[48] P. Datta *et al.*, *Phys. Rev. C* **69**, 044317 (2004).

[49] P. Joshi *et al.*, *Phys. Rev. Lett* **98**, 102501 (2007).

[50] E. O. Lieder *et al.*, *Phys. Rev. Lett* **112**, 202502 (2014).

[51] C. Liu *et al.*, *Phys. Rev. C* **88**, 037301 (2013).

[52] S. Roy *et al.*, *Phys. Lett. B* **710**, 587 (2012).

[53] Y. X. Luo *et al.*, *Nuclear Physics A* **919**, 67 (2013).

[54] P. Moller *et al.*, *Atomic Data and Nuclear Data Tables* **59**, 185 (1995).

[55] S. H. Liu *et al.*, *Phys. Rev. C* **84**, 014304 (2011).

[56] I. Stefanescu *et al.*, *Eur. Phys. J. A* **42**, 407 (2009).

[57] S. Lalkovski *et al.*, *Phys. Rev. C* **87**, 034308 (2013).

[58] W. Nazarewicz, P. Olanders, I. Ragnarsson, J. Dudek, G. A. Leander, P. Moller, and E. Ruchowska, *Nucl. Phys. A* **429**, 269 (1984).

[59] W. Nazarewicz and S. L. Tabor, *Phys. Rev. C* **45**, 2226 (1992).

[60] J. H. Hamilton *et al.*, *Prog. Part. Nucl. Phys.* **35,** 635 (1995).

[61] W. R. Phillips, I. Ahmad, H. Emling, R. Holzmann, R. V. F. Janssens, T. L. Khoo, and M. W. Drigert, *Phys. Rev. Lett.* **57**, 3257 (1986).

[62] S. J. Zhu *et al.*, *Phys. Lett. B* **357**, 273 (1995).

[63] M. A. Jones *et al.*, *Nucl. Phys. A* **605**, 133 (1996).

[64] S. J. Zhu *et al.*, *Phys. Rev. C* **60**, 051304 (1999).

[65] Y. X. Luo *et al.*, *Phys. Rev. C* **66**, 014305 (2002).

[66] W. R. Phillips, R. V. F. Janssens, I. Ahmad, H. Emling, R. Holzmann, T. L. Khoo, and M. W. Drigert, *Phys. Lett. B* **212**, 402 (1988).

[67] L. Y. Zhu, S. J. Zhu, M. Li, J. H. Hamilton, A. V. Ramayya, B. R. S. Babu, W. C. Ma, J. O. Rasmussen, M. A. Stoyer, and I. Y. Lee, *High Energy Phys. and Nucl. Phys.*-Chinese Edition **22**, 885 (1998).

[68] Y. J. Chen, S. J. Zhu, J. H. Hamilton, A. V. Ramayya, J. K. Hwang, M. Sakhaee, Y. X. Luo, J. O. Rasmussen, K. Li, I. Y. Lee, X. L. Che, H. B. Ding, and M. L. Li, *Phys. Rev. C* **73**, 054316 (2006).

[69] Y. J. Chen, S. J. Zhu, J. H. Hamilton, A. V. Ramayya, J. K. Hwang, Y. X. Luo, J. O. Rasmussen, X. L. Che, H. B. Ding, and M. L. Li, *High Energy Phys. and Nucl. Phys.*-Chinese Edition **30**, 740 (2006).

[70] J. G. Wang *et al.*, *Phys. Rev. C* **75**, 064301 (2007).

[71] S. J. Zhu *et al.*, *Phys. Rev. C* **59**, 1316 (1999).

[72] W. Urban *et al.*, *Phys. Rev. C* **54**, 945 (1996).

[73] H. J. Li *et al.*, *Phys. Rev. C* **90**, 047303 (2014).

[74] Ts. Venkova *et al.*, *Eur. Phys. J. A* **28**, 147 (2006).

[75] J. D. Robertson *et al.*, *Phys. Rev. C* **40**, 2084 (1989).

[76] M. Shmid *et al.,* Proc. Int. Conf. Nuclei Far from Stability, Helsingor, Denmark, Vol.2, p.576 (1981); CERN-81-09 (1981).

[77] F. Schussler *et al.*, Proc. Int. Conf. Nuclei Far from Stability, Helsingor, Denmark, Vol.2., p.589 (1981).

[78] F. Hoellinger *et al.*, *Phys. Rev. C* **56**, 1296 (1997).

[79] M. Sakhaee *et al.*, *Phys. Rev. C* **60**, 067303 (1999).

[80] T. Rząca-Urban *et al.*, *Phys. Rev. C* **86**, 044324 (2012).

[81] S. J. Zhu *et al.*, 3th Int. Conf. on "**Fission and prop-erties of neutron-rich nuclei, Sanibel 2012**", eds. J. H. Hamilton & A. V. Ramayya, World Scientific, 1998.

[82] R. L. Gill *et al.*, *Phys. Rev. C* **27**, 1732 (1983).

[83] P. Moller *et al.*, *Atomic Data and Nuclear Data Tables* **98**, 149 (2012).

[84] R. Krücken et al., *Phys. Rev. Lett* **88**, 232501 (2002).

[85] R. F. Casten et al., *Phys. Rev. Lett* **87**, 052053 (2001).

[86] L. J. Lv, Journal of Chifeng University (Natural Science Edition) **23**, 5, (2007).

[87] P. A. Butler, *Acta Phys. Pol. B* **24**, 117 (1993).

[88] S. J. Zhu *et al.*, *J. Phys. G: Nucl. Part. Phys.* **21** L75 (1995).

[89] www.nndc.gov; W.D.Kulp, Priv. Comm. (2009).

[90] J. K. Hwang *et al.*, *Phys. Rev. C* **62**, 044303 (2000).

[91] J. K. Hwang *et al.*, *Phys. Rev. C* **82**, 034308 (2010).

[92] T. Rząca-Urban *et al.*, *Phys. Rev. C* **82**, 067304 (2010).

[93] S. H. Liu *et al.*, *Phys. Rev. C* **84**, 044303 (2011).

[94] T. Malkiewicz *et al.*, *Phys. Rev. C* **85**, 044314 (2012).

[95] J. Dalmasso *et al.*, *Nucl. Instrum. Methods* **221**, 564 (1984).

[96] E. M. Baum *et al.*, *Phys. Rev. C* **39**, 1514 (1989).

[97] H. Yamamoto *et al.*, *J. inorg. nucl. Chem.* Vol. **42**, 1539 (1980).

[98] P. F. Mantica *et al.*, *Phys. Rev. C* **48**, 1579 (1993).

[99] R. C. Greenwood *et al.*, *Nucl. Inst. Meth. Phys. Res.* A **390**,95 (1997).

[100] N. K. Aras *et al.*, *Can. J. Chem.* **61**, 780 (1983).

[101] Y. Kojima *et al.*, *Eur. Phys. J. A* **19**, 77–81 (2004).

[102] B. Pfeiffer *et al.*, J.Phys.(Paris) **38**, 9 (1977).

[103] U. Keyser *et al.*, Proc.Intern.Conf.Atomic Masses and Fundamental Constants, 6th, East Lansing (1979), J.A.Nolen, Jr., W.Benenson Eds., Plenum Press, New York, p.485 (1980).

[104] BrIcc v2.3S, conversion coefficient calculator [http://bricc.anu.edu.au/]; T. Kibedi, T. W. Burrows, M. B. Trzhaskovskaya, P. M. Davidson, and C. W. Nestor Jr., Nucl. Instrum. Methods Phys. Res. A **589**, 202 (2008)

[105] Gabriela Thiamova *et al.*, *Phys. Rev. C* **86**, 044334 (2012).

[106] S. Yamada, A. Taniguchi, and K. Okano,J. Phys. Soc. Jpn. **64**, 4047 (1995).

[107] W. Urban *et al.*, *Phys. Rev. C* **79**, 044304 (2009).

[108] Y. Kojima *et al.*, *Nucl. Inst. Meth. Phys. Res.* A **564**,275 (1996).

[109] G. S. Simpson *et al.*, *Phys. Rev. C* **81**, 024313 (2010).

[110] M. Shibata *et al.*, *Eur. Phys. J. A* **31**, 171 (2007).

[111] K.Okano and Y.Kawase, NEANDC(J)-140/U (1989).

[112] J. K. Hwang *et al.*, *Phys. Rev. C* **80**, 037304 (2009).

[113] D. G. Burke *et al.*, *Phys. Rev. C* **18**, 693 (1978).

[114] A.K Jain, *Zeitschrift für Physik A* **317**, 117 (1984).

[115] T. B. Brown *et al.*, *Phys. Rev. C* **66**, 064320 (2002).

[116] M. Hellström *et al.*, *Phys. Rev. C* **46**, 860 (1992).

[117] M. Hellström *et al.*, *Phys. Rev. C* **47**, 545 (1993).

[118] S. J. Zhu *et al.*, *J. Phys. G* **21**, L57 (1995).

[119] X. Q. Zhang *et al.*, *Phys. Rev. C* **57**, 2040 (1998).

[120] C. Gautherin *et al.*, *Eur. Phys. J. A* **1**, 391 (1998).

[121] G. S. Simpson *et al.*, *Phys. Rev. C* **80**, 024304 (2009).

[122] E. Y. Yeoh *et al*., *Eur. Phys. J. A* **45**, 147 (2010).

[123] Y-C Yang *et al.*, *J. Phys. G: Nucl. Part. Phys.* **37**, 085110 (2010).

[124] J. B. Wilhelmy *et al.*, *Phys. Rev. Lett.* **25**, 1122 (1970).

[125] E. Chiefetz *et al.*, *Phys. Rev. C* **4**, 1913 (1971).

[126] N. T. Brewer *et al.*, Nuclear structure 2012; 5th Int. Conf. on "**Fission and properties of neutron-rich nuclei, Sanibel 2012**", eds. J. H. Hamilton & A. V. Ramayya, World Scientific, 2013.

[127] R. Bengtsson *et al.*, *At. Data Nucl. Data Tables* **35**, 15 (1995).